POLITECNICO DI TORINO

Master of Science in
Electronics Engineering

Master's Thesis

An approach to sustainability evaluation and characterization of a C60-based device

Supervisors
Prof. Mariagrazia Graziano
Prof. Gianluca Piccinini
Prof. Maciej Krzywiecki
Dr. Fabrizio Mo
Dr. Yuri Ardesi

Candidate
Alessandro Sciarrone

Academic Year 2023-2024

Summary

Climate change has become an urgent global issue. Among the anthropic agents, the electronic industry has a significant impact on it, accounting to abount 0.45% of the global greenhouse gases emissions. Therefore it is interesting to evaluate the environmental footprint of this growing sector and possible alternatives to the current technologies, focusing on the semiconductor industry. In this context, the fullerene C60 is a well-documented molecule, constituting a well-known organic material, e.g., used in thin film. In this work, the C60 is investigated as potentially low-environmental impact organic material for the implementation of electronic devices. In particular, both a sustainability evaluation and a characterization of a microelectronic device is performed. The former is based on a proposed scheme focused on the environmental impact of the fabrication: from the synthesis of the material (12.7 GJ/Kg C60 and 48.55 L/Kg C60 of o-xylene loss) and the device fabrication (300 MJ of energy) up to the energy consumption during the usage. Concerning the second, both ab-initio computations and measurements on the fabricated structure have been employed, with a structure based on a top-gate bottom-contact thin film transistor with Bi as contact metal. The results brought to the definition of the energy band diagram, by comparing computed levels on the bulk structure with the photoelectron spectroscopy measurements and Kelvin probe scanning microscopy. The latter, together with atomic force microscopy, provided the roughness of the different uniform surfaces for both their potential distribution and topography. The obtained results motivate further analyses on metal-organic junction, oxide and fabrication process, posing the basis to the study of an optimized device capable to be competitive in the global market.

Acknowledgements

I am grateful to Professor Maciej Krzywiecki and Fabrizio Mo, who have supported me throughout this work, providing me with the information I needed to develop it, allowing me to get to know their field of research and giving me the confidence to develop my ideas and make them concrete, as well as for Yuri Ardesi and Professor Mariagrazia Graziano. I would also like to thank the whole team of the ESpeFuM Laboratory at Politechnika Śląska, who warmly welcomed me, and in particular Aleksandra Przybyła, Justyna Juszczyk-Synowiec and Professor Barbara Solecka, who took care of the measurements and provided insights into their disciplines. My final thanks go to my family for supporting and helping me all the way here, and to my friends and all the people I have had the opportunity to share this journey with.

Contents

List of Tables

List of Figures

Part I

Introduction

The climate crisis is an issue that has an effect on our lives, both directly, through climate change, and indirectly, through a modification of ecosystems, which in turn constitute the environment in which we live.
Therefore, the urgency of tackling this problem and trying to mitigate it as much as possible, if not neutralise it, confronts us with the need to make a personal contribution to achieving these goals.
The ways in which we can follow this path can be several, from adopting a more sustainable lifestyle, to creating greater awareness of the issue, to becoming participants and advocates in collective actions that aim to educate people and combat the problem, regardless of the size of their sphere of influence.
All these possibilities seek to find common living conditions, which can be compatible with the ecosystem in which we live, but allowing all of us to have the same opportunities in terms of health conditions and freedom of choice, without increasing the already largely present huge uneven life conditions.
Therefore, this requires both a reduction of resource consumption to the bare minimum and an improvement in technology to optimise the use of resources.
The latter is the direction that the discourse in this thesis wants to take, starting from an in-depth understanding of the most impactful problem, such as climate change, and the contribution that the electronics-related industry has in this scenario (referring mainly to the semiconductor industry), to the study of technological solutions that can reduce it, if not eliminate it.

Part II

Climate change

Chapter 1

The climate crysis

The climate crysis, also referred as climate change, is a combination of several phenomenons, all caused by the anthropic action on the environment, due to gaseous emissions. Each of them has an impact on the ecosystems and consequently on our lives. They consist in global warming , ocean acidification and ozone layer depletion.
Moreover the different phenomenons are linked each other, since the effect of one phenomenon could enhance the cause of the other one (for instance more the ozone layer is depleted more UV rays could enter into the atmosphere warming the globe, so increasing its temperature) and sometimes they also presents some positive feedback (for instance the increase of CO_2 into the ocean makes the capability to absorb it by means of calcification decrease).
Therefore the ecosystems are stressed by these alterations of their normal condition, the one registered before the industrialization era, being forced to change in some way in order to adapt to the different environmental conditions. This stress could be sustained until the changes are no more reversible, reaching the so called tipping points.
So for each phenomenon the effects and the causes will be highlighted, and consequently the possible solutions that have been (and could be) adopted.

1.1 Global warming

The global warming consists of an increase of the global temperature, because of an increasing greenhouse effect.
This retain heat on the surface close atmosphere warming it, the lands and the oceans, by means of the greenhouse gases (GHGs), which absorb the infrared (IR) radiations coming from the Earth, avoiding to a larger part of them going out the atmosphere. However the reduction of outgoing energy, through IR radiations, despite a constant external source, the Sun (in average over a whole year), perturbs the energetic equilibrium (incoming energy equal to the outgoing one). As result the Earth has to heat up itself in order to emit more energy , by means of IR radiation. So increasing the atmospheric concentration of GHGs, the Earth will become warmer.
This phenomenon is what in this last century and a half is happening in a strong manner, reaching an increase of the mean surface temperature of about 1.1 °C [47], as it is shown in figure 1.1.

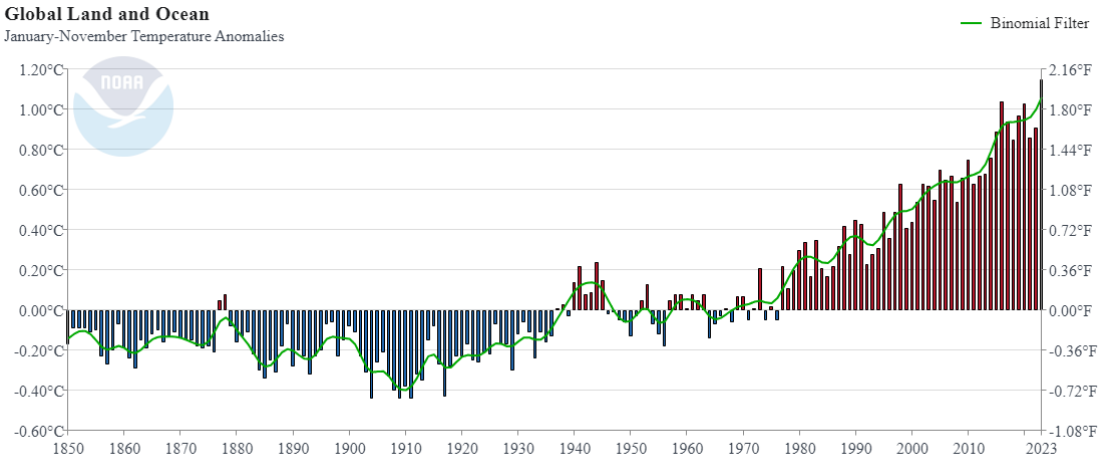

Figure 1.1: Global land and ocean surface temperature[47]

Among the GHGs we can find CO_2, methane, vapour water, nitrous oxide, ozone, chlorofluorocarbons, hydrofluorocarbons and perfluorocarbons, each of them contributing with a different strength and amount to the overall greenhouse effect, as it will be shown when discussing quantitatively this phenomenon.
However they are not the sole contributing agents, in fact among them there are also some natural events and other anthropic ones, in general referred as climate variability and change (including also the GHGs). They can be due to internal variability (e.g. oscillations as El Niño Southern Oscillation and ocean current changes, which alters the heat transfer, or life, affecting the carbon and the water cycles) or external climate forces(e.g. GHGs, orbital variations, volcanism, whose product reduce incoming sunlight or aerosols). Aerosols are one of the main negatively contributing to the global warming by cooling of[0

to 0.8]°C[25]. This statement is fundamental to understand that the effect of pollution, which contribute to the formation of aerosol, hide partially the effect of the GHGs and so if not present the global warming could be higher, providing a further reason to fight against global warming causes.

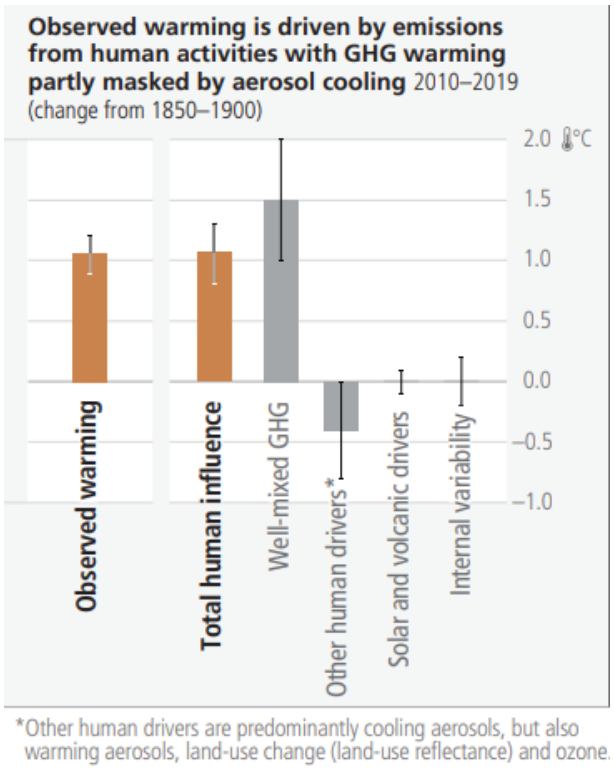

Figure 1.2: Contributions to global warming[25]

Indeed the global warming has an impact on several ecosystems. The main effects are visible through the land warming, the ocean warming, the glacier and permafrost melting, each of them causing phenomenons which can perturb ecosystems and affect our lives, starting from the mostly exposed region of the Earth, usually the warmer ones.
Finally this abrupt climate change makes difficult the ecosystems and living species to adapt, compromising their existence.

1.1.1 Land warming

Global land temperature increases in average by 1.59 °C ([1.34 to 1.83]°C) above 1850-1900 levels during the 2011-2020 period[25]. The land warming results to be the highest one compared to the ocean one and also taking into account the the overall global warming states at 1.09 °C([0.95 to 1.20]°C).
This temperature increase facilitates the water evaporation, so causing soil to dry more easily than before leading to droughts, wildfires and floods, since a dry soil results to be

more compact and less capable to absorb water.

1.1.2 Ocean warming

Oceans are a huge reservoir of Earth heat (they cover 70% of the Earth's surface and absorbed 90% of the warming produced in last years), despite this its temperature increases in average by 0.88 °C ([0.68 to 1.01]°C) above 1850-1900 levels during the 2011-2020 period[25]. The increase of temperature can lead to different effects on environment and ecosystems. So also in this case we can observe perturbations on ecosystems and their normal lifecycle as we can see in the changing of ocean currents and in the coral reef bleaching.

Marine species distribution

The increasing temperature moves the region at a certain temperature at higher latitudes. In this way the marine species move toward higher latitude in environments where other species already exist, this create a competition among them. In some cases the foreign species are invasive one, putting in danger the new hosting ecosystem. In other cases a warmer environment favour the proliferation f a certain species (i.e. harmful algal blooms (HABs)).

Coral Bleaching

Corals are highly sensitive to changes in temperature. When ocean temperatures rise even slightly above the normal range, corals expel the symbiotic algae (zooxanthellae) that live in their tissues and provide them with nutrients through photosynthesis. Thus leaving them white and more susceptible to disease, so to death.
The decreasing of surfaces covered by coral reef cause a reduction of barrier to strong wave for coastal area and also an alteration of the surrounding ecosystem, toward a lower diversity one[56].

Ocean deoxygenation

Ocean deoxygenation is mainly caused by an impact of temperature on both oxygen solubility and circulation, mixing and oxygen respiration[54]. This threaten the normal life in the ocean , reducing the possibility to survive and so the richness of living species and also creating some region with very low or no content of oxygen.

Ocean Heatwaves

Ocean warming cause an increase in the frequency, duration, and intensity of marine heatwaves. These extreme temperature events can have devastating effects on marine ecosystems, causing mass die-offs of species, widespread coral bleaching, and disruption of fisheries. Unlike atmospheric heatwaves, marine heatwaves can last for months, making recovery for affected ecosystems much more challenging.

Thermal Expansion and Sea Level Rise Thermal Expansion

As ocean water warms, it expands. This thermal expansion is a major contributor to sea level rise, which is strengthened by the ice melting occurring by the high temperature. Even a small increase in temperature can lead to significant rises in sea levels over time, which threatens coastal communities and low-lying islands, with higher possibility of floods.

Melting of marine based ice

Warmer ocean temperature enhance the decline of sea ice, lowering the salinity of nearby sea and altering the environment where polar species live.

Impact on Marine Food Webs

The warming of surface waters stratify the ocean, creating a more pronounced layer of warm water on top of cooler, nutrient-rich deeper waters. This stratification can limit the upwelling of nutrients to the surface, where phytoplankton (the base of the marine food web) reside. Reduced phytoplankton productivity affects the entire food web, so species at all levels.

Changes in Ocean Currents

Temperature, salinity and pressure influence ocean currents, which are strong participant to regional climate, since they move heat. In the global warming scenario two concurring phenomenons act to perturb those currents, and they are: evaporation at central latitudes, which increase salinity and so density, and ice melting close to the poles, where salinity decrease, as well as for the density. An example is the strength decrease of the Atlantic Meridional Overturning Circulation (AMOC)[41], where the pressure gradient decrease because of:

- subpolar water warming faster than subtropical one, so decrease the temperature gradient
- subpolar water have an incresing salinity with respect to the subpolar one, because of evaporation an decrease in salinity of the latter. So density of water at subpolar latitude, even if coming from the subtropical regional, is not high enough to go into the deep water as fast as before, hence weakening the deep water AMOC.

1.1.3 Atmospheric warming

Naturally also the near surface atmosphere has an increased temperature, in 2018 registered to be increase by 1.18 °C with respect to the mean level in the period 1961-1990[53]. Also in this case there a is a perturbation to the system Earth.

Higher water vapor

The higher evaporation rate increase the humidity and the amount of vapor water. This one is a greenhouse gas, hence the evaporation behaves as a positive feedback.

Extreme precipitation

The higher temperature increase the capability to retain water vapor. As a consequence the possibility of having an extreme precipitation increase, in fact the registered average annual maximum precipitation amount in a day has significantly increased since the mid-20th century[41].

1.1.4 Sea ice, ice sheet and glacier melting

As already mentioned for the ocean warming the increasing temperature in both ocean and atmosphere, with the consequent melting, lead to sea level rise and reduction on saline concentration. Moreover their loss reduce the reflective surface of the Earth, since at their place there will be the darker ocean or lands. This causes a further increase in land and ocean temperature.
As example of the related loss, according to [74] in 2019 the arctic sea ice corresponds to half of the surface detected in the 1970s.

1.1.5 Permafrost melting

Permafrost is the ground that remains frozen for two or more consecutive years. It can be made of soil, rocks, and ice, so there is also organic matter that preserved over the years and is not completely decomposed. Moreover it is stratified in an active layer that thaw regularly during summer and refroze in colder seasons, such that some plants can grow on it and the beneath always frozen layer. Permafrost extends over 11% of the global surface[50] and is gradually thawing due to the global warming.
The consequences of its thawing are several from the ecosystem point of view to the effect on local population.

Release of greenhouse gases

The exposure of unfrozen permafrost allow the decomposition of organic matter in it, by means of bacterial. Their digestion cause emission of CO_2 and methane (a much stronger GHG than CO_2)[67]. Thus it acts as a positive feedback to the climate change and it can be considered as a tipping point.

Ecosystems disruption

Naturally the alteration of the environmental conditions strongly affects the ecosystem based on it forcing it to move toward higher latitudes, where this conditions are still met. Moreover the melted ice distributes beneath the nearby permafrost enhancing its

melting and also accumulating in lakes, hence modifying also the geological conformation of territory.

Impact on indigenous populations

Several infrastructure in these areas are built over permafrost. Therefore is lack or weakness can constitute a source of collapse of the soil, so of the structures at their time.

Potential for ancient pathogens

Permafrost could exist also for several thousand of years [67], so some pathogens (e.g. viruses) can be brought to life again, being expose in a world with many different species from their originary ones, so probably more exposed to them.

1.1.6 Impacts on ecosystems and human lives

All of these induced phenomenons have strong impact on ecosystems and our human lives. The former have to adapt to the new climate conditions, and this means that some species have to migrate to colder regions (toward the poles for land species and deeper regions for water species), so interacting with other ecosystems with in certain cases negative results, for instance the incoming specie can be aggressive toward the native ones (e.g. the commonly known blue crabs, which with warmer marine temperature can easily reproduce into Mediterranean Sea and consume a lot of clams as food, overcoming their reproductive rate). While the plants can become more vulnerable to parasites and weaker, so contributing to the desertification.
This huge stress on ecosystems can so endanger the existence of some living species.
Consequently, since we rely on these ecosystems, by means of agriculture, water accessibility and breeding/hunting, also human lives can be endangered, especially in those region where these phenomenons are stronger, for instance compromising the water access, because of harder droughts. Moreover the highest rate at which extreme weather conditions occur damage more frequently crops and in some cases also buildings. This poses concerns firstly on the access to the food and then also on the economical side of our society.
Moreover the exposure to such events changes from region to region, and usually the one most involved are the poorest ones, which have less access to facilities allowing them to deal with these problems, and all the native populations who strictly rely on the ecosystems where they live.
Indeed the climate change is worsening the conditions of those populations who actually pollute less.

1.2 Ocean acidification

The increase of CO_2 in the atmosphere is the cause of ocean acidification, where the carbon dioxide dissolves into the oceans water, leading to a decrease of pH. Indeed the gaseous CO_2 dissolves into the water following the Henry's law, in practice its concentration in water is proportional to the partial pressure of the gas on the water. While the

dissolved CO_2 together with the water forms carbonic acid, which at their time dissociate into a proton and carbonate ion.

$$CO_2(aq) + H_2O \rightleftharpoons H_2CO_3 \rightleftharpoons HCO_3^- + H^+ \rightleftharpoons CO_3^{2-} + 2H^+ \tag{1.1}$$

Therefore the two acid dissociation introduce in the water a greater number of proton, hence decreasing the pH, affecting the biocheical equilibrium[71].
Considering that around 20% of the CO_2 introduced into the atmosphere has been absorbed by the ocean[71], the impact of increasing carbon dioxide has an important impact on marine ecosystems (i.e. reduced calcification).

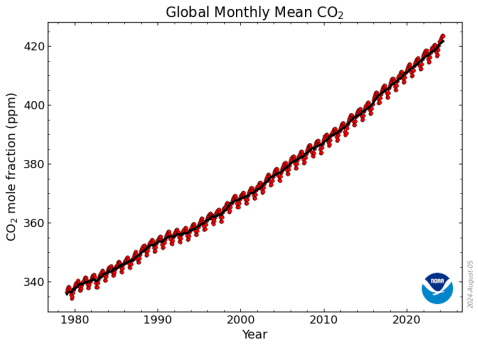

(a) Trend of CO_2 from 1980 to today

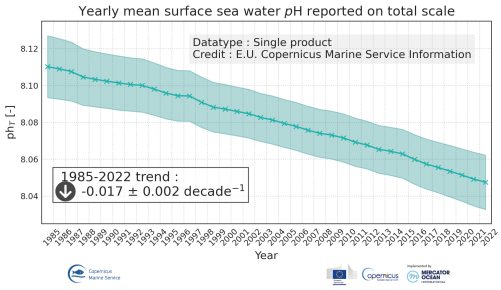

(b) Trend of pH from 1985 to 2022

Biological impact

The decrease of pH can alter the biological equilibrium, for instance by disrupting physiological and biochemical factors (e.g alteration on enzyme activities and flagellar motion for cell motility), influencing the chemical availability of essential micronutrients[71] and changing the meatbolism[43].

Calcification reduction

Many organisms base their lives on calcium carbonate ($CaCO_3$), as it is the constituent of shells and exoskeleton. Its creation depends on the equilibrium of carbonate and calcium ions with calcium carbonate, hence ocean acidification take part to this equilibrium by means of carbonate ions concentration[15].

$$HCO_3^- \rightleftharpoons CO_3^{2-} + H^+ \tag{1.2}$$

$$Ca^{2+} + CO_3^{2-} \rightleftharpoons CaCO_3 \tag{1.3}$$

Indeed the acidification of the water, so the increase of protons, moves the equilibrium of the relation described by equation 1.2 toward the left side. In fact protons are produced

by dissociation of both carbonic acid (H_2CO_3) and bicarbonate (HCO^-), while carbonate ions (CO_3^{2-}) are the production of the lone bicarbonate dissociation. Therefore the concentration of carbonate decreases with a CO_2 increase, hence moving the equilibrium of the relation (presented in equation 1.3) toward a condition with less $CaCO_3$[15]. This equilibrium condition is graphically well explained by the Bjerrum plot.

This can endanger the marine species based on calcification (e.g. corals, species belong-

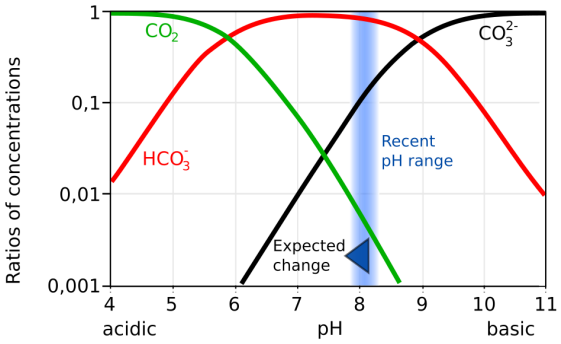

Figure 1.4: Global land and ocean surface temperature[25]

ing to phytoplankton, molluscs and so on), so indirectly affecting the food web and species depending on them[15].

1.3 Ozone layer depletion

Ozone layer is the area in the stratosphere (within 15 km to 50 km from the Earth's surface) characterized by an high presence of ozone (O_3). More precisely this layer is located in altitudes ranging from 30 km to 35 km and it is responsible of absorption of many ultraviolet radiations (UV), which are harmful to our bodies (e.g. causing skin tumors). The absorbed radiation are mainly the higher energy UVC (100% of absorption), followed by UVB (90% of absorption) and finally the lowest energy UVA (50% of absorption)[70]. Instead in case of ozone residing in the lower troposphere (up to 15 km of altitude), so close to the surface, it constitutes a risk for the health[70].

DATA onOZONE DEPLETION The ozone depletion is caused by the so called *ozone depleting substance* (ODS), among which there are chlorofluorocarbons, bromofluorocarbons and halogens. These compounds interfere with the ozone-oxygen cycle, responsible for the presence of ozone in the troposphere.

Ozone-oxygen cycle

The ozone in the stratosphere is formed starting from oxygen molecules O_2, which dissociate into two oxygen atoms (also called radicals, because of their capabilities to easily react) by means of the energy provided by UVC radiations. The oxygen radicals reacts with oxygen molecules to form ozone.

However ozone is not a stable molecule, hence , when stimulating by the energy provided by UVB radiations, dissociate into an oxygen radical(represented with a dot) and an oxygen molecule[48].
O_2 + energy(UVC) $\longrightarrow$ 2 O -> O_2 + O $\longrightarrow$ O_3 -> O_3 + energy(UVB) $\longrightarrow$ O_2 + O

Ozone depleting substances

The ozone depleting substances are[16]:

- Chlorofluorocarbons (CFCs)
- Halons or bromofluoromethanes
- Carbon tetrachloride (CCl_4)
- Methyl Chloroform ($C_2H_3Cl_3$)
- Bromide based compounds
- Chlorobromomethane(CH_2BrCl)
- Hydrochlorofluorocarbons (HCFCs)

These substances are harmful for the chloride and bromide radicals, which acts as catalysts in the cleavage of ozone molecules. Moreover some of these compound acts as strong greenhouse gases.
The principle behind the catalytic behavior is based on the splitting of the compound by means of radiations, giving as results the aforementioned radicals (indicated by a dot represent an unpaired electrons, at the basis of the reaction).
$CFCl_3$ + energy(radiations) $\longrightarrow$ $Cl\cdot$ + $\cdot CFCl_2$
Therefore the remaining radicals reacts with the ozone to form their oxide forms and leaving an oxygen molecules (the same reactions occurs with bromide radicals)[49].
$Cl\cdot$ + O_3 $\longrightarrow$ ClO + O_2
ClO + O_3 $\longrightarrow$ $Cl\cdot$ + 2 O_2
In fact the radicals does not create a stable compound, coming back to the original states in the next reaction with ozone, hence having a catalytic behavior. This cycle persist until the radicals precipitate to the troposphere.
However after the application of the Montreal protocol(in 1987) rules in 1989, the emissions of ODS decreased below the level at which their effect is equivalent to the rate of ozone forming, so the ozone depletion is starting to be recovered [33].

1.4 Tipping points

Tipping points are critical thresholds in the Earth's climate system, beyond which a small change can lead to significant and often irreversible impacts. Once these thresholds are crossed, the system may enter a new state, which can result in dramatic changes in climate patterns, ecosystems, and even the overall stability of the climate system. Today they

are not well understood, in fact their definition can vary among different organization working in this kind of analysis (e.g. IPCC and NOAA). Following the Sixth Assessment report of the IPCC[35], they are the following one, together the effects forecasted in the 21th century in case of continuing increase in temperature :

- Global Monsoon: increase
- Tropical forest: increase in vegetation
- Boreal forest: moving toward the poles
- Permafrost carbon : decline in frozen carbon
- Arctic Summer sea ice:complete loss
- Arctic Winter sea ice: moderate winter decline
- Antarctic sea ice:moderate winter and summer declines
- Greenland ice sheet:mass loss
- West Antarctic ice sheet and shelves: mass loss
- Global ocean heat content: oceans will continue to warm
- Global sea-level rise: continued rise
- AMOC: decline
- Southern MOC: decrease in strength
- Ocean acidification: continued increase of CO_2
- Ocean deoxygenation:increase hypoxia and deoxygenation rates

Chapter 2

How to face the climate change - GHGs emission reduction

The causes of the climate change are attributable to the increase greenhouse effect and the high concentration of CO_2, as already described. Therefore there is the need of quantifying their impact in order to forecast how much reduction on emissions is needed to not go toward the tipping points and have a stable environmental condition. This is the starting point to define exact rules for governments and industries in order to have an effective plan, capable to not require an abrupt change in behavior and so damages to the economy.

2.1 Evaluation of GHGs impact

Greenhouse gases are several and their contribution to the greenhouse effect can vary, depending on their radiative forcing, indeed their capability to absorb the infrared radiation emitted by the Earth. In fact the greenhouse effect take into account two aspects:

- the energy balance between incoming energy (light from the Sun) and outgoing energy (reflected light and infrared radiation emitted by the Earth) should be null at equilibrium;

- the Earth can be treated as a black body, so its temperature determine the wavelengths of the radiation emitted, so having a temperature around 300 K the radiated energy will be with infrared wavelength.

Greenhouse gases (GHGs) are capable to absorb this energy re-emitting part of it back, while the remaining in the free space throughout upper layers of atmosphere, which have much less capability to absorb these radiations. Therefore more heat is retained by GHGs more infrared radiations the Earth has to produce, in order to satisfy the energetic balance.

2.1.1 Quantification of GHGs impact

The effect of each greenhouse gas can be evaluated by means of different parameters and depending on the lifetime of the compound, so on the time horizon in which the effect has been evaluated:

- radiative forcing, so the change in the net radiative flux due to a change of an external driver. So in case of an increase of CO_2, it is the change flux related to the amount of the added gas after a certain time horizon. This characterizes the GWP (Global Warming Potential) metric.

- temperature change, so the effect on the temperature after a certain period due to a quantity of added GHG into the atmosphere, constituting the GTP (Global Temperature change Potential) metric.

In this discussion GWP is the metric taken into account, because it can be easily referred as the more commonly known CO_{2eq}. In fact the unit of this metric is the radiative forcing of a unit mass of CO_2. Some of the GHGs are listed in table 2.1, taking into account few compounds for each species[23] and GWP evaluated over two time horizons, 20 years and 100 years.

2.1.2 Scenario

The global surface temperature has increased by 1.1 °C above 1850-1900 in 2011-2020, still showing a positive trend[25], as shown in figure 1.1. The cause is attributable to increase in GHGs emissions as shown in figure 1.4.
Among all GHGs, the main contributors to global warming are[59]:

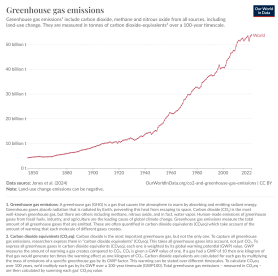

Figure 2.1: Trend of total GHGs emissions from 1850 to 2022[59]

- Carbon dioxide CO_2: 75.01%;

- Methane CH_4: 19.47% ;

- Nitrous oxide N_2O: 5.51%.

Name	Chemical formula	Lifetime (Years)	GWP 20-Years	GWP 100-Years
Carbon dioxide	CO_2		1	1
Methane	CH_4	12.4	84	28
Nitrous oxide	N_2O	121	264	265
Chlorofluorocarbons				
CFC-11	CCl_2F	45	6900	4660
Hydrochlorofluorocarbons				
HCFC-21	$CHCl_2F$	1.7	543	148
HCFC-23	CHF_3	222	10800	12400
Chlorocarbons and Hydrochlorocarbons				
Carbon tetrachloride	CCl_4	26	3480	1730
Methyl chloroform	CH_3CCl_3	5	578	160
Bromocarbons, Hydrobromocarbons and Halons				
Methyl bromide	CH_2Br	0.8	9	2
Halon-1201	$CHBrF_2$	5.2	1350	376
Fully fluorinated species				
Nitrogen trifluoride	NF_3	500	12800	16100
PFC-14	CF_4	50000	4880	6630
Halogenated alcohols and ethers				
HFE-125	CHF_2OCF_3	119	12400	12400

Table 2.1: Some of the greenhouse gases

Therefore is important to understand the sources of these emissions, in order to have a clear idea on sector to focus on to contrast the climate change.

The knowledge of the impact of the detected emissions in the previous decades and the physical reason behind the current situation, scientists are trying to create mathematical models to forecast the possible scenarios in case of different trends for the emissions. In particular the possible climate change scenarios can be described by the Shared Socioeconomic Pathways (SSPs), which are the projected socioeconomic global changes up to 2100, and the Representative Concentration Pathways(RCPs), representing different levels of emissions and the consequent radiative forcing.The two metrics result to be complementary representing the stage of the society at which emission reductions will occur(the former) and the amount of warming due to a certain amount of emissions(the latter).
Regarding SSP scenarios, the possible scenarios are 5 and sometimes are associated to the respective expected radiative forcing in the year 2100 (ranging from 1.9 to 8.5 $\mathrm{W\,m^{-2}}$, so from best to worst emission scenario):

SSP1-1.9 (Sustainaibility-Taking the green road)

SSP2-2.6 (Middle of the road)

Source	CO_{2eq}(100-years)	CO_2	CH_4	N_2O
Tot (billion tonnes of CO_{2eq})	48.45	35.66	8.44	3.13
Electricity and heat	31.33%	42.37%	0.14%	1.87%
Transport	15.05%	19.91%	0.51%	4.67%
Manufacturing and construction	12.84%	17.33%	0.19%	0.84%
Agriculture	12.12%	0	41.95%	74.35%
Fugitive emissions	6.65%	0.75%	34.96%	0.21%
Industry	6.46%	4.57%	0.11%	8.50%
Buildings	6.15%	7.6%	2.78%	1.16%
Waste	3.41%	0	17.89%	4.63%
Land-use change and forestry	2.87%	3.28%	1.31%	3.47%
Aviation and shipping	1.94%	2.61%	0.02%	0.24%
Other fuel combustion	1.20%	1.59%	0.12%	0.07%

Table 2.2: Gas emissions by sector in 2020[58]

SSP3-4.5 (A rocky road)

SSP1-7.0 (A road divided)

SSP1-8.5 (Taking the highway)

So taking into account the SSPs scenarios, together with a categorization due to the expected temperature increase depending on the emission level (categories C1 to C8 described in[25]), the expected emissions and increase in temperature are represented in

2.2 Regulation

The scheme at the basis of the determination of rules to follow is based on the quantitative determination of the changing phenomenons, the anthropic forcing and the economic requirements useful to pursue the wanted goals[72].
The starting points are the Earth's observations of all the climate, biological and chemical phenomenons. It occurs by organizations as Copernicus, WMO, NASA and NOAA, followed by related researches useful to quantify the phenomenons and create more accurate forecast models .
Therefore all of these information are gathered by the IPCC (Intergovernmental Panel on Climate Change) in scientific reports, providing the instruments to the international

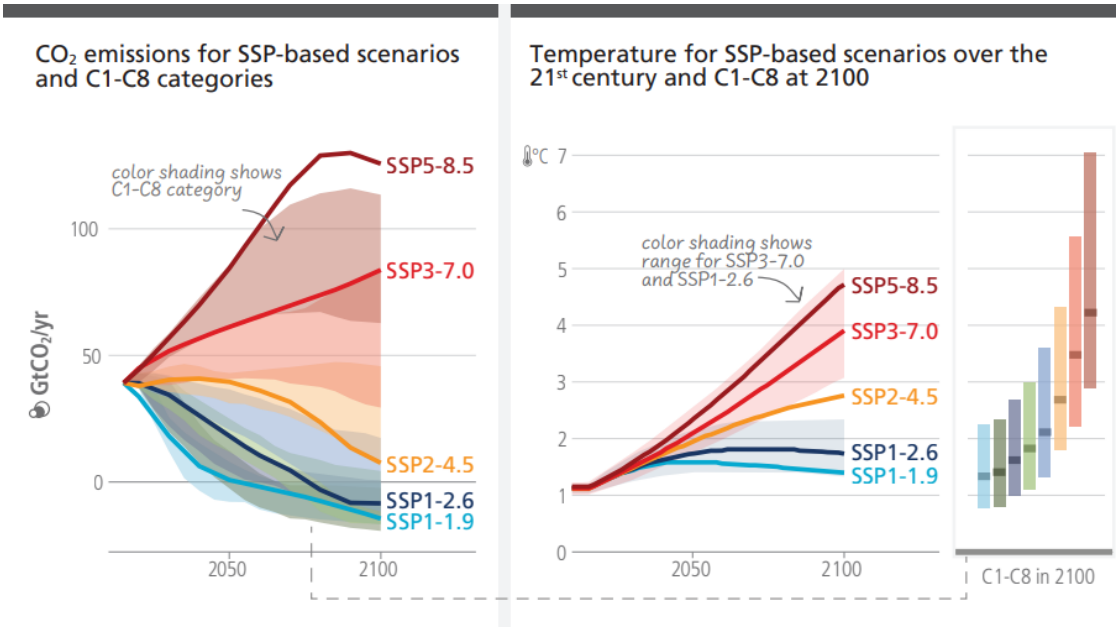

Figure 2.2: SSPs scenarios:global CO_2 emissions and temperature increase

institutions to determine a proper road to contrast the climate change.
At this purpose the international treaty Conference of the Parties (COP, but also known as UNFCCC-United Nations Framework Convention on Climate Change) has been created. Entering in force in 1994 it engages all the parties to fulfill the *"stabilization of greenhouse gas concentrations in the atmosphere at a level that would prevent dangerous anthropogenic [i.e., human-caused] interference with the climate system"*[69], also respecting eventual future protocols (i.e. Kyoto protocol in 1997). Moreover after the Paris agreement (2015) the conference takes it into account as reference.
The COP of conferences are taken each year to agree all the parties on the the action plan to follow and to update the Nationally Determined Contributions (NDCs), so the commitments of the singular countries to reduce GHGs emissions. In order to give guidelines to the creation of NDCs each five years (starting from 2023) the Global stocktake has been introduced

2.2.1 Kyoto protocol

Kyoto protocol was stipulated in 1995, even if entering in force since 2005, after at least 55 countries with an overall polluting emissions of 55% of the total ones had ratified the protocol. The aim of the protocol is the reduction of GHGs emissions by asking a certain reduction of emissions to each party, in order to have an amount of GHGs present in the atmosphere for which the climate change will stop. In order to achieve this is important to reach the net zero emission goal. Furthermore the protocol guarantees the party to not respect the required reduction in case they are engaged to reduce emissions in third countries, where the taken actions require less fundings. This mechanism is regulated by

means of a trading one, which assign a value to the fulfillment or not of the target and a value to the effort in GHGs emission reduction in a third country.The assigned value is quantified by the so called Kyoto units.
Indeed this is carried out in accordance with the Kyoto mechanisms[32]:

- **Emission tradings**: Parties may exchange Kyoto units, in such a way that if one party has reached its target can provide its credits to help another one to be within its target. In this way the overall emissions cap can be still fulfilled.
- **Joint implementation**: A Party can receive credits by funding projects to reduce emissions or enhance sequestration in another one.
- **Clean development mechanisms**: Credits can be obtained by projects of emission reduction, reforestation or afforestation in a countries that have not committed themselves to limiting anthropogenic emissions.

Parties that does not satisfy the requirements to be within the Kyoto mechanisms can be suspended in taking part to it by a specific committee.

2.2.2 Paris Agreement

The Paris agreement has been signed by 195 countries (also called parties) of 198 belonging to the United Nations. Its aims are[55]:

- keeping the temperature increase well below 2 °C above pre-industrial levels, pursuing to limit the temperature increase to 1.5 °C;
- increase the ability to adapt to adverse consequences of climate change, by committing to reduce GHGs emissions, in order to not threaten the food production;
- making finance flows consistent with low GHGs emissions.

Furthermore the parties have to improve their policies every five years. Therefore the Global stocktake has been introduced from 2023 to assess the global effort and provide guidelines.

2.2.3 Strategies for carbon reduction

The fulfillment of all the governmental and international policies can be achieved by several strategies focused on[24]:

- **energy supply improvement**: so working on diversification of energy source, moving more and more toward renewable energy.
- **optimization of land, water and food use**: reducing wastes and emissions of CH_4 and N_2O, or having a better managements of lands and forests, restoring ecosystems, up to adopting more sustainable diets.

- **More efficient settlements and infrastructures**: reducing energy loss in buildings due to heat dissipation, efficient energy use of lightening, and having fuel efficient or electric vehicles and shipping.
- **More efficient industry**: reducing emissions, improving recyclability and energy efficiency.

Chapter 3

The environmental impact of the semiconductor industry

In the climate change scenario it is important to evaluate each possible contributor, and among them the increasing semiconductor industry can have its part. The sphere of influence that this sector can impact are several, starting from the emissions also due to the high energy demand, going toward water and mineral deployment, up to the generated waste, that can be strongly polluting.

3.1 Atmospheric emissions

The emissions of semiconductor factories are mainly characterized by GHGs, fluorinated GHGs (whose relevance is due to the high GWP) and VOCs (Volatile Organic Compounds).
A representative value of the order of magnitude of GHGs emissions of the sector are the emissions of the top six companies accounting to the 58% of the global share of wafer manufacturing capacity in 2020[44](Samsung Electronics, TSMC, Micron, SK Hynix, Kioxia and Intel), which are stated to be 132×10^6t CO_{2eq}. Indeed, assuming the related emissions accounts to the 58% of the overall ones in the sector, the latter are estimated to be 229×10^6t CO_{2eq}, so 1/224 of the global GHGs emissions (51.46×10^9 t CO_{2eq}[59]).
These emissions are characterized by Scope 1, Scope 2 and Scope 3 emissions together, where they are defined as:

- **Scope 1**: direct emissions due to the industrial processes
- **Scope 2**: indirect emissions due to energy demand and production (they can vary depending on the self-production system and the source nationally employed in the country where the plant is located)
- **Scope 3**: indirect emissions not related to the energy needs and for instance due to purchased materials, distribution of the products and end-of-product life.

Averagely the overall emissions are divided into 52% Scope 3, 32% Scope 2 and 16% Scope 1 emissions. Regarding the Scope 1 emissions they are characterized by 45% of perfluorocarbons(PFCs), 16% of CO_2, 15% of NF_3, 9% of N_2O, 7% of other heat transfer fluids (HTFs), 6% of hydrofluorocarbons (HFCs) and 2% of SF_6. Indeed PFCs assume a strong role for their high global warming potential[44]. While the Scope 3 emissions are difficult to estimate and evaluate because of both a not standardized methodology and differences among companies in the stages they are in charge of (i.e. TSMC does not report information on sold product, because this stage of the product life is managed by a third company). Also VOCs emission are concerning for endangering human health and the environment. They can be release from wafer fabrication, manufacturing processes, PCBs manufacturing and assembly. These processes can produce compounds as alcohol, ketones, acetate and aromatic compounds, xylenes, acetone,iso-propyl, ethyl acetate, styrene, methanol in addition to the non-VOCs acids(sulfuric, hydrochloric, phosphoric, nitric, acetic), chlorine and ammonia[6].

3.2 Energy consumption

Energy consumption is important for evaluating the Scope 2 emissions and therefore understanding the possibility to reduce the carbon footprint, depending on the territory where the plant is located. In fact the emissions related to the energy production varies a lot among different countries (as briefly shown in table 3.1), because of different deployment of energy sources. Therefore the reduction of carbon footprint can occur from both governmental (so on the national scale) and private (so on company scale) investments on renewable energies or low-carbon sources(i.e. gas instead of coal).

Country	Production fuel mix factor ($kgCO_{2eq}$ per kW h)
Poland	0.76
Italy	0.32
Sweden	0.0057
USA	0.42
Saudi Arabia	0.51
Cina	0.54
South Africa	0.90

Table 3.1: Country specific electricity factors- January 2022[9]

3.2.1 Electronic industry related energy demand

3.3 Water management

Semiconductor industry requires large amount of water, a representative case is the TSMC one: in 2021 three fabs located in the Hsinciu science park needed of $547\,000\,t\,d^{-1}$ of water

accounting to the 10.2% of the overall demand in the region[68].
This large requirement is attributable to the ultrapure water (UPW) needed for rinsing the wafer after fabrication steps (i.e. photolithography). The UPW theoretically should contain no impurities (e.g. ions and organic compounds), which could be remained attached to the wafer reacting with it or creating unwanted layer contamination, that can destroy or alter the structure and so compromising the electrical performances. Moreover, after each process, the water used for rinsing contains the removed contaminants, some examples reported in [34] are shown below:

Process	Contaminants
Backgrinding and dicing	Si particles
Photolithography	Tetramethylammonium hydride (TMAH) and chlorine
Pretreatment and wet etching	Inorganic acid,alkalis and oxidizing agents(hydrogen peroxide)
Subprocesses(e.g. maintenance and jig cleaning)	Organic solvents

Table 3.2: Water contaminants produced in manufacturing processes[34]

Therefore the management of wastes and water supply affect the surrounding communities, since it can be the cause of water shortage during droughts and the pollution of the water.
In fact several semiconductor companies are working to improve the footprint of the factories from this point of view through several strategies:

- diversification of the sources,
- enhancement of water recycling.

The latter is the most challenging, but needed in the long term, because of the need of UPW from wastes containing silica and organic solvents, prone to remain even after the treatment. Despite this technologies capable to filter out this contaminants exist[34], as it is shown by the already occurring water recycling[68].

3.4 E-waste

The electronic equipments wastes (also known as waste electrical and electronic equipment, WEEE) are assuming more relevance over the years, because of the increasing number of devices under use and the increasing technology integration within furniture, clothes and tools. In fact, in 2022 62 billion kg of e-waste has been generated[7], whose 22.3% is documented as formally collected and recycled in an environmentally sound manner. Instead another 25.8% is estimated to be collected and recycled outside the formal systems[7]. Instead the devices put on the market in the same year were 96 billion kg, showing obviously the same increasing trend of e-waste.

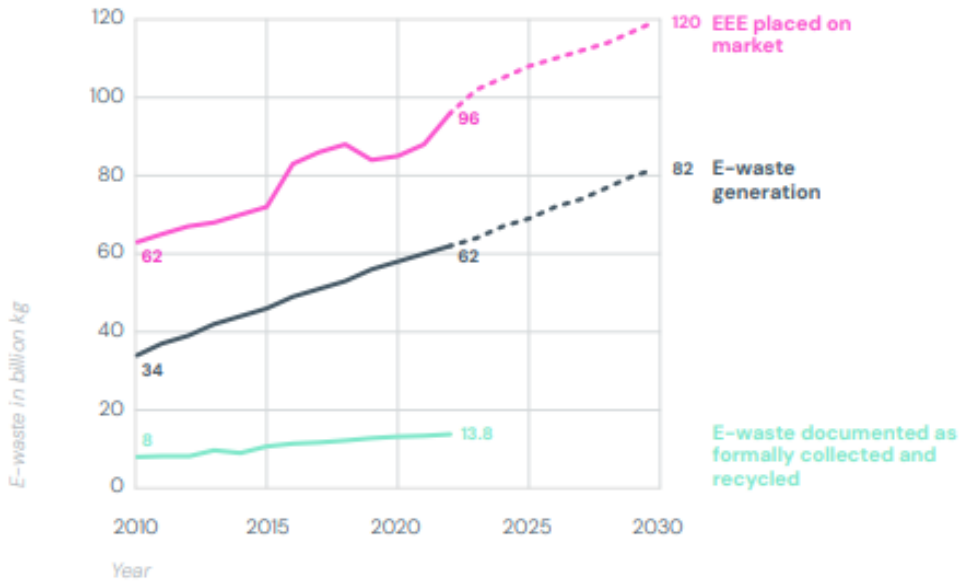

Figure 3.1: Trends of sold electronic and electrical devices, their wastes and their recycling[8](from 2010 to 2022 and forecast of the next years)

In the classification of electrical and electronic equipment (EEE) batteries and other electricity storage device are not included, because of a different end-of-life treatment, as well as for EEE installed in automotive apparatus, since not considered as stand-alone devices. While the considered EEE are:

- temperature exchange equipment
- screens and monitors
- lamps
- large equipment (e.g. washing machines)
- small equipment (e.g. vacuum cleaner)
- small it and communication equipment (e.g. mobiles)

WEEE are composed by many valuable materials, that can be recycled and therefore useful for fabrication of new devices. In fact the material composition is estimated to be made by 31 billion kg of metals (50% of the overall amount), 17 billion kg of plastics (27.4%) and the remaining 14 billion kg (22.6%) comprising other components, such as some alloys, composite materials, glass and concrete, or materials that could not yet be properly quantified in the datasets.
Recycling metals, including also semimetals, is important since they constitute the major part of EEE, hence, if they can be recycled, the related mining and extraction processes

can be significantly reduced. This is important to reduce GHGs emissions due to these processes and also the consecutive impact on the surrounding environment, through pollutant releasing and geological modifications.
This can be faced starting from the amount of needed materials for the production of 62 billion kg of EEE, and from the actual capabilities to recycle them, so from the net need of materials. Therefore the materials with both high and no-low recovery rates are listed in tables 3.3 and 3.4, respectively. The latter are critical raw material, so they are concerning also for the remaining available amount. In fact it is important to reduce the most as possible their demand.

Metal category (percentage of recovery)			Metal	E-waste amount
Total metals (60%)			Fe	24 billion kg
			Al	4 billion kg
			Cu	2 billion kg
			Ni	0.52 billion kg
	Other metals (4%)		Zn	280 million kg
			Pb	70 million kg
			Sn	44 million kg
			Co	34 million kg
			Sb	28 million kg
		Precious metals (20%)	Ag	1200 thousands kg
			Au	270 thousands kg
			Pd	121 thousands kg
			Bi	47 thousands kg
			Os	12 thousands kg
			Rh	5.1 thousands kg
			Pt	2.6 thousands kg
			Ir	0.6 thousands kg
			Ru	0.4 thousands kg

Table 3.3: Metals in e-waste with high recovery rates[8]

3.5 Critical raw material deployment

The urgent need of nullifying or reducing the carbon emissions asks for a further development of new technologies (batteries, electrical mobility, renewable energies and so on), which are based on certain material. Most of them are extracted in few regions of the world, both for availability and economical-historical reasons. In the case of Europe great part of the needed materials are supplied from outside, hence making it vulnerable to fluctuations of foreign markets and geopolitical decisions of other countries.
Therefore the European countries define periodically the list of these material of interest, also named Critical Raw Materials (CRMs), as shown in figure 3.2 for 2020. However in a global perspective this classification is still interesting to be considered, since the progress demanding them is in common with all the other countries, independently on the

Material	E-waste amount
Nd	7248 thousands kg
Y	1814 thousands kg
Dy	501 thousands kg
Pr	429 thousands kg
Ho	422 thousands kg
La	395 thousands kg
Ce	361 thousands kg
Re	357 thousands kg
Eu	277 thousands kg
Tb	133 thousands kg
Gd	97 thousands kg
Er	37 thousands kg
Sm	32 thousands kg
Li	6.1 thousands kg
Ge	5.3 thousands kg
Sc	2.2 thousands kg

Table 3.4: Critical raw materials in global e-waste with no or low recovery rates[8]

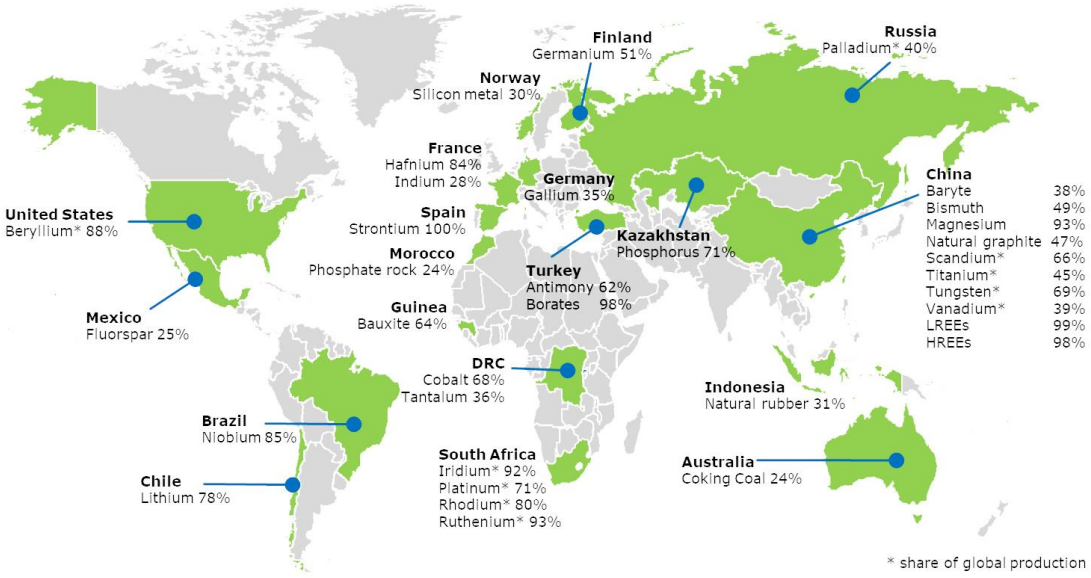

Figure 3.2: Biggest supplier countries of CRMs to the EU in 2020[12]

extracted amount of material. A comprehensive list of CRMs updated to 2020 is available at [12].
This puts concerns on the impacts related to the increasing demand of CRMs, and so to their mining:

- environmental impact,
- social impact,
- incoming scarcity of some of the materials.

3.5.1 Environmental impact

Mining in general can threaten the environment in several ways, from the modification on the surface lands, so exposing areas previously covered by vegetation, useful to keep stable the soil, up to the pollution. The latter can be caused by losses of the extracted materials (which could be heavy metals, radioactive materials, acidic compounds as sulfuric acid or other toxic substances) that can flow away from the mining site through the water used for the extraction or to cool down the equipment.
Furthermore mining is responsible for 4% to 7% of greenhouse gases emissions, because of the electricity and fuels employed for the equipment and the transportation needed to deliver the extracted materials[13].

3.5.2 Social impact

The pollution produced by extraction can endanger the nearby populations, but in addition to this they can be subjected to conflicts and labour exploitation at the basis of the control of these richness resources in regions not well developed economically. In fact in these areas the population is more vulnerable to exploitation since more exposed to lack of primary needs, pushing them to make work also children, often at expenses of their basic education. Example of this exploitation are child labour, violence and very poor safety rules registered in cobalt mines in the Democratic Republic of Congo[46].

3.5.3 Incoming scarcity of some of the CRMs

The increasing and continuing demand of minerals extraction is bringing mining to go deeper and explore new sites, this can be occur until the costs related to new excavations are economically sustainable for the mining company and the whole sector basing on them[22]. Therefore material scarcity is concerning for future generations development.

Chapter 4

Toward a more sustainable electronic

By looking at the environmental impact of the sector, the possible actions to mitigate it can be accounted. In fact the critical raw material issue together with the e-waste disposal ask for a proper choice of the materials, that still have to preserve the electronic performances of the state of art devices. Therefore materials that are easy to find and synthesize, rather than no polluting when disposed, are required.
Nonetheless, also the energy demand and the pollutant emissions have to be limited, and this can be done by selecting the proper fabrication processes, which can also affect the choice of the material to use.
All of these choices can be supported by means of an evaluation of the impact of the device over all its life: from the material extraction to the end of life treatment. A well known method is the Lifecycle Assessment (LCA). Indeed these concepts are those ones defining the world of the green electronics.

4.1 Transient electronics

Materials suitable to solve the e-waste problem are transient, being characterized by the property of self- degrading. Instead the problem of the critical raw materials is simpler while considering a novel technology, since they can be chosen taking into account their availability and often they coincide with not degradable materials.
Therefore the aim is to have devices the easily degrades in the environment, while being not harmful, even after degradation, hence going toward a transient electronics. Indeed the material has also to be not toxic, hence a useful property mentioned in literature is the biocompatibility, so the capability to not be harmful to the surrounding organisms. In fact many studies on biomedical applications works on transient electronics that has to be also biocompatible[11][10].
Instead regarding the degradation of a material, it is a complex phenomenon and in some case cannot be complete, at least within a period comparable to days,weeks or months. Indeed it is important to know how it occurs, and so what it is needed for a complete

degradation. According to Li et al. [36] the biodegradation mechanism occurs in three phases biodeterioration, biofragmentation and assimilation.

Biodeterioration

Occuring by means of abiotic factors, it consisits of mechanical, light, thermal and chemical degradations, where the materials go toward oxidation, hydrolysis or breaks in their crystalline structure.

Biofragmentation

It is due to both aerobic and anaerobic digestion. The fromer acts in shorter time than the second, producing higher volume mass, while the latter is responsible for methane production, so it can be exploited for green fuel production. Moreover many times it occurs together with biodeterioration.

Assimilation

Finally the by-products of the biofragmentation can be absorbed by microbial cells, going toward further chemical transformation, by means of metabolic pathways. The processed compounds are absorbed by the organism itself or other ones after expulsion.

Therefore the complete biodegradation is not trivial, in fact the possible degradation level can be defined as:

- Type I: the molecule or the material is fragmented in monomers and oligomers, which cannot be degraded naturally. This occurs because the difficulty of cleaving C-C bonds. Therefore the biodegradation is partial.
- Type II: the compound is completely disrupted into products that can be assimilated in nature.

Within these specification the materials for each functional part of an electronic device have to be found, so for electrodes, active region, dielectric, substrate and encapsulation. For this purpose some of the materials cited in literature are grouped in table 4.1. For electrodes typically metals are employed, even if sometimes in literature organic materials are considered as doped conjugated molecules (so with π bonding) or carbon nanotubes[36]. However these ones present not complete biodegradation or even toxicity where dimensions are in the nm range, so metals are preferable. Instead regarding metals some of them have to not be considered since toxic, such as lead, chromium and mercury[36], while other ones are not biodegradable(i.e. Ag, Pt and Cu). Regarding gold it is not biodegradable but it is edible, hence it can be included as transient material, but it is a critical raw and conflict material so it is also controversial. The remaining metals (e.g. Mg and Zn) as well as for some of their alloys, dissolves in water and are not toxic[36][11][30].
Active material can be either organic or inorganic. The latter are the conventional ones, so Si and Ge, but also metal oxides as ZnO and ternary oxides as ITO and FTO. Si and Ge are

commonly considered not biodegradable, but if they are enough thin (e.g. 100 nm, where the layer is called nanomembrane-NM) their dissolution time is within days or weeks. The same rules can be applied to the other mentioned materials. Moreover looking at the dissolution products of Si they are silicic acid $Si(OH)_4$ and protons[30][11], which are compounds naturally present in our body; the only issue is related to the dopant elements, but if present in very low concentration they should not cause any harmful effect. The same reasoning can be applied to silicon and magnesium oxides and nitrides considered as suitable transient insulating and incapsulating materials[10].
Instead organic materials can range from natural to synthetic ones. The former can be easily found in nature (e.g. β-carotene) and so are biodegradable, while the latter can degrade partially, having mostly a type I degradation, always because of C-C bonds difficult to cleave[36].
Regarding insulating and encapsulating materials, they can be organic too. In particular also in this case there are some natural or nature inspired, as well as for synthetic ones. Among the latter an interesting one is the poly(lactic-glycolic acid) PLGA made by polylactic acid (PLA) and polyglycolic acid (PGA), whose ratio determine the dissolution rate of the material[10].
Substrate materials are mainly organic materials, since the common silicon or in general inorganic substrate requires several centuries to biodegrade, as a consequence of thicknesses in the order of some 100 µm. Also in this case there are some natural or nature-inspired materials and other ones synthetic[30]. Indeed nature-inspired materials are those one that can be synthesized or processed from natural sources, but present structure similar to the present in nature (i.e. paper and indathrene yellow G, which is a derivative of natural anthraquinone)[36].
In general the differences between organic and inorganic materials consists of the easy of the deposition process (peculiar of organic materials) and the electrical performances (better in inorganic ones), where in case of organic materials flexible devices can be manufactured.
Furthermore, another useful consideration regards materials for RF electronics, where the commonly used inorganic semiconductor GaAs is toxic in the environment for the presence of arsenic, but its performances are higher than organic semiconductor and also than silicon. However a strong improvement from the biodegradability point of view is the deployment of biodegradable substrate (i.e. cellulose nanofibril,CNF, [29], therefore strongly reducing the amount of semiconductor material to the only needed one. This is the same concept applied when using Si as active material for transient electronics. In these cases common microfabrication techniques can be still applied, but the front end of line has to be screen printed onto the new substrate [29][30].

Finally dissolution rates and so the required time can be tuned by means of their dependency on temperature, pH and aggregation or deposition method, hence providing the capability to tune the lifetime of a device[61][10].

	Electrodes	Active material	Dielectric and Encapsulation	Substrate
Inorganic	Mg	Si	SiO_2	
	AZ31B	Ge	Si_3N_4	
	Zn	Si-Ge	MgO	
	Fe	ZnO		
	W	SnO_2		
	Mo	ITO		
		FTO		
Natural organic		β-carotene	Polysaccharides	Silk
		Indigo	Polypeptides	Cellulose and paper
		Indathrene yellow G		Chitin
		Indathrene brilliant orange RF		Shellac
		Furan-based		Collagen
		Melanin		
Synthetic organic	Carbon nanotube		PLGA	
	Polypyrrole(PPy)			Polycaprolactone (PCL)
	Polyaniline(PANI)			
	Polythiophene(PT)			
	PEDOT			
	PEDOT:PSS			

Table 4.1: Summary of main materials found in literature [30][36][11][10]

4.2 Green processing

The material choice has to be supported by a sustainable deposition, where solvents and a certain amount of energy are required and, consequently, some substances are released into the environment.
Indeed new deposition and synthesis methods have to be taken into account, with the aim to reduce energy demand and releasing of toxic substances, by using less solvents and substances that when released are not harmful to the environment[42]. Therefore the choices has to take into account the 12 principles of green chemistry, hence with the possibility that they can affect also the choice of the materials for a device.

4.3 Lifecycle Assessment

Together with all the considerations aforementioned, a method that can evaluate and compare different technologies in the same area of interest (e.g.solar cell, transistor for digital application and LED) can be useful to optimize the technology and to evaluate if it is satisfactory from the sustainability point of view.
A possible method is the lifecycle assessment (LCA), which provide a standardized method for this kind of evaluation, analyzing the environmental impact of a certain product over predefined stages of its life: raw material extraction, materials manufacture, product manufacture, use stage and end of life. In the various stages also the recycling, and reuse of the product or materials have to be taken into account. In particular this analysis is composed by 4 stages:

- **Goal and scope definition**: where the purpose of the assessment is defined (e.g., improving sustainability, comparing products), together with the life cycle stages included and the specific environmental impacts to be assessed (e.g. GHGs emissions, water demand, toxicity).
- **Inventory analysis**: where all the inputs, including energy, and outputs, so emissions and waste, in each stage of life are gathered in an inventory (Lifecycle inventory, LCI).
- **Impact assessment**: where the impact categories of interest are evaluated, basing on the contribution of each element present in the LCI.
- **Interpretation**: where the quantitative results are analyzed, in order to draw conclusions and eventually identify new strategies.

Part III

Theoretical and technological background

Chapter 5

Theoretical background

The sustainability analysis on C_{60} has to be supported by a study on the possibility to have a device based on it. In particular, as first step, it is important to study the metal-organic interface, with a selected metal (in our case it will be the Bismuth). This analysis can be performed through both virtual simulations of the structure and measurements of its properties. Thus, the theoretical basis of both the computation behind simulations and physics of the interface are shown subsequently.

5.1 Simulation

The virtual simulations, used to compute the properties of the structure under study, can be based on different computation methods: the *ab-initio* and the semi-empirical ones. The latter combines more accurate simulation results (i.e. *ab-initio*) and measurements, while the former is based on models describing the physical behavior, starting from the Schrödinger equations.
For our structure, based also on an organic material (in fact C_{60} contains 60 carbon atoms), the *ab-initio* method is taken into account and combined with the Linear Combination of Atomic Orbitals (LCAO) theory. In particular LCAO theory allows the definition of molecular orbitals (Ψ_α) through the linear combination of atomic orbitals (Φ_i), where each molecular orbital is defined by an eigenfunction, so a wavefunction solution of the Schrödinger equation:

$$\Psi_\alpha = \sum_i c_{\alpha i} \Phi_i$$

Another important distinction to take into account, before proceeding on, is the difference in physical models between the bulk of an inorganic materials and the bulk of organic ones. In particular the former have atoms covalently bonded, in a single crystal, allowing the wavefunction to be delocalized over the entire volume of the crystal. Instead, regarding organic crystals, the molecules are bonded each other through Van deer Waals forces, so wavefunction are confined[26].
Indeed this difference has effects on the physical modeling, which in case of inorganic bulks can be based on the Bloch theorem , due to the periodic potential in the crystalline

structure, which simplify the description. While for organic solid the outer electrons remain confined within the molecule volume, hence the electronic structure preserves that of an isolated molecule[26]. This difference motivates the choice of the aforementioned method and the subsequent described modeling.
As a result, the problem is a many body one (because of the many electrons and nuclei interacting each others), where all particles in the molecule and their mutual interactions have to be considered. It can be described by Schrödinger equation, :

$$\hat{H}\Psi = \epsilon\Psi$$

In general the Hamiltonian can be expressed as the sum of the kinetic energy and the potential energy of the electron, where the former is related to both nuclei particles and electrons, while the potential describes the nuclei-nuclei interaction V_{nn}, the nuclei-electron interaction V_{ne} and the electron-electron interaction V_{ee}.

$$\hat{H} = \hat{K} + \hat{V}$$

$$\hat{K} = \hat{K}_n + \hat{K}_e = -\sum_{j=1}^{Nn} \frac{\hbar^2}{2m_n}\Delta R_j - \sum_{i=1}^{Ne} \frac{\hbar^2}{2m_e}\Delta r_j$$

$$\hat{V} = V_{nn} + V_{ne} + V_{ee}$$

However this problem has too many variable that the solution cannot be found, in fact there is need of some simplification, in order to define a problem whose solution can be found [45]:

- **Tight binding approximation** : where inner electrons are considered tightly bounded to the nucleus, such that together with the nucleus they can be considered as an ion, while the remaining outer electrons are considered as valence ones.
- **Born-Oppenheimer approximation** : which considers the kinetic term of the nuclei and the nuclei-nuclei potential negligible, because of their substantially lower velocity with respect to electrons.

In this way the hamiltonian is reduced to :

$$\hat{H} = -\sum_{i=1}^{Ne} \frac{\hbar^2}{2m_e}\Delta r_j + V_{ne} + V_{ee}$$

Where V_{ne} describes the interaction of ions with electrons. However the V_{ee} term includes the interaction among each couple of electrons, so it can be simplified, describing it as the interaction of a single electron with a charge density. Thus the problem can be solved as one electron problem, if the charge density is considered unique independently on the electron, such that it can be added to the actual charge density. It can be possible by assuming that the charge difference introduce by a single electron is negligible with respect to the overall one. The resulting simplified model is the Hartree model, which moreover allows to define the overall wavefunction as the product of the single electron wavefunctions, thus significantly simplifying the calculation of the overall wavefunctions.

However this representation describes also the possibility of a self-interaction for the electron and it does not take into account the impossibility of two electron to be in the same place at the same time, repulsing each other. This can be considered by introducing another potential term, called exchange-correlation potential V_{XC}, hence taking into account the quantum mechanical properties of the electrons. This addition to the Hartree model defines the so-called Hartree-Fock model.
Moreover additional potential energy terms have to be considered in case of polarization of the molecule, both for electron cloud rearrangement (i.e. when the atom or molecule is nearby another one attracting or repulsing them), called pseudopotential, and for an external field applied (i.e. by means of an electrode)[64].

$$H = K + V_H + V_{XC} + V_{ext}$$

$$V_H = V_{ne} + V_{ee}$$

$$V_{ext} = V_{pseudo} + V_{gate}$$

Furthermore all the potentials can be defined through the electron density, which represent the probability of an electron to be found in a position of the space, independently on its energy. Therefore it can be a measure of the spatial charge density when multiplied by the electron charge. In particular it can be defined starting from the probability of finding each electron, so from their wavefunction.

$$n(\vec{r}) = \sum_i |\Psi_i(r)\vec{|}^2$$

This approach, at the basis of the density functional theory (DFT), helps to reduce the complexity of the problem, since the electron density is defined over 3 variables, while using wavefunctions as inputs, each of them depends on 4 coordinates, which have to be multiplied by the number of the electrons. The resulting hamiltonian is called Kohn-Shannon haimltonian.
However in this problem the electron density is still defined starting from the wavefunctions at the different energy levels, which are obtained through the solution of the Schrödinger equation, thus being a recursive problem. This can be solved by an iterative approach, in particular by the Self Consistent Field (SCF) method. It starts from an estimation of the potentials, from which the eigenfunctions Ψ_i and the eigenvalues E_i can be calculated. Afterwards they are used to defined the electron density, which determines the potentials, hence the eigenfuctions and the eigenvalues can be again calculated. This process is repeated until a certain tolerance has been respected.
Moreover in this solving procedure the eigenfunctions can be represented by means of a basis set with a finite number of basis functions, according to the LCAO theory.
Regarding the solution of this problem there is still an important issue: the relationship between the electron density and the potential energy cannot be defined. Therefore there should be estimations of them, which can be optimized depending on the wanted computing performances or accuracy and on the structure under study.
This working scheme lays behind the *ab-initio* method taken into account, where, in particular, the eigenfunctions are represented by means of the atomic orbitals, according to the LCAO theory. As a result of the aforementioned considerations, in order to

perform a simulation, there's need to define the pseudopotential, the basis set5055, the exchange-correlation potential and the Hartree potential, in an optimal way depending on the situation[64]. The latter in particular is computed considering that it is defined by the charge distribution, so it can be obtained through the Poisson equation:

$$\nabla^2 V_H[n(\vec{r})] = -\frac{e^2}{4\pi\epsilon_0} n(\vec{r})$$

Indeed here the second order differential equation can be solved by different methods and starting from different boundary conditions (needed to fix the solution), depending on the optimal choice for the case under study.

5.2 Surface and interface physics

Regarding the measurements methods in this discussion they are mostly related to the surface and are also intended to evaluate the behavior at the interface. Therefore it could be useful to introduce some concepts of the physics at the surface and interfaces, rather than the conduction in nanodevices, where the active region is represented by one or few molecules.
In particular, regarding the surface, it is important to compare the behavior of the material here with respect to the bulk, hence the bandstructure and the density of states (DOS) are properties useful for this comparison, and also for the behavior at the interface. Indeed the bandstructure identify the ranges of energies, which can and cannot be occupied by the electrons. The ranges of energies, or bands, are not singular energy levels, but a group of close energy levels that are shifted with respect to the lone atom energy levels, in order to not be superimposed. This occur because of the Pauli's exclusion principle, where electrons cannot have the same quantum numbers, including the spin.
This concepts is at the basis of the Density of States (DOS), which describes the number of electronic states per unit of volume and energy. From the DOS the number of occupied states can be obtained by multiplying it with a occupation distribution function (i.e. the Fermi-Dirac distribution). From here the valence band (or HOMO in case of a molecule) and conduction band (or LUMO) can be extracted, since they are the highest occupied energy level (or electronic state) and the lowest unoccupied one.
Finally the work function is another important parameter, which describes the difference between the vacuum and the Fermi energy levels, where the former coincides to the energy of a free electron (so without the influence of the nearby material) and the latter defines the occupation of the states, being the center of the Fermi-Dirac function.
Once known these parameter, useful to define the band diagram and to study the behavior at the interface, it is important to assess the difference occurring at the surface and at the interface.

5.2.1 Surface

The abrupt change in the potential energy, due to the transition from the material to the vacuum, causes the wavefunction to be extended into the vacuum side. In fact the

probability of having an electron in the vacuum near the surface is not null.
As a result there's a negative charge in the vacuum nearby the surface, which results from a partial depletion of electron at the surface of the material, hence creating an electrical dipole. Its strength can be also influenced by the crystallographic orientation. Therefore the presence of this dipole has effects on the work function, which change on the surface with respect to the bulk, and can differ depending on the crystallographic orientation[26].

5.2.2 Interface

The behavior at the surface is at the basis of what happens at the interface in fact the extension of the wavefunction out of the border of the materials from both sides cause a rearrangement of the electrons and the dipoles. This can be described by two phenomenons: Pauli pushback effect and screening effect.
The former describes the behavior of the metal surface over which a molecule is physisorbed. In particular the molecule and the metal electrons repulse each other modifying the dipole at the metal surface. As a result the metal work function at the surface diminishes.
Instead the screening effect describes the orbital rearrangement due to the presence of the metal surface inducing a reduction of the HOMO-LUMO gap, which is the equivalent of the bandgap for inorganic bulk materials.
Moreover in addition to this electronic structure modification the way the energy levels are aligned can favour the motion of electrons toward either the metal or the molecule. As a result the lack of an electron in the molecule shifts its energy spectrum (or the DOS) toward lower energy levels, contrary to what happen to a gain of an electron. Therefore this charge transfer can allow to a new energy alignment that favour another charge transfer, occurring until an equilibrium has been reached.
Going back to the energy spectrum modifications at the interface, they tends to vanish in favour of the bulk behavior while increasing the distance from the interface. However the distance needed for reaching the bulk conditions varies depending in the dielectric constants, the difference between the bulk vacuum levels of the two materials (known as built-in potential) and the density of electrons[26].

5.2.3 Conduction at nanoscale

Generally the conduction in a material between two electrodes occurs when electrons can move toward lower energy along the path from one electrode to the other one. This occur when there are energy levels of the active material between the two Fermi levels of the electrodes.
The energy levels distribution is represented by the density of states. However when the active material is within the dimensions of nanometers, and especially when it is characterized by only one molecule, the transmission of electrons, throughout it, it is influenced by the interaction electrode-molecule, also known as coupling. In particular a stronger coupling enhances the conduction, or more specifically reduces the time needed to an electron to move from the electrode to the molecule.
Therefore at each energy level the possibility of electrons to move throughout the molecule

is described by the transmission spectrum. Indeed it quantify the possibility of an electron to move from the source electrode to the drain one, where the source is considered as the electrode where the lowest voltage is applied, when it is positive. Furthermore the possibility of a transition depends on the available energy levels per energy, hence on the density of states.
As a result the current caused by a voltage applied between source and drain, can be described as the integration over the energy of the transmission spectrum multiplied by the difference between the two Fermi distribution at the two electrodes. Where the transmission spectrum is defined by the coupling coefficients γ defined per each energy levels and the DOS distribution.

$$I_{DS} = \frac{2q}{\hbar} \int_{-\infty}^{+\infty} T(E)[f(E, E_{FS}) - f(E, E_{FD})]dE$$

$$T(E) = \sum_i \pi \frac{\gamma_{i,S}\gamma_{i,D}}{\gamma_{i,S} + \gamma_{i,D}} DOS(E)$$

Chapter 6

Technological background

The comprehension of the experimental setup is important in order to have the possibility to have reproducible study and also to understand possible non idealities that can occur. In particular the device has been fabricated by thermal physical vapor deposition and afterwards analyzed by means of several methods in order to study the surface and interface behavior of such structure: atomic and scanning Kelvin probe force microscopy, photoelectron spectroscopy and impedance spectroscopy.

6.1 Physical Vapor Deposition(PVD)

The physical vapor deposition here adopted is based on the thermal evaporation of the material that has to be deposited in high vacuum conditions (from 10^{-3} to 10^{-7} mbar). The PVD system under use included a crucible, the sample holder, a quartz microbalance and a shutter.

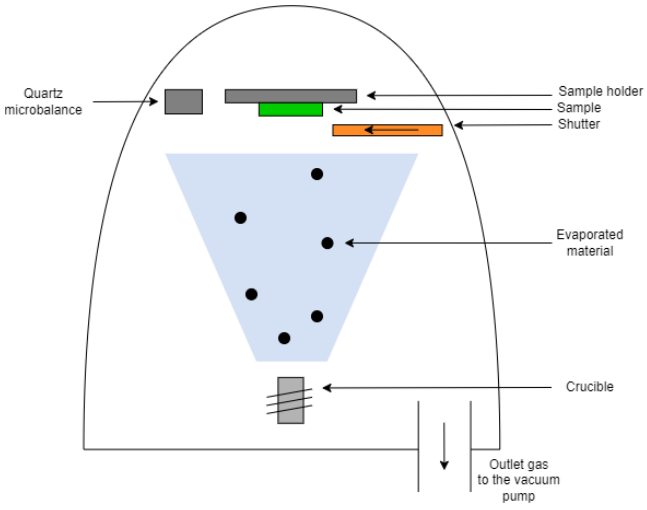

(a) Scheme of a vacuum deposition system

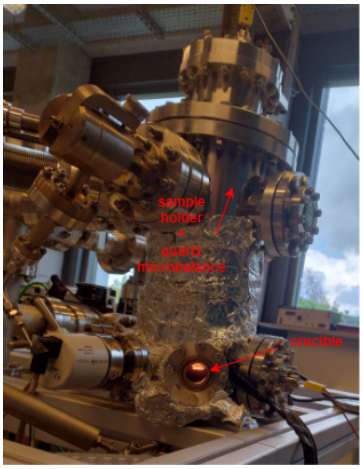

(b) Structure of the used deposition system

Crucible

Placed at the bottom of the chamber, it contains the material to evaporate and is heated up by a resistive filament wound around it, while its temperature is sensed by a termocouple placed nearby.

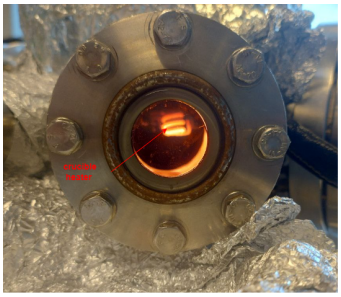

Figure 6.2: Crucible and its heater

Shutter

Above the crucible (in the case of the Bismuth deposition system, while below the sample holder in case of the C_{60} deposition system) there is the shutter, which is useful to stop the flux of evaporated material, hence stopping the deposition. Indeed the evaporation cannot be stopped instantaneously, so there is need of an external control to stop the deposition.

Sample holder

At the top of the chamber, it holds the sample where the evaporated material has to be deposited. It has to feature to be heated up, by a separated heater, while the temperature is sensed by a termocouple on the holder itself. As a consequence, the external heating system asks to periodically rotate the holder in order to have a uniform heating of the sample.

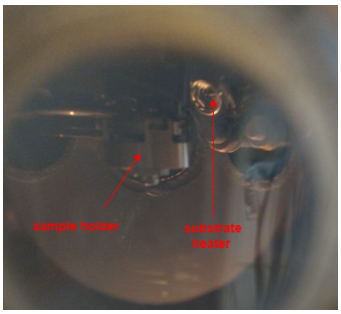

Figure 6.3: Sample holder and its heater

Quartz microbalance

The thickness of the deposited material can be monitored during deposition. In particular it occurs by means of the quartz microbalance, which is a quartz crystal resonator, whose resonance frequency varies depending on the amount of material deposited on it. Therefore, if place close to the sample the thickness of deposited material is the same, hence it can be known by means of the relation between shift in the resonance frequency and deposited thickness.

The deposition procedure requires some precautions, in order to obtain a well organized deposited structure. It can be obtained through a slow deposition process, especially in case of organic materials, because of the Van der Waals bonding instead of covalent one and of larger dimensions, with respect to inorganic materials (which can have higher deposition rates). In fact if the deposition rate increase too much there is need to stop the deposition by closing the shutter, decreasing the crucible temperature until the wanted deposition rate has been reached, after which the deposition can be resumed. Further help to the crystalline organization can be provided by substrate heating, but in this case careful should be given to the reached temperature, which can enhance another crystalline organizations above certain thresholds or damaging the material if too high.
In particular, the deposition rate is influenced by temperature of the crucible and pressure in vacuum chamber, which depends on the amount of evaporated material, hence on the temperature too. Thus the temperature has to be controlled by means of the power applied to the resistive heater. Examples of the deposition parameters regards the material deposited in this study (i.e. C_{60} and Bi) represented in table 6.1.

	Temperature (°C)	Deposition rate (Å s^{-1})	Pressure (mbar)
C_{60}	270	0.03	6×10^{-7}
Bi	375	0.15	7.5×10^{-8}

Table 6.1: Mean values for deposition parameter present in the used vacuum systems

6.2 Atomic Force Microscopy (AFM)

Atomic Force Microscopy (AFM) is a method to investigate the topography of a surface, by measuring the height at the points scanned on the area of interest, hence belonging to the scanning probe microscopy class. The height is measured by the electrostatic interaction between the probing tip and the sample at the investigated position.
In particular the system is composed by a tip attached to a cantilever, which deflects depending on the interaction tip-sample, so if it is more or less attractive (or repulsive, depending on the working mode). The deflection of the cantilever is a measure of the height of the sample, hence it is measured by a laser ray impinging over the cantilever, close to the tip position, indeed where the deflection is higher. The reflected ray is then

collected by a photodiode. The monitoring of the shifts of the ray with respect to an initial point on the photodetector indicates the deflection of the cantilever. As a result the feedback system acts in order to bring the cantilever to the starting conditions (deflection or amplitude and phase oscillation) by changing the height of the cantilever itself. Therefore this procedure is repeat for each point scanned by the AFM, belonging to the area under study. Moreover the scanning is performed twice on the same row, in order to have a control of a correct scanning settings, which in the opposite case can cause artifacts in the obtained topographic image.

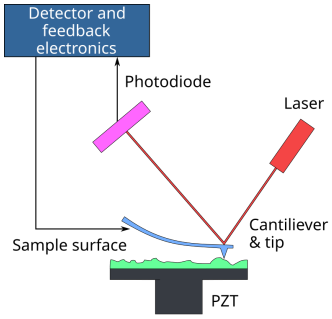

Figure 6.4: Scheme of AFM working principle

Regarding the electrostatic interaction between the tip and sample it can be either attractive or repulsive, depending on the distance from the surface, but still being within 10 nm distance. In this distance range two main electrostatic forces occur:

- **Repulsive interaction forces**: it is due to Pauli's exclusion principle for which two electron clouds cannot superimpose, hence the tip cannot reach distance 0 nm.
- **Van der Waals forces**: they originates from the interaction between the dipoles formed at the sample and tip surfaces.

In particular getting closer to the surface the repulsive force become dominants, against being at a moderate distance, even if still within 10 nm, where Van der Waals forces become more important. Such behavior dependent on the distance is well describe by a picture taken from [66].

Depending on the distance of the tip from the surface different working modes for the AFM exist: Contact mode, Tapping mode and Non-Contact mode.

Contact mode

The tip works in the repulsive region, where changes in height of the sample correspond to changes in force applied to the cantilever, hence to a greater or lower deflection, with respect to the starting one. This difference encodes the height difference with respect to the initial conditions.
In this case the tip works statically: it preserve the same position if there are no changes in the height.

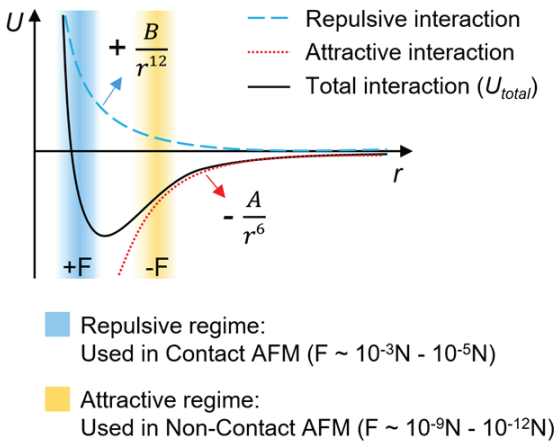

Figure 6.5: Forces acting close to the surface

Tapping mode

Instead with this working mode the tip oscillates moving within both the repulsive region and the attractive one, hence working in a dynamic mode. The oscillating frequency is close to the resonance one, as a result when the tip is subject more to repulsive forces, rather than attractive ones, the natural frequency changes. This is reflected to the oscillation amplitude, since the oscillating frequency is controlled by the system. Indeed the cantilever has a resonator frequency response , hence, if the device works at the same frequency but its natural frequency shifts, the amplitude will vary depending on the slope of the frequency response and the amount of the shift, as shown in figure 6.6 (taken from [65]).

Non-contact mode

In the two previous modes there is a tip-sample contact, against to the non-contact mode in which the tip work in the Van der Waals forces region. However without looking at the distance difference with respect to the tapping mode, the operative mode is the same, hence with an oscillating cantilever whose amplitude and phase changes are evaluated for determining the sample height.

Among the discussed working modes the best results to be the Non-Contact mode, since the close contact with the surface can cause damage to both the sample and the tip. In fact in case of damage the spatial resolution and the accuracy decreases, hence the Non-Contact mode is the used one.

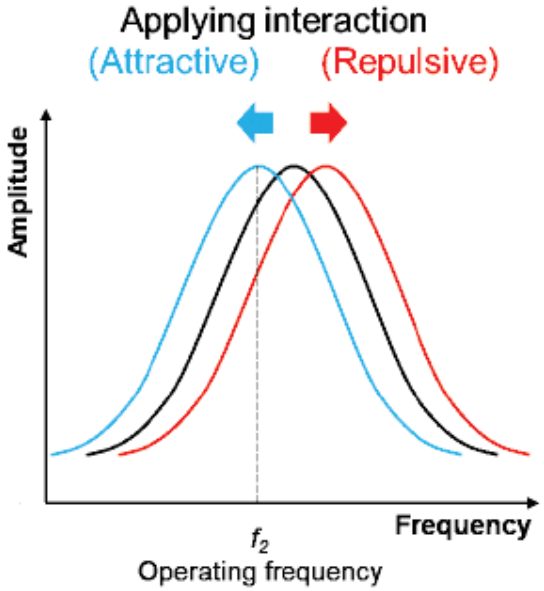

Figure 6.6: Frequency shifts due to interaction forces

6.2.1 Data analysis

After the measure has been completed, the obtained topographic image could need to have some post-processing, in order to remove some unexpected behavior of the structure under study (e.g. an inclination of the sample substrate, that it is not present in the deposited structure) or to extract useful information (e.g. roughness).

6.3 Scanning Kelvin Probe Force Microscopy (SKPFM)

The scanning probe microscopy idea can be used also to analyse the surface potential. Indeed the surface can have different potentials on different positions, depending mainly on the crystalline organization and the presence of different materials. Thus they cause a charge distribution over the surface, reflected by the different potentials.
A figure of the potential over the surface can be obtained by applying a voltage to the tip and looking at its interaction with the electrostatic field produced by the surface charges. Their influence is dominant at a distance further than the one where Van der Waals forces are dominant (i.e. electrostatic forces can be sensed even at 1 µm distance). Thus the scanning is performed twice: the first time in Non-Contact mode for topography measurement at the Van der Waals distance, while the second time the scanning is performed at higher distance to only sense the electrostatic forces. In particular they deflect the cantilever as all the other aforementioned forces.

This the operation mode describes the Electrical Force Microscopy, but the procedure can be speed up by acquiring both signals of height and potential during the same scanning. In fact by adding a lock-in amplifier to the system, it can control an AC voltage

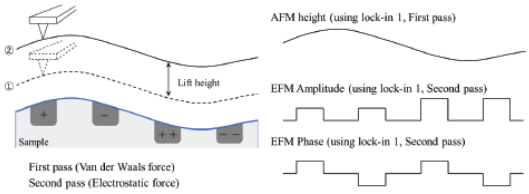

Figure 6.7: Electrical force microscopy

V_{AC}, in addition to the bias one V_{DC} and the cantilever oscillation one. In particular the latter is needed to control the height of the tip, through the feedback system internal to the microscope.
As a result there are 2 AC voltages applied: one related to the cantilever oscillation and the other one to the polarization of the tip. Thus the two AC voltages have to be at frequency far each other, such that they can be filtered. In fact the polarization voltage applied to the tip is:

$$V_{applied}(t) = V_{DC} + V_{AC} sin(\omega t)$$

Instead the voltage difference with the surface, which determine the electrostatic force acting on the tip, is:

$$V(t) = V_{DC} - V_{surface} + V_{AC} sin(\omega t)$$

The resulting electrostatic force can be expressed by means of the distance d tip to the sample and the capacitance C present among the two. This can allow a clear view of the frequency components of the signal obtained from the electrostatic forces.

$$F = qE = q\frac{V}{d} = C\frac{V^2}{d}, \qquad \text{q = unit charge} \qquad \text{E = electric field}$$

$$\begin{aligned} F(t) = \frac{C}{d}V(t)^2 = \frac{C}{d}[(V_{DC} - V_{surface})^2 + \frac{1}{2}V_{AC}^2] \\ +2\frac{C}{d}(V_{DC} - V_{surface})V_{AC} sin(\omega t)] \\ -\frac{1}{2}\frac{C}{d}V_{AC}^2 cos(2\omega t) \end{aligned}$$

Therefore the expression of the force can be decomposed in a DC component, ω and 2ω components. In the case of scanning Kelvin probe force microscopy (SKPFM) the ω component is taken into account and the bias voltage is varied in order to be equivalent to the surface potential, thus nullifying the term.
Actually the applied bias voltage has to take into account the difference between the surface and the tip work function. In fact when the tip and the sample surface are far each other their energy levels are aligned by the vacuum level. Instead when connecting the sample to the tip, they are aligned by the Fermi levels, in order to have the same distribution of electron around the same energy. Thus electrons must flows from the side with higher Fermi level toward the other side, hence creating a charge difference, for the

depletion or accumulation at the surfaces, which characterizes a difference in the vacuum levels between the tip and the sample surface, called contact potential difference (CPD). Therefore such potential difference can be nullified by applying a proper voltage V_{CPD} between the two sides.

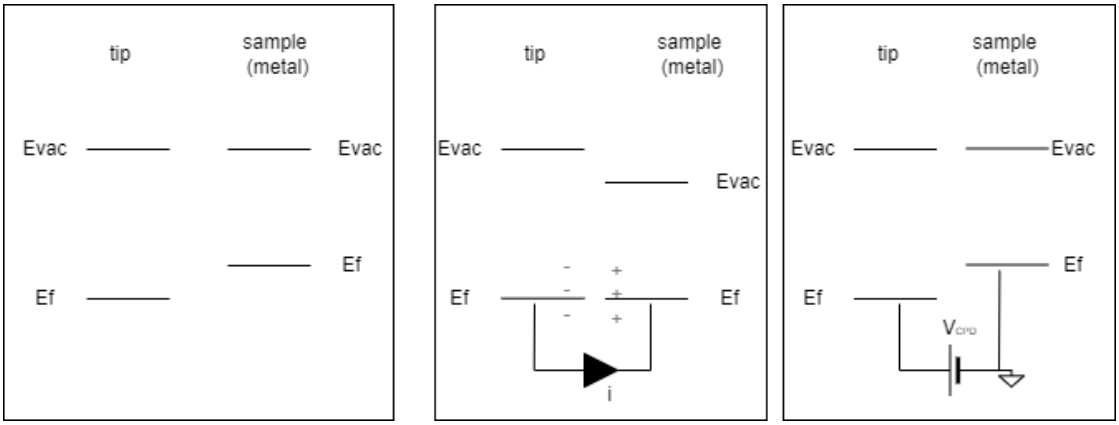

Figure 6.8: Interaction between the tip and the sample, in case of electrical isolation, connection and a voltage applied between them (from left to the right).

As a consequence, in order to obtain the surface work function (see equation 6.1), there is need to know the tip one, which usually is not specified by the manufacturer, hence requires a calibration procedure (see equation 6.2) based on a reference material.

$$\Phi_{Sample} = \Phi_{Tip} + eV_{CPD} \tag{6.1}$$

$$\Phi_{Tip} = \Phi_{Reference} - eV_{CPD} \tag{6.2}$$

Furthermore, the applied voltage use as reference the sample, so there is need of an electrical connection with the sample in a proper place, in order to guarantee the Fermi level alignment between the tip and the surface of the sample. In fact in our study, 2 electrical connections were performed in order to know the most suitable for the structure under study.

6.4 Photoelectron spectroscopy

Photoelectron spectroscopies are spectroscopy methods based on the photoelectric effect, hence they are useful to derive the energy spectrum of a material by means of electron emission after an excitation, caused by an incident photon. In particular they are X-ray and ultraviolet ray photoelectron spectroscopy, also known as XPS and UPS, respectively. The former is based on high energy photon rays (typically above 1000 eV)[63], in fact it can excite the core electrons of a material, so those ones closer to the nuclei (e.g. the ones residing in the orbital 1s).Therefore it is useful to evaluate the chemical state of the material under study and can provides information about other properties (e.g. crystalline

organization and charging). Instead the UPS, adopting rays with energy below 50 eV[63], is suited for analysing the outermost electrons, hence the valence ones. As a result it is useful to extract both the work function and the distance of the conduction band (or HOMO, depending on the material nature) from the Fermi level.

6.4.1 Instrument setup

The instrument setups to perform such measurements are equivalent except for the ray source, in fact both XPS and UPS are performed in the same system. Thus the discussion will be focused on the XPS measurement setup and then the differences with respect to the UPS will be shown.
The X-ray source is created through an electron gun emitting electrons toward the anode emitting photons as a consequence. The wavelength of the emitted photons depends on the anode material, for instance the mostly common Mg and Al emit photons at 1253.6 eV and 1486.6 eV[63], respectively. However is some cases (i.e. Mg anode) there could be a further less intense emission line, which affects the measurement, or also there could be need to reduce the linewidth. These two issues can be solved by introducing a filter of the emission spectrum (called monocromator), based on the diffraction mechanism.
Therefore the x-rays generated by the anode, are filtered through the monocromator and afterward hit the sample surface, with the selected energy hν. Here for the photoelectric effect electrons gain energy, hence are promoted to higher energy levels or if the energy is sufficiently high can leave the surface. In particular the energy required for an electron to leave the surface, from a certain energy level, has to be higher than the sum of the binding energy (BE, indeed the energy required to move to the highest energy level) and the work function of the material (Φ_{sample}, indeed the minimum energy needed to eject an electron from the surface). The eventual remaining energy characterizes the kinetic energy of the travelling electron $KE_{surface}$, if there no energy loss during the path toward the outermost part of the surface[63].

$$h\nu = BE + \Phi_{sample} + KE_{surface}$$

Afterward the electrons have to be collected and their kinetic energy has to be measured, in order to extract the binding energy, hence the energy spectrum. Detectors useful to gather the electrons are typically electron multipliers[63]. However high kinetic energies worsen the accuracy of the detectors, in fact, during the path from the sample surface to the detectors, extraction lenses are present, in order to slow down electron[63]. Further improvements on the accuracy can be done by analyzing a small part of the energy spectrum, and this can occur through a filtering system realized by a concentric hemispherical analyzer, taking into account the most common solution. In particular, in this kind of analyzer, the voltages select the electrons by their kinetic energy (the resulting range is called pass energy): the outer hemisphere is more negative than the inner one, as a result electrons with higher energy tend to collide to the outer side, contrary to those ones with lower energy tending to collide with the inner one. Indeed electrons going out from the extraction lenses pass throughout this polarized path, where the pass energy is selected by means of the applied voltages, reaching at the end the detectors.
One important issue in this measurement is the unknown work function of the sample,

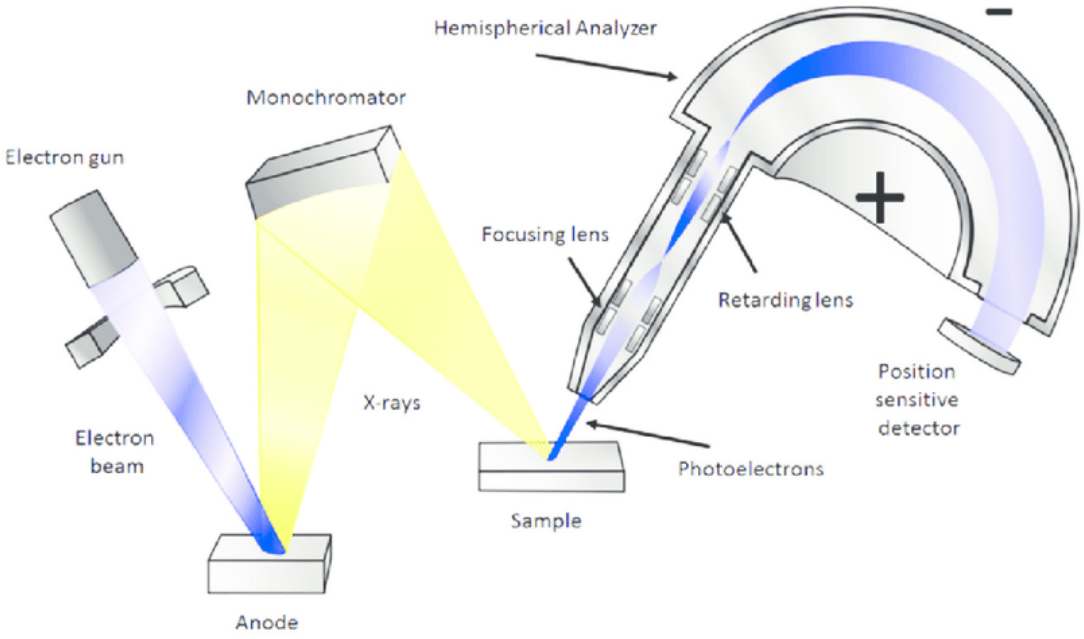

Figure 6.9: Schematic representation of an XPS system.

which should be measured by the method itself. This issue can be solved by electrically connecting the sample surface with the detector. In fact the energy levels are consequently aligned and the electron preserve its energy, hence when reaching the detector, the kinetic energy will differ by the same amount of work function difference such that:

$$BE = h\nu - \Phi_{spectrometer} + KE_{measured}$$

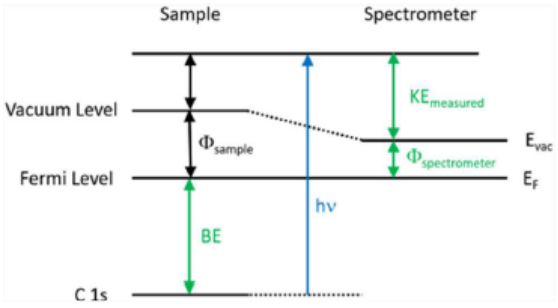

Figure 6.10: Band diagram of sample surface and spectrometer when electrically connected[63]

Furthermore the measurement has to be conducted in ultra high vacuum conditions (i.e. pressure below 10×10^{-8}mbar), because of possible scattering of electrons with free

molecules in the atmosphere and of physiosorption of contaminant particles, which can alter the surface properties of the sample under study.
Finally, regarding UPS measurements, the source is based on He and provides two emitted spectral lines at 21.2 eV and 40.8 eV.

6.4.2 XPS

In the XPS measurements the peak position provide information on the elements and the related orbitals , since each element has a unique spectrum. However the picture of the energy spectrum often is not so obvious, since there are multiple components contributing to the peak or it can be found at energy slightly shifted with respect to the one expected from the lone atom. Thus a short review of the possible components contributing to the spectrum is shown below[63], with the aim to introduce the reader to the possible issues present in this kind of analysis, leaving more detailed considerations to the references found in literature[63][39][60]:

- **Background signal**: photons can excite electrons far from the surface several nanometers, but when they acquire enough energy to escape from the surface they have to travel throughout the material up to the surface. In this path electrons can collide with other electrons and nuclei loosing energy. Thus, when reaching the surface, their kinetic energy is lower than the one they would have if emitted directly at the surface. In fact they result to have higher binding energy and as a consequence at binding energies higher the the actual one they contribute to the so called background signal. This component does not provide any information about the chemical and physical state of the material, hence it has to be subtracted to the spectrum in order to properly fit and estimate meaningful components. Indeed it can be estimated by several methods, among which the most common is the Shirley one[63].

- **Chemical environment**:elements in a material are bounded each other also through covalent bounds, sometimes causing hybridization of s and p orbitals[63]. Thus the rearrangement of atomic orbitals, characterizes another component shifted with respect to the expected one. For instance in a single covalent bond of a carbon and an oxygen atoms the electrons resulted to be more attracted toward the oxygen, since it has higher electronegativity. Thus the carbon atom has a partial positive charge, because of a partial lack of these electrons closer to the oxygen, hence carbon electrons have higher binding energy. The values of these shifts are usually summarized in proper databases[73][62].

- **Doublets due to spin-orbit coupling**: spin-orbit coupling is a relativistic effect caused by the interaction of the electron motion and its spin into an electric field. This interaction causes different contribution to the hamiltonian, hence to the energy, which can be visible in XPS by means of the splitting of spectral lines associated to the same orbital, except to those ones related to the s orbitals where this effect is not present. In fact the spin-orbit coupling is at the base of the fine structure[63].

- **Asymmetric peak shape**: in metals the lineshape in the XPS spectrum can be asymmetric, with a tail toward higher binding energies. This occurs because there are many unfilled state just above the Fermi level, hence some electrons can be excited to these states by the emitted electrons, which as a result lose energy. Thus the measured binding energy is higher[63].
- **Shake-up peaks**: similarly to what happens for metals, in other cases valence electrons can be excited toward higher states (e.g. from π to $\pi*$ orbital), resulting in an energy loss equal to this transition. As a result some peaks at higher binding energies than the expected one are present[63].
- **Shake-off peaks**: the phenomenon at its basis is the same of shake-up peaks, but in this case the valence electrons acquire enough energy to escape from the surface[63].
- **Satellite peaks**: in case of a non-monochromatic X-ray source, the emission spectrum can present a secondary line, with a certain shift from the main one. Thus a peak with the same shift can be visible in the XPS spectrum, if it is not covered by the main peak. In fact this artifact can be removed by adopting a monochromator[63].
- **Excitation of plasmons**: another loss, in metals, can occur through the excitation of plasmons[63].
- **Multiplet splitting**: there could be a presence, especially in transition metals, of further peaks due to the presence of multiple final states, in presence of unpaired electrons. This results in a further unexpected peak splitting[39].
- **Full width half maximum(FWHM)**: the broadening of peaks can depend on several factor, starting from the instrument contribution through the extraction lenses and the spectrometer, up to the linewidth of the X-ray source and to the lifetime of core holes, rather than x-ray damage and different charging among different places in the surface.[39]

Moreover there are two further issues to take into account while fitting the XPS spectrum, which are not directly related to the material properties, but have influences on the XPS spectrum:

- **Adventitious carbon**: surfaces, unless in ultra high vacuum conditions, are strongly subjected to physiosorption of compounds present in the atmosphere, so especially if the sample has spent some time out of the vacuum system. These compounds are usually of organic nature, but they cannot be defined clearly, since they depends on the surrounding environmental conditions, which cannot be taken under control. Thus in the energy spectrum there could be a carbon peak even if the sample does not contain compounds carbon-based. However these carbon species have been shown to be not graphitic [73] and the common chemical bonding are summarize in literature[73], as well as for other element bonding.
- **Charging**: in some cases the electrical connection of the sample with the instrumentation, as previously seen, is not enough to introduce all the electrons that has

been emitted, especially in insulator materials. Thus a positive charge starts to accumulate and electrons have more difficulty to escape from the surface, subsequently to photon excitation, hence they show have higher binding energy. In fact in these cases the peaks are shifted, and as reference, usually, carbon peak is taken into account[63].

Finally XPS can be useful to determine the stoichiometry of the surface under analysis. However the atomic concentration cannot be obtained by direct comparison of peak areas, but they have to be divided by a proper sensitivity factor (also called RSF), specific for each transition. Thus the obtained value can be compared to the other ones in order to obtain its concentration[63].
Furthermore, this procedure is convenient to be performed on the survey spectra, the energy spectrum measured over all the possible energy range (from a binding energy equal to the x-ray source energy up to 0 eV).

6.4.3 UPS

Instead regarding UPS measurements work function and ionization potential can be measured. In particular the measured spectrum can be defined both in terms of kinetic and binding energy, as already seen for XPS measurement their relationship.
Talking about the binding energy, the reference value equals to 0 eV and coincides with the Fermi level, hence in case of a bandgap and , more specifically, a difference between the Fermi and the HOMO level (or conduction band) there is no electron emitted from this energy range. As a result in these energies the measure will be null.
While going toward deeper energy levels, that are occupied by electrons, those ones start to be stimulated and emitted with a certain kinetic energy, until the ultraviolet rays (in our case with energy equal to 21.2 eV have enough energy to stimulate electrons to escape. This occurs when the binding energy and the work function together start to be higher than the incoming UV-rays.
Consequently to these considerations the energy spectrum taken out from the measurement extend over an energy range equal to $h\nu - \Phi - (E_F - HOMO)$, and close to the Fermi level the difference $E_F - HOMO$ can be found. Thus toward the highest energies the work function Φ can be measured, where both energy range can be seen by the proximity to 0 counts per second of the measured spectrum (as shown in picture 6.11a).
Moreover for organic materials it can be possible to observe the highest occupied energy levels (i.e. HOMO, HOMO-1 and so on), by means of the peaks present in the region of the spectrum close to the Fermi level (as shown in picture 6.11b).

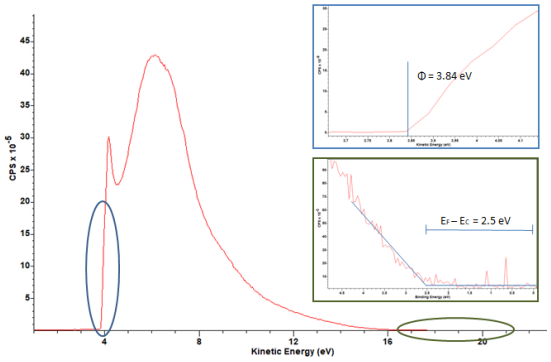

(a) UPS measurement of Bismuth, with native oxide top layer

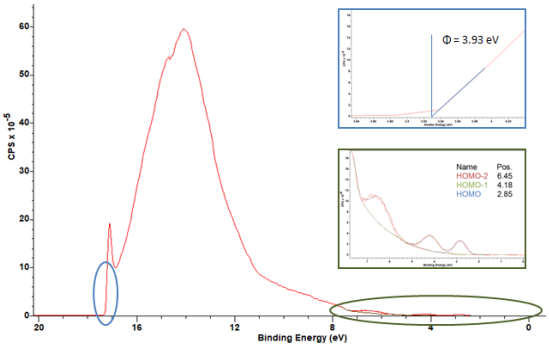

(b) UPS measurement of C_{60}

Part IV

Sustainability evaluation

Chapter 7

Sustainability evaluation

The evaluation here conducted wants to follow the concepts of LCA (LifeCycle Assessment analysis), without taking into account its rules. In particular the analysis wants to be a so called cradle-to-grave one, hence looking at:

- the material extraction;
- the material manufacture;
- the product manufacture;
- the use of the product (so the energy required to work and eventual wastes);
- the end of life, so the disposal of the product, hence also the recyclability of the wastes or its biodegradation.

For each of these stages it is important to consider the input (so materials and required energy) and the wastes, looking also at their possibility to be recycled or degraded in nature, without negatively affecting it.
Therefore the proposed method follows these requirements aforementioned, while having the perspective of the choice of the material to use for an electronic device.
Indeed the material is evaluated at first for its toxicity and degradation, in order to look at first at the capability to be disposed in a non polluting way (or most likely less polluting). Then, looking at the synthesis and the deposition of the material, the focus is both on the energy required and the emissions and the liquid and solid residuals of the process. Moreover in these two stages even the residuals and emissions should be evaluated by the toxicity and disposal or effect on the environment, as already done for the material of interest. Finally the usage of the device can be evaluated by its power consumption and lifetime.

7.1 Environmental compatibility

The environmental compatibility is intended in the meaning of the disposal, in particular with the aim to not have any residual material after the end of life.
In detail toxicity, degradation mechanisms and by-products bio-absorbability are taken into account.

7.1.1 Toxicity

Toxicity is mostly evaluated by the worst case scenario in a qualitative way, by looking at the possible effect that it could cause on human(or mammals) body and environment. While, wherever it is possible to have it, a useful quantitative indicator is LD50 (Lethal Dose 50%), where it is indicated the amount of substances that provided to the assay (in vitro cells or in vivo animals) causes the death of half of the population under study. However it is important if there are inflammatory responses in the body, that in the long term could compromise the health of the assay.

7.1.2 Degradation mechanisms

The degradation possibilities of the material are important to target the best way of disposal of it. Where a good disposal is intended to be the one whose wastes can perfectly integrate with the nature being part in the biogeochemical cycles of the nature, without polluting the environment.
Therefore among the possibilities we can find two groups: biodegradation mechanisms and other methods.

Biodegradation mechanisms

In this case it is expected that the material decomposes by means of reaction that occur in the natural environment, which could be the oxidation, the mechanical work due to erosion and fracture or the inclusion in metabolic pathways. In this last case the study become much more complicated because it should consider several species if in open environment or in case of controlled close environment it can consider just one species (e.g. in the case of larval eating plastics [14]).
In this scenario it is important to consider that the residual of the biodegradation should not be toxic at their time, hence they could be used in some metabolic pathways. Indeed the inclusion in some metabolic pathways, without any compromising effect to the species digesting it, is the ideal case where the substance can be released safely in nature.

Other methods

Other methods of degradation can be pyrolysis, combustion and use of reagents. In these case it is important to evaluate whether they can be useful to produce some energy (in case of combustion and pyrolysis) and the emission and the residuals of the process. Moreover the energy required for the process is an important parameter.

7.1.3 By-products bioabsorability

Once the degradation mechanisms occurred there are some residuals and they should be integrated perfectly in the natural cycles, as already in the biodegradation section. Otherwise their toxicity has to be evaluated.

7.1.4 Further useful analysis: Recyclability

Moreover in this scheme as an alternative path to the disposal is important to consider the recyclability, so the possibility to collect the material from the fabricated device and the percentage of collected material with respect to the present one, rather than the energy and the wastes involved in the recycling process. However this analysis has not been conducted on the chosen material.

7.2 Synthesis

The synthesis of a material is characterized by several processes that have an impact on the environment:

- extraction of the raw material, it occurs mostly mechanically (e.g. in case of fullerenes tetralin extraction);
- conversion of the raw material (e.g. in case of fullerenes tetralin pyrolysis to generate soot);
- separation of the material of interest from other species, by means of solvents, filters or other processes.

Each of these step can include the use of energy ad solvents, and can cause some emissions, which could be GHGs, pollutants or not dangerous ones. So for each of the released substances its environmental impact has to be evaluated according to section 7.1.

7.3 Deposition method

Also the deposition has similar issues to the synthesis, in particular there are several methods for depositing a material on a surface, where there could be need of some solvents or a lot of energy, with also some emissions due to possible wastes or evaporation of the solvents themselves. In fact the deposition is a process that has to be optimize to reduce the overall impact of a product.

7.4 Device power consumption

Finally the device power consumption is another important quantity to know. In an electronic device, in this case a transistor the contributions to this are given by the dynamic and static power consumption.

Moreover also the lifetime of the product is important to be estimated, since a greater working time for the product will ask for less production of it, so less impact on the environment.

7.5 Further considerations

Looking at this scheme it lacks of the definition of some quantitative parameter measuring the impact of each section. Moreover it is important to have a database where all the sustainability information on solvents and materials are contained within in order to facilitate such evaluation (this feature is already contained in some LCA tools).
Therefore some aspects will not be evaluated in detail hereinafter.

Chapter 8

Fullerenes

8.1 Environmental compatibility

In this section the

8.1.1 Toxicity

Toxicity studies show results in contrast each other, ranging from proofs of toxicity (for instance through the death or inflammatory response in the assay) to the non-toxicity or even anti-inflammatory response[27][28][40].
However, for a final evaluation, only the toxic response of C_{60} will be taken as reference point, as evidence of toxicity of this material. While the other results discussed in literature will be taken into account to consider which could be the possible causes of a different interaction with biological systems.
Moreover it has to be noted that the studies cited in the analyzed reviews[27][28][40] have different conditions, which could be the causes of a different biological response to the presence of the fullerenes, that have been analyzed in separate manner. So summarizing, the possible aspects that can affect the toxicity are:

- **exposure to light**, which excites the fullerenes to a state that reacting with the oxygen, that at its time it is excited to a state (singlet state[27]) that is very reactive, so enhancing oxidation reactions in the assay. So even the presence of oxygen is fundamental, but it is assumed as a natural condition in biological systems.
- the **dose of exposure**
- **time of exposure**
- **derivatization of the fullerene or the fullerene species**, which can affect the solubility, so the diffusion into the biological system, or the capabilities to react.
- **preparation of the fullerene solution**. Indeed if not properly derivatized fullerene are not soluble so there are some other options to create a solution: "solvent to water

exchange" protocol (through the use of a solvent that is later eliminated by evaporation), dispersion into a solvent(most likely organic one) and mixing for an extended period with water (e.g. by sonication). The creation of a solution is fundamental in order to make the fullerenes be absorbed by the biological species. In these cases the residual of solvent is important, beacause it can be the cause of toxicity.

- **dimensions of the aggregate**, where the direct consequence is the active surface area. So a smaller aggregate have larger area capable to react with surrounding species.

Furthermore the main cause the toxicity has been found to be the production of reactive oxygen species (the so called ROS) by means of fullerenes (or its derivatives) presence. As a result from several studies on aquatic animals (which could have a different toxicological response with respect to other animal and not species)[40] it has been found a LC50 mean value of around 5 ppm for sonicated C_{60} (or with diameter below 0.45 µm) and around 400 ppb for filtered solution (where the filtered C_{60} aggregates are expected to be smaller). Instead regarding the mammals cells (i.e. rats) the fullerenes are excreted by means of feces and urines, while the remaining part accumulates into the body, mainly into the liver (81.6% of whole accumulated C_{60})[27].

8.1.2 Degradation mechanism

8.1.3 By products bio-absorbability

8.2 Fullerene synthesis

The fullerenes synthesis has been analyzed basing on a previous LCA (LifeCycle Assessment) study, focused on the energetical point of view. Here the focus tries to be also on the wastes created during the process through some estimations. In particular it can be divided into 2 steps.
The first one is the creation of a soot which is partially constituted by many kinds of fullerenes (C60,C70,and other higher order ones), together with other carbon species. The soot can be also defined as carbon black, so this suggest that the remaining compounds can be used as carbon black (for instance in supercapacitors applications). It can be produced by means of toluene or tetralin combustion and also by radiofrequency or arc plasma with graphite as feedstock (so consisting in a vaporization of graphite by electric arc)[5].
The second step is the extraction of the fullerene of interest from the soot, followed by purification steps in order to obtain a high purity material (99.5% or >99.9% of C60). The extraction and purification is based on the different solubility in organic solvent of the fullerenes with respect to the other compounds present in the soot and also among the different species of fullerenes.
Then there could be even a functionalization procedure, which is not of our interest.
In this concept the quantitative energetic evaluation is strictly based on the values found by Anctil et al.[5], while the focus will be on the byproducts of the whole process and their amount (whether it can be estimated quantitatively).

8.2.1 Soot synthesis

Soot synthesis methods have been analyzed through an LCA approach by [5], comparing them by the energetic demand for the whole synthesis process, from the raw material (toluene and tetralin for pyrolysis methods and graphite for arc and RF plasma techniques) to the purification and functionalization of the fullerenes. So for our purpose we start with the results obtained in this study and shown clearly in a graph reported by them.

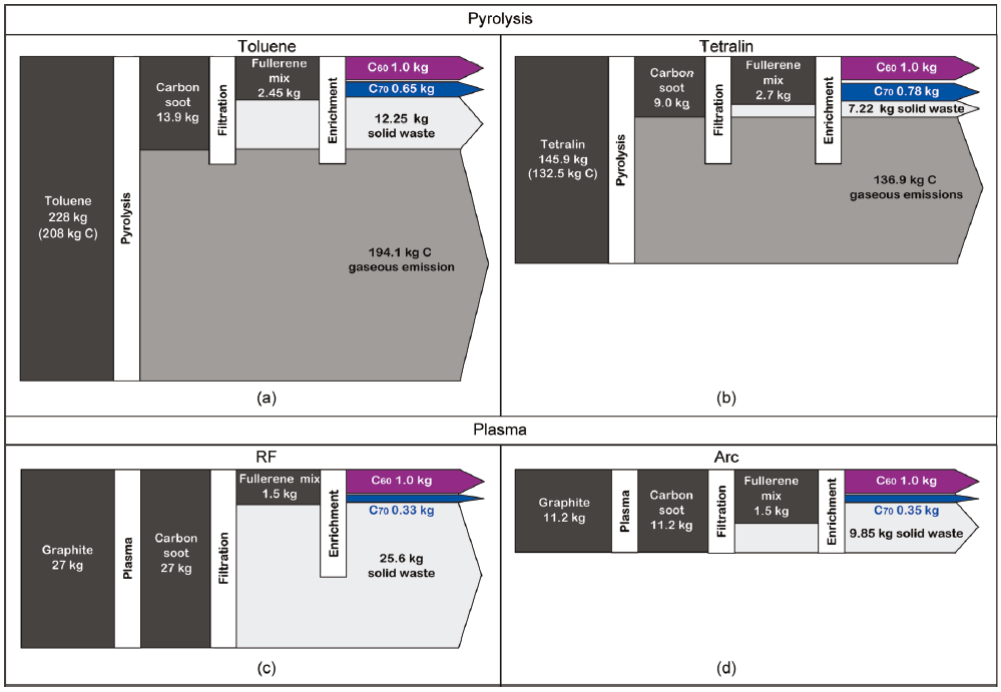

Material flow for the four synthesis methods (a) pyro-toluene, (b) pyro-tetralin, (c) RF plasma, and (d) arc plasma.

Figure 8.1: Energetic comparison and raw material need for each synthesis process (picture taken from [5])

The energetic comparison suggests the tetralin pyrolysis as the most efficient method to obtain 1 kg of C_{60}. However the pyrolysis methods (both toluene and tetralin based) produce a large amount of carbon based gaseous emissions, not present in RF and arc plasma methods, while these last one have larger solid waste, but it has to be evaluated how this wastes can be reused, if possible. Indeed there's need to study the gaseous emissions and the recyclability of the solid wastes.
Regarding gaseous emissions, the evaluation starts from the conditions at which the tetralin combustion occurs to obtain an optimum yield for fullerene production. From there we can determine which are the products of the combustion reaction. Indeed the tetralin pyrolysis requires the following conditions[4] to obtain the maximum fullerene yield (2.03%, with the respect to the fuel, while 30% with respect of the soot, whose 40% made up by C_{60} ones):

- $\phi = 2.8$, where ϕ is the equivalence ratio defined as $\phi = \frac{\frac{n^{fuel}_{hydrocarbon}}{n_{O_2}}{}^{fuel}}{\frac{n^{stoichiometric}_{hydrocarbon}}{n_{O_2}}{}^{stoichiometric}}$.

  Indeed it indicates how much hydrocarbons is contained in excess with respect to the stoichiometric relation, involving a complete combustion.

- $T = 1920\,°C$, referring to the adiabatic flame temperature, so the temperature at constant volume (no work) of an ideal gas.

- $C/O = 1.08$, where it represents the ratio between carbon atoms and oxygen ones.

- $P = 40\,\text{Torr}$.

In these conditions there is no study in literature on the tetralin combustion to our knowledge, in particular the closest environment[37] is characterized by T =1127 °C, $\phi = 1.5$, P =1 atm and 1000ppm of tetralin concentration, highly diluted by N_2, with a residence time in the reactor of 0.1 s. In fact the detected compounds (as shown in the supporting informations) can be an indication of which substances can be emitted in a pyrolysis based fullerene synthesis.

mols of products	tetralin			
	1000ppm	145.9Kg	m. mass(kg/mol)	CO2eq(kg)
CO	5.91E-03	6.52E+03		
O2	2.98E-03	3.29E+03		
H2	1.50E-03	1.66E+03		
CO2	9.26E-04	1.02E+03	1.00E-03	1.02E+00
C2H2	7.54E-04	8.32E+02		
CH4	2.81E-04	3.10E+02	0.016043	7.75E+00
C2H4	1.58E-04	1.74E+02		
C6H6	6.41E-05	7.07E+01		
C10H8	3.93E-05	4.34E+01		
CH2O	2.23E-05	2.46E+01		
toluene	1.62E-05	1.79E+01		
PHIC2H (Phtalic acid)	1.45E-05	1.60E+01		
indene	1.35E-05	1.49E+01		
C4H4	1.20E-05	1.32E+01		
PC3H4	1.09E-05	1.20E+01		
C2H6	8.69E-06	9.59E+00		
CPD (cyclopentadiene)	6.81E-06	7.52E+00		
AC3H4	6.67E-06	7.36E+00		
styrene	3.18E-06	3.51E+00		
benzofuran	1.71E-06	1.89E+00		
EtBenzen	4.56E-07	5.03E-01		

The detected compound are many hydrocarbons (whose toxicity has to be evaluated) and the most common oxygen, carbon monoxide (whose toxicity is well known), hydrogen,

carbon dioxide and methane. Considering as GHGs CO_2 and CH_4 an estimation of the CO_{2eq} can be performed by considering 28 as global warming potential (GWP) over a 100 year period [1], obtaining 8.77 kg for 1 kg of C_{60} production, assuming to use 145.9 kg of tetralin. However this is still far from the actual scenario, due to the different ambient condition and an unknown residence time into the reactor. We can expect to have a better combustion at higher temperatures, with more simple hydrocarbons and carbon oxides, at expenses of more complex hydrocarbons.

8.2.2 Purification

The purification process instead consists of many steps, which can change depending on the methodology and on the purity needed. The procedure starts by separating the whole fullerenes family from the other species constituting the carbon soot[31][18], which can contain species such as amorphous carbon,impurities of polycondensed aromatic hydrocarbons and multilayer carbon nanotubes. It is based on the different solubility of fullerenes into a certain organic solvent, with respect to the other species present in the soot.
Indeed, following the procedure indicated by Grushko et al.[18], the soot is mixed with the organic solvent (e.g. toluene or o-xylene) and then stirred at 2-3 revolutions per second. The fullerenes well dissolved into the solvent will pass throughout the filter, while the other carbon species not well soluble will be retained by the filter.
The results of this step is what we define from here on fullerene mix, from which the fullerenes of interest (C_{60} in this study case) have to be separated from the other species, reaching the desired purity. For the electronic grade C_{60} the best condition is the highest purity as possible, so the target should be a purity >99.9%, but in this study the amount of solvent and energy required are estimated for a target purity >99.5%.
This final separation can occur through several methods, some of them are:

- chromatography [18], where the different solubilities of the different fullerenes (C_{60}, C_{70} and higher order ones) are traduced into a different elution times. In the application under study the C_{60} has to have higher solubility in the chosen solvent with respect to the other fullerenes in the same solvent.

- crystallization [31], through the use of crystallizers and solidliquid separators, and basing on the dependency of the solubility of the fullerene mix in the solvent on the temperature, hence exploiting different temperatures to supersaturate the solution and obtain the solid phase of the desired fullerene. So the differences between fullerenes (C60,C70 and so on) in solubility with respect to the temperature allow the solid precipitation of only one species. In order to obtain the desired purity the solution undergoes throughout different steps of crystallization, even with different temperatures, such that the solubility can be tuned at the best to obtain a precipitation.

- complexation [20], based on the tuning of the solubility of the different fullerene species by means of a compound who can selectively react with all the species with the exception of C_{60}, in order to make them precipitate, while leaving the C_{60} still dissolved into the solvent. In this way it can be filtered out and then crystallized through the use of another chemical (isopropanol[20]).

In this scenario Heidari et al.[20] compared the three different methodology stating the complexation as the best one, basing on a quantitative approach for the evaluation.
Despite this, in order to obtain detailed informations also on the amount of solvents (and eventually complexant agents) the Grushko's studies[18] seem to be more comprehensive, so it is the one this study will focus on. However the other two methods are useful to be known in order to find and evaluate at whole the best process, for the environmental

point of view.

Quantitive informations

The quantitative informations about the chromatographic process come from the detailed study of the process, which starts with a carbon black produced by electric arc evaporation and can be divided into three sections and will lead to a 99.5% purity C_{60}:

- extraction of fullerenes from the carbon black, also called fullerene black (FB)
- enrichment of the extract by fractional concentration
- production of pure C_{60} fullerene by means of flash cromatography

In this scenario it has to be noticed the soot is not produced by means of tetralin pyrolysis so the percentage of fullerenes on the overall soot are different, possibly causing different efficiencies for the same process, in terms of purification steps or cycles and amount of solvent needed. Indeed the soot under discussion from now on consist of meanly 7 wt% of fullerenes (where wt% refers to the mass percentage), at their time divided into 65-88 wt% C_{60}, 12-30 wt% C_{70} and 1-5 wt%$C_{n>70}$. While for the pyrolysis based soot the percentage of C_{60} is stated to be around 40%. However for quantitative evaluation this differences have been neglected, accounting the first stage of purification to lead to the same concentration results. Moreover the differences in molar weight between C_{60} and C_{70} have been considered negligible for sake of simplicity in the percentage considerations. Indeed with these assumptions an estimation of the overall fullerenes mass can be obtained, by considering the input mixture containing 7 wt% of fullerenes species, divided at their time into 75.5% of C_{60}, 24.3% of C_{70} and the remaining for higher order fullerenes (where these values have been taken from the output of the first purification step, considering that it cannot influence the fullerenes proportions). Consequently, considering the input mass of 1 kg of fullerene black, the mass of C_{60} and C_{70} are respectively 52.85 g and 17 g.

Extraction of fullerenes The starting fullerene black can be purified by non-fullerene species through its better solubility into the solvent. It has to guarantee an high solubility of fullerenes, low boiling point, low fire and explosion hazard, low toxicity and low cost. A good solvent is the o-xylene, where the C_{60} and C_{70} solubilities at 25 °C are respectively 8-10 and 15 $\mathrm{g\,L^{-1}}$. Hence the extraction process consists of stirring, through a mechanical stirrer at 2-3 revolution per second, so dissolving the fullerene black into the o-xylene. Then the solution is filtered under 5 $\mathrm{kg\,cm^{-2}}$ of N_2 pressure, producing the fullerenes rich solution and a deposit of carbon black (so the fullerene black with very low content of them) and the solvent. Finally this remaining solvent is partially recovered by a vacuum evaporator, as well as for the fullerene rich solution. The entire process is repeated 3 times, requiring $\mathrm{kg}_{FB_{soot}}$, whose 9% is irrecoverably lost (so around 0.99 $\mathrm{L\,kg^{-1}}$). While the efficiency of the extraction process is stated to be around 92-95%, so a good assumption can be considering that the 93% of the fullerenes present in the starting fullerene

black have been collected, obtaining the so called fullerene mix.

Fractional concentration In this stage the fullerene mix contains still an high percentage of different species (around 75.5% of C_{60} and 24.3% of C_{70}), such that it is not suitable for the electronic grade applications. Hence a further purification is needed and, in particular, the cromatography could be the first solution, but in order to make the sorbent life time the longer as possible, there's need of a further purification step.
As a consequence there's need of enriching the extract by means of fractional concentration, reaching a 96% C_{60} rich solution. It consists of dissolving the previously obtained fullerene mix into o-xylene up to 85 °C until a saturated solution is formed and then filtering the latter on a vacuum filter at the same temperature, so obtaining a C_{60} rich deposit and a C_{70} rich filtered solution. The chosen dissolution temperature and filtration guarantees a better dissolution of C_{70}(21.8 mg mL^{-1} at 80 °C) and a worse for C_{60} (4.4 mg mL^{-1} at 80 °C)[3], in this way the solution is easily C_{60} saturated allowing its deposit onto the filter.
This process undergoes 3 cycles in order to reach a final composition of $C_{60}O$ 2.2 wt%, C_{60} 94.9 wt% and C_{70} 2.9 wt%. The 3 cycles products are shown in the table below (basing on the work of Grushko et al.[18]), where the deposit is used as input for the following cycles, while the filtrate is the waste of the filtering. However the latter can be included at its time into the cycles, in order to improve the efficiency of the process.

cycle		deposit		filtrate	
		C60 (%)	C70 (%)	C60 (%)	C70 (%)
1	% w.r.t start	79.50%		79.50%	20.50%
	partial % w.r.t input	87	13	31.4	68.6
	partial % w.r.t start	69.1	10.3	6.4	14.3
2	% w.r.t start	66.30%		13.2% (100%-66.3%-20.5%)	
	partial % w.r.t input	92	8	75.4	24.6
	partial % w.r.t start	60.996	5.3	9.95	3.247
3	% w.r.t start	79.50%		5.50%	
	partial % w.r.t input	96.7	3.3	84.6	15.4
	partial % w.r.t start	58.79	2	4.65	0.847

Table 8.1: Fractional enrichment

cycle	input mass (g)	solubility (mL/g)	solvent required (L)
1	70	10	0.7
2	55.65	19	1.06
3	46.41	15	0.7

Table 8.2: Fractional enrichment: input and output

The required solvent has been estimated to be 2.5 L, where also in this case it can

be recovered through the vacuum evaporation, for which a possible estimation on the losses can be the same obtained for the extraction process, so 9% of loss (corresponding to 0.225 L). While regarding the final deposit (whose mass is 60.8% of the starting one) consists by its 96.7% of C_{60}, so they are 78% of the starting C_{60} fullerenes.
In order to decrease the loss of fullerenes, the filtrate from the 2^{nd} and the 3^{rd} cycles, which contain >75.4% of C_{60} concentration, can be included in the 1^{st} cycles of another enrichment procedure. Indeed it can be seen that the amount of C_{60} contained in both filtrates of the 2^{nd} and the 3^{rd} cycles is 14.6% of the starting ones. So , taking into account that the percentage of C_{60} deposit at the end of the enrichment procedure is 78% of the starting amount (as it happens to the deposit), than the added amount that can be obtained by reusing the filtrates is 11.4%. As result the obtained C_{60} is 89.4% of the starting ones, by using this recycling procedure which does not need of further filtration steps, if included in those ones of a new fullerene mix batch.

Flash cromatography The obtained C_{60} powder pure at 96% needs a further purification, that can be done by means of chromatography.
This process consists of separating the components of mixture(called *analyte*), dissolved into a fluid solvent (called *mobile phase* or *eluent*), by means of their different retention time into the stationary phase, so the time they need to pass throughout the whole stationary phase. So the setup of chromatography consists in a column in which the stationary phase has been placed at the bottom, while it is fed at the top by the dissolved mixture. Then the latter flows into the stationary phase , where the separation occurs, and the filtered solution is kept at the bottom of the column.
In the this study, following the results obtained by grushko e t al.[18], the cromatography method is the flash chromatography, which speeds up the purification process by means of an increase of pressure, with respect to the ambient one.
The solvent used is the o-xylene, due to its previous use and good C_{60} solubility (around $9\,\mathrm{g\,L^{-1}}$ at 25 °C), while the stationary phase is activated carbon.
Hence the saturated solution of C_{60} is supplied at a velocity of around$0.45\,\mathrm{mL\,min^{-1}\,cm^{-2}}$, until 0.1% of C_{70} is present at the output solution. Then the stationary phase has to be washed with the solvent untill the C_{60} concentration does not exceed $0.2\,\mathrm{g\,L^{-1}}$. Moreover the solid phase of the purified and filtered out materials can be obtained as before by means of vacuum evaporation.
The yield of the process is around 75%, while the remaining C_{60} are irrecoverably loss (15%) or being part of a material whose C_{70} concentration exceed 0.5%, which can be recycled by running it into the previous processes, but here it won't be considered. While the C_{60} purity is around 99.5%.
Nonetheless the solvent usage can be estimated, by means of the C_{60} solubility and its weight (46.2 g, so amounting to 5.1 L, without considering the washing of the cromatographic column. Assuming an irrecoverable loss of 9%, as for the previous steps, in the recycling process, the stated loss amount to 0.462 L.

Overall results The analysis can estimated the overall efficiency (62.3%) and the overall o-xylene loss (1.68 L), in order to obtain 34.6 g of C_{60} in a 99.5% pure mixture, from 1 $kg_{FB_{soot}}$. Indeed, a more complete overview can be provided by the following table. Furthermore among the wastes there are also carbon black, resulting from all the wastes

	IN				OUT			
	C_{60}	C_{70}	others	o-xylene(L)	C_{60}	C_{70}	others	o-xylene (loss)
extraction	52.85 g	17 g	898 g	11 L	52.85 g	17 g	-	0.99 L
enrichment	52.85 g	17 g	-	2.5	46.177 g	1.41 g	1.07 g	0.225
flash crom.	46.177 g	1.41 g	1.07 g	5.13	34.6 g	-	-	0.462

Table 8.3: Input and output for each purification step

of the filtered substances of each purification step, and the activated carbon, after it cannot be used anymore in the chromatographic column.
Moreover part of these processes can be included in the production line of C_{70}, dividing part of the environmental impact into 2 materials.

8.3 Deposition methods

8.3.1 Power consumption of its deposition

In order to evaluate the energy consumption needed by a technology based on fullerene, a case study is the one later analyzed whose structure will be the following.

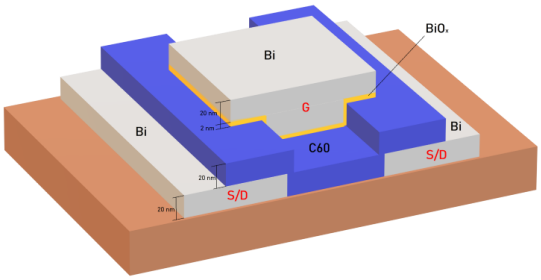

Figure 8.2: 3D model of the transistor

Hence an estimation of the possible fabrication steps can be done basing of what done to fabricate it in laboratory (as it can be seen in chapter 10). Indeed they can be the following ones (even if they do not represent an optimized solution, for instance the first problem could be the alignment of the gate with respect to the source and drain electrodes):

1 : masking of the Source and Drain electrodes, so a photoresist deposition and a subsequent photolithography are needed.

2 : deposition of Source and Drain electrodes, by means of thermal physical vapor deposition and a subsequent removal of photoresist.

3 : masking of the active area (photoresist deposition and photolithography are required).

4 : deposition of the active material C_{60} and photoresist removal.

5 : masking of the gate electrode (photoresist deposition and photolithography are required).

6 : deposition of the gate oxide and gate electrode. Indeed the first deposition of Bi (2 nm thick) is followed by exposure to the air in order to oxidize it, followed by the Bi deposition for the gate electrode. Finally the photoresist removal is needed.

- : afterward there would be needed a passivation of the overall structure and the creation of contacts to connect the Front end of line (FEOL) with the upper interconnection layers, but in this case study they are not analyzed.

In this framework also the photoresist deposition and the photolithography are not analyzed, since the masking has been done manually.
Indeed the analysis will be focused on the energy consumption of the 3 needed depositions, for which the current and the voltage applied to the crucible and to the substrate heating system (only for the Source and Drain deposition) have been considered.
Moreover the pumping system power consumption has to be evaluated. In particular the PVD system includes 2 chambers (connected each other, one for the storage and the other one for the deposition), each of them requiring two pumps, the turbomolecular and the backend ones.In addition to the pumps, there's also the chiller which distribute water at 20 °C to the pumps, in order to cool them. The schematic of the deposition system for the Bi is represented in picture 8.3. However the schematic and the values of power consumption are considered to be valid also for the C_{60} deposition.

Therefore, in order to estimate the power consumption of a deposition system the data on the power provided to the crucible have been taken (as it can be seen from pictures 8.4a,8.4b and 8.5b), starting from the voltage and current coming from the power supply.

Instead regarding the remaining part of the system (pumps and chiller, since the fans are considered to be negligible in power consumption) the power consumption is summarized in table 8.4.

Moreover, regarding the working time of the system, it requires around 6 h to be both started up and turned off.
However this analysis has to be compared to other similar one on fabrication processes, hence it can be considered at a laboratory scale or at an industrial one. The former one is simple since it has to be considered only the process regarding the fabrication of only one sample. The latter is much more complicated because needs to have an entire production line been designed (as mentioned at the start of this section). Therefore the analysis here conducted is intended to be compared with other fabrication processes at laboratory scale,

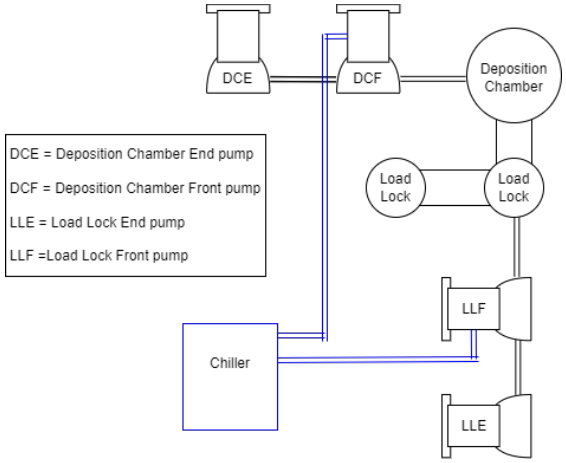

Figure 8.3: Schematic of UHV deposition system

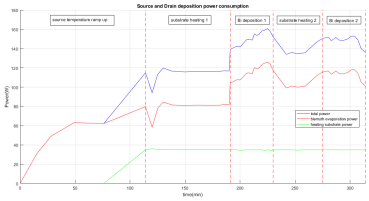

(a) Source and Drain deposition power consumption

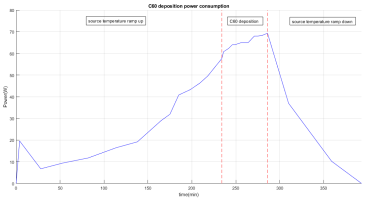

(b) C_{60} deposition power consumption

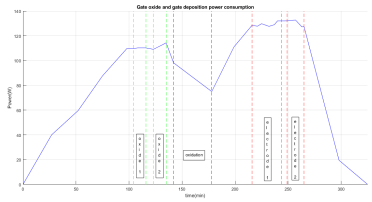

(c) Gate oxide and gate deposition power consumption

assuming they could be a good indicator of what could happen at large scale(i.e. in a proportional way).
Therefore, following the first kind of analysis, the deposition of Bi occurred on the two samples in two different time intervals, so the part of time used for the deposition of the second sample has to be neglected, as shown in figures 8.5a and 8.5b, and summarized in table 8.5. As a consequence the overall time is 28 h, with an overall power consumption of 300 MJ (with 171.3 MJ and 128.7 MJ corresponding to the deposition time and the on and off time of the system).

device	power (W)	device
LLF	100	Agilent TV 81M
LLE	483	Agilent SH-100 Dry Scroll Vacuum Pump
DCF	233	Turbovac 450i and Turbo Power 800100V0003
DCE Isolation valve	7.5	VPI251205060
DCE pump	1035	Varian PTS03001UVPIEU
chiller	1120	S&A CW-6000AI
tot	2978.5	

Table 8.4: Power consumption of all the deposition steps

deposition step	energy consumption (MJ)	time required(min)	power consumption (W
Source and Drain	1.40	294 (242 + 52)	96.7
C_{60}	0.68	393	28.98
Gate oxide and Gate	1.22	273	74.77
tot	3.3	960	57.29

Table 8.5: Power consumption of all the deposition steps (where the C_{60} deposition time is characterized by the registered 242 min and 52 min for reaching starting conditions, so no power to the heater

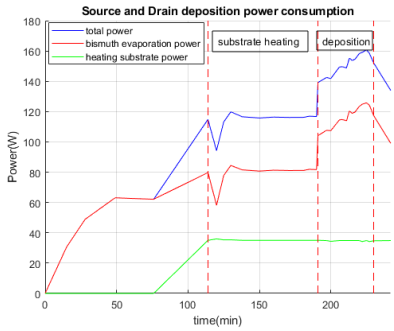

(a) Source and Drain deposition power consumption estimation

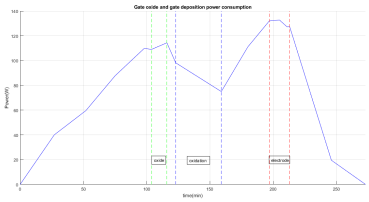

(b) Gate oxide and gate deposition power consumption estimation

8.4 Conclusions

The aforementioned results show that the synthesis of C_{60} pure at 99.5% requires 12.7 GJ and 48.55 L of o-xylene each kg_{C60}, starting from the tetralin combustion. While the deposition requires 171.3 MJ and 128.7 MJ for the deposition and the turning on and off of the UHV system, respectively. The direct greenhouse gases emissions (i.e. Scope 1 emissions) are not evaluated for the possible differences between the tetralin pyrolysis characterized by emissions in literature and the one used for the soot production, which can affect the actual emissions. In fact the shown data are useful in order to take into account if this process can contribute to GHGs emissions and pollution, but not to quantify

them.
However the indirect GHGs emissions, due to energy demand(i.e. Scope 2 ones), can be evaluated by knowing the emissions produced by unit of energy in the country where the synthesis and deposition occurred (as summarized in table 3.1). Indeed in Poland each kW h is responsible for the emission of 0.76 kg of CO_{2eq}, hence the synthesis process produces 2681 kg of CO_{2eq} each kg_{C60}, while the deposition is responsible for 63.3 kg of CO_{2eq} emission.

Part V

Study on devices

Chapter 9

Simulations

In this study simulations can be useful to support and understand better the measurements. In particular it is not expected always an exact match of the results obtained with the two methods, but their comparisons will be useful to understand better the structure and the interface behavior.
The analyses performed in this way aim to determine the energy diagram of bismuth and C_{60} and study a molecular junction based on these two materials.

9.1 Energy diagram

In order to determine the energy diagram it is important to know the valence and conduction band edges (if we refer to an inorganic material) and the vacuum level. While in case of organic materials the valence and the conduction edges correspond to the HOMO and LUMO levels, in addition to which other lower energy levels could be of interest (i.e. HOMO-1 and HOMO-2).
Therefore, bandstructure and density of states can be useful information for determining all the energy levels with the exception of the vacuum level. In fact the latter is a surface properties, hence in the simulation software under use (i.e. QuantumATK), there is need to compute the chemical potential in a structure which consider the vacuum too, so not in the bulk.
Hereinafter the settings at the basis of the simulations are summarized, without taking into account the settings set by default.

Looking at the chosen settings, the potentials and basis set have been chosen by taking into account both the accuracy of the results (i.e. in the QuantumATK manual[64] are enlisted the errors related to each basis set-pseudopotential choice for each element) and the time requirement. Therefore the presented choice suited to be good for the problem under study, which consider both inorganic and organic material.
Regarding instead the numerical accuracy settings the k-points sampling has been chosen to be greater than 7 in each direction as suggested by the manual[64].
The considerations introduced until now are general for every computation considered in this study. While in these two particular cases, in the numerical accuracy section the

Computation setting	Bulk Bi (012 and 111)	Bulk C_{60}
LCAO calculator		
LCAO Basis set		
Exchange correlation family	GGA	GGA
Functional	PBE	PBE
Pseudopotential	FHI	FHI
Basis set	DZP	DZP
Dispersion correction	Grimme DFT-D3	Grimme DFT-D3
Numerical accuracy		
Density mesh cutoff	90 Ha	75 Ha
Occupation method	Methfessel -Paxton	Fermi-Dirac
Broadening (K)	1000	1000
k-points sampling	A:18 B:10 C:18	A:20 B:20 C:20
Poisson solver		
Solver type	FFT	FFT
Boundary conditions	Periodic	Periodic
Tolerance	10^{-4}	10^{-5}
Bandstructure		
	default	default
Density of states		
k-point sampling	A:18 B:10 C:18	A:10 B:10 C:10
Bands above Fermi level	All	10

Table 9.1: Settings for bulk computation

occupation method has been chosen different on bismuth simulation, since it is a metal, hence *Methfessel-Paxton* method is the most accurate[64].
Moreover the structure is a bulk periodic structure, so the Poisson solver under use is FFT one, as suggested from the manual[64]. Finally regarding the density of state analysis the requirements on C_{60} have been loosen, in order to avoid running out of memory, hence the sampling as been halved in each direction and the bands above the Fermi level have been reduced from all to 10.
Going back to the structures under analysis the crystallographic orientation has been taken from literature, where bismuth results to be mainly organized with (012) as crystalline orientation [38][75] and C_{60} organizes mostly in face cubic centered structure with (111) crystalline orientation and lattice constant of 14.198 Å[21][17][2]. However for the molecular junction simulation the accepted crystallographic orientation for bismuth as electrodes is (111), hence the bandstructure and the DOS have been computed also in this case, adopting the same settings for the computations.

The simulated bandstructure and DOS , in case of the two bismuth configurations are compared each other, and they result in consistent results. In fact even if the bandstructures present some differences the two DOS functions coincide. Indeed in case of

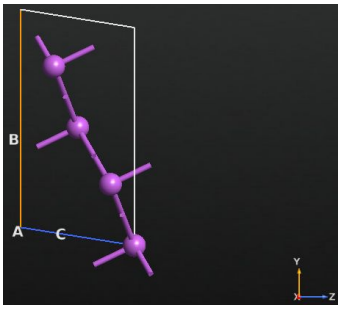

(a) Bi (012) simulation unit cell

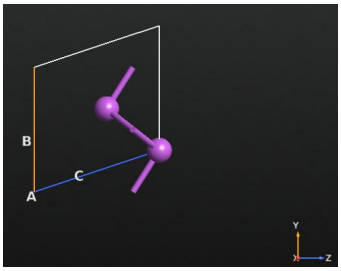

(b) Bi (111) simulation unit cell

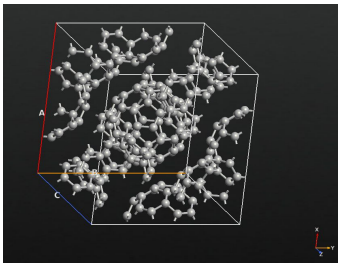

(c) 60 (111) simulation unit cell

(012) orientation the bandstructure presents a bandgap, that is not present in the (111) orientation. This discrepancy can be attributed to the different perspective at which the material has been looked, being confirmed by a unique DOS function. Therefore in this case, the one of a metal, it is important to know only the work function, which will be seen later.

Regarding C_{60} a bandgap and the energy levels related to the orbital are visible. Indeed the indirect and direct bandgap almost coincide, with a difference of 0.02 eV, being stated to be 1.04 eV. Moreover it is well centered on the Fermi level, in fact the LUMO level is 0.52 eV above it and the HOMO level 0.54 eV below.

In the same way as for Bismuth, the bandstructure and the density of state describe the same energy levels, hence there extracted levels coincides. In fact through a rough estimation of the band's center position, it has be found the peak position of the DOS. In particular it can be possible to compare these values with the ones resulting from the UPS measurement.

	Simulations	UPS measurement
LUMO	0.86 eV	-
HOMO	−0.78 eV	−2.85 eV
HOMO - 1	−2 eV	−4.18 eV
HOMO - 2	−3.6 eV	−6.45 eV

Table 9.2: Comparison between calculated and measured energy levels of C_{60}, referred to the Fermi energy level, supposed to be at 0 eV

At this point it is useful to compute the work function. For this purpose it is necessary to simulate the behavior at the surface, indeed the previously employed bulk is exposed to the vacuum, in such a way that the electronic cloud can expand into the vacuum. However from a computational point of view the short-range localized basis set are not sufficient to represent the extension of the electronic cloud out of the surface, hence there is need of additional ones into the vacuum. They can be considered by adding ghost atoms into the

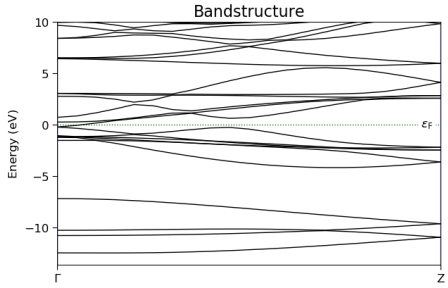

(a) Bi (012) bandstructure

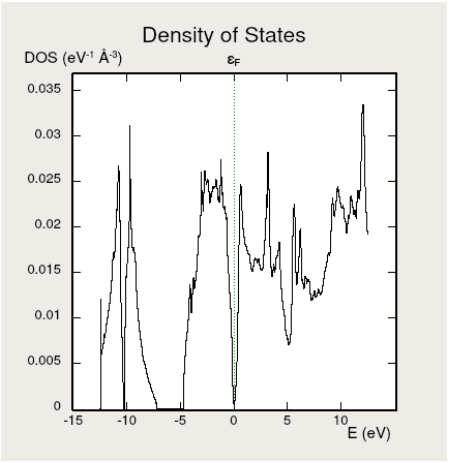

(b) Bi (012) density of states

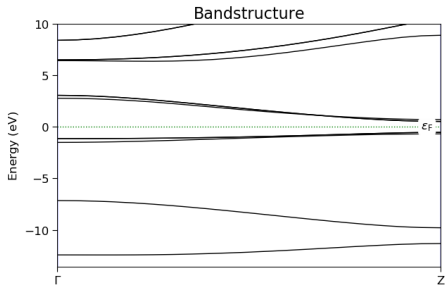

(c) Bi (111) bandstructure

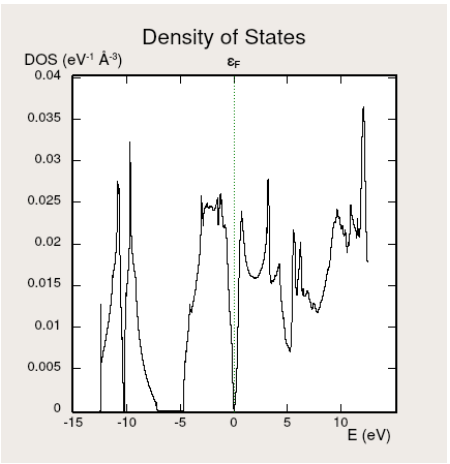

(d) Bi (111) density of states

Figure 9.2: Bi bandstructure and density of states depending on crystallographic orientation

vacuum near to the surface[57], which are represented by those atoms without bonding, as instead the normal ones are (as represented in picture 9.4. Moreover the tutorial taken into account[57] suggests to have on the left side another vacuum region extended enough to be longer the the basis set tails. In fact the left vacuum regions are 5.84 Å and 3.56 Å for Bi and C_{60}, respectively, while the longest basis set tails are 3.81 Å and 2.96 Å. The different conditions between the left and the right sides ask for different boundary conditions over this direction[57]: the left side has Neumann boundary conditions, against the right side with Dirichlet ones.

As a result for the aforementioned considerations the computation settings differ from the bulk calculation and are highlighted hereinafter:

Combining the obtained results in this calculation and the previous ones, the energy

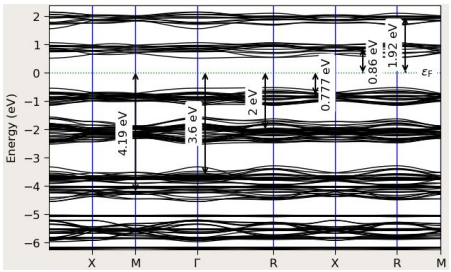

(a) C_{60} bandstructure

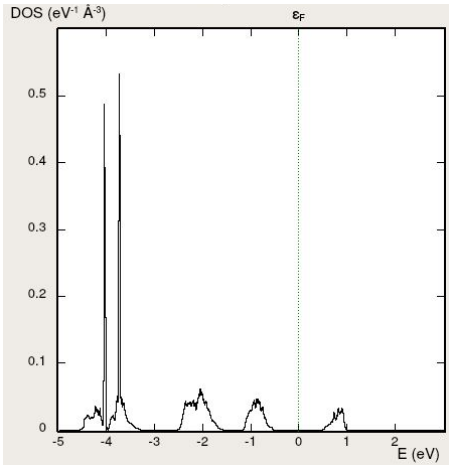

(b) C_{60} density of states

Figure 9.3: C_{60} bandstrucutre and density of states

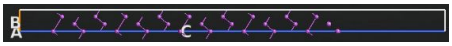

(a) Bi(111) work function simulated structure

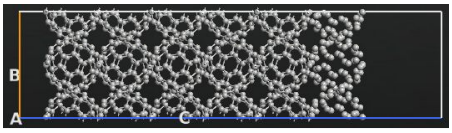

(b) C_{60} work function simulated structure

Figure 9.4: Computed work functions

diagram can be obtained and compared with the experimental results, coming from UPS measurements. In particular the work function taken into account is the one related to the bismuth deposited over the substrate, while the bismuth deposited over the fullerenes have work function higher than 0.3 eV, so most likely it is influenced by the interaction with the C_{60} beneath.

The obtained work function from simulation results to be almost consistent with the experimental results, with a variation of 0.2 eV. Such variation can be associated to oxidation of the surface of the Bismuth and to several crystalline orientations present in the sample.
While instead the values obtained for the C_{60} differ consistently from the measured ones, even if they result to be almost consistent with other simulation results found in literature [2]. This discrepancy can be due to the interaction of C_{60} with the beneath layer of Si_3N_4.

Computation setting	Bi (111)	C_{60}
LCAO calculator		
LCAO Basis set		
Basis set	SZP	DZP
Numerical accuracy		
Density mesh cutoff Occupation method k-points sampling	30 Ha Fermi-Dirac A:7 B:7 C:7	75 Ha Fermi-Dirac A:7 B:7 C:7
Poisson solver		
Solver type Boundary conditions Tolerance	Multi-grid A,B:Periodic LeftC:Neumann RightC:Dirichlet 10^{-4}	Multi-grid A,B:Periodic LeftC:Neumann RightC:Dirichlet 10^{-4}

Table 9.3: Settings for work function computation

	Bi(111) computed	UPS measurement
Φ	3.69 eV	3.89 eV

Table 9.4: Energy levels for Bi(111): comparison between computed and measured values

	C_{60} computed	UPS measurement
Φ	-	3.93 eV
LUMO	0.86 eV	-
HOMO	−0.78 eV	−2.85 eV

Table 9.5: Energy levels for C_{60}: comparison between computed and measured values

9.2 Molecular junction

A possible application of Bi-C_{60} junction is the molecular junction, where 2 bismuth electrodes work with one fullerene.

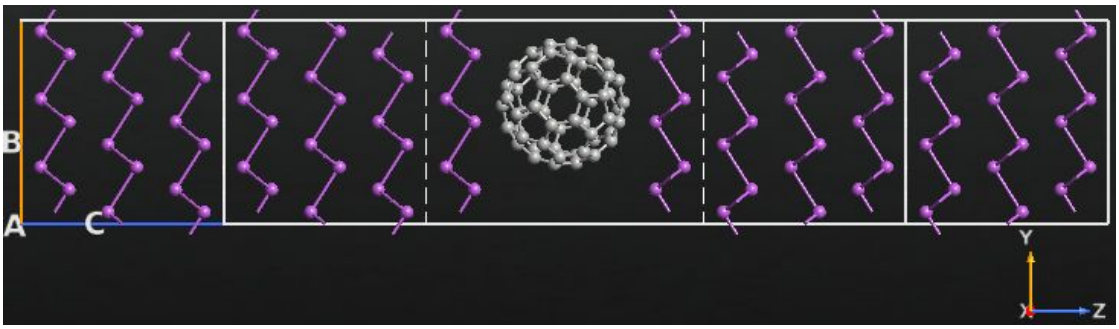

Figure 9.5: Molecular junction structure

In this case the transmission spectrum is fundamental in order to derive the IV curve, where the current is the result of a voltage difference applied among the two electrodes. In

particular the transmission spectrum is evaluated from energy levels 8 eV below the Fermi level up to 4 eV above it, while the bias applied ranges from −2 V to 2 V. Furthermore another useful analysis regard the density of state, which compared to C_{60} an Bi ones can describe how much the electrodes influences the DOS of the active material (i.e. the fullerene in the middle). Nonetheless the structure has been characterized by the mechanical forces present in it, in order to understand if the device is working or not in condition of mechanical stress and understand if it is compressive or tensile one. The mechanical stress can determine the rearrangement of molecular orbitals, hence a different electrical response.
In order to perform the aforementioned analyses, the chosen settings are the following one. In particular the energy range of the transmission spectrum and the DOS have been chosen in order to investigate the LUMO and few of the above levels with the HOMO and some of the below levels.

Computation setting	Chosen values
LCAO calculator	
LCAO Basis set	
Exchange correlation family	GGA
Functional	PBE
Pseudopotential	FHI
Basis set	C:DZP Bi:SZP
Dispersion correction	Grimme DFT-D3
Numerical accuracy	
Density mesh cutoff	75 Ha
k-points sampling	A:7 B:7 C:37
Poisson solver	
Solver type	[Parallel] Conjugate gradient
Boundary conditions	A,B:Periodic C:Dirichlet
Forces	
IV Curve	
Energies	[-8, 4]eV
Points	121
Voltage biases	[-2,2] V
Points	11
Device density of states	
Energies	[-8, 4]eV
Points	121

Table 9.6: Settings for device computation

The resulting current-voltage curve is shown in figure 9.6, where a null current is present at 0 V applied to the electrode, while when a non null bias is applied the curve have the same behavior for both negative and positive biases. In particular the negative voltage side of the characteristic present the opposite currents at opposite voltage, when

compared to the positive voltage side. Thus the following considerations can be applied only on the positive voltage side of the curve, since they would be the same as on the opposite side.
The characteristic present two important feature that can be confirmed when looking at the transmission spectra: the first one is the change of slope at 0.4 V and the second one is a slightly quadratic increase in the curve after the previously mentioned threshold.
The presence of a threshold at quite low voltages suggests that this device can be used as a diode, with an off state at 0 V and an on one at 0.5-0.6V, where there is a current around 20 µA. However the ratio I_{ON}/I_{OFF} has to be evaluated, in order to address this device to a specific application or if there is need of some optimizations.

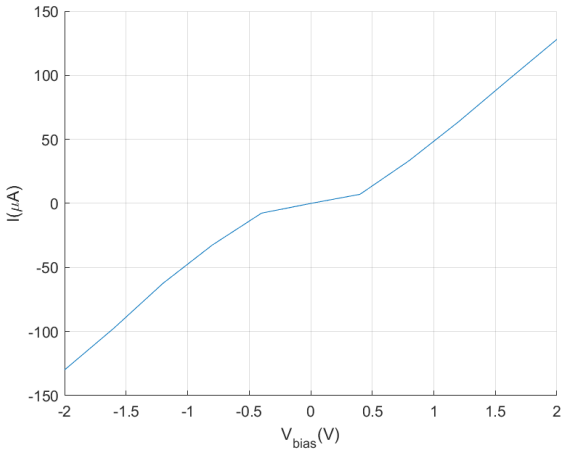

Figure 9.6: Simulated IV curve

The IV curve has been computed starting from the transmission spectra obtain at each bias voltage, by integrating it over the energy as explained in the theoretical chapter. In fact, by looking at the spectrum it can be noticed that it changes when the bias is applied, in particular a peak starts to be present and grow together with the applied voltage, as it can be seen from picture 9.7. This peak is centered into the bias window, indeed the region of the energies between the Fermi levels of the two electrodes. Such feature of the spectrum lead to a quadratic growth of current over the voltage, because both the area of integration and the spectrum increase in a linear way, or better the second one is supposed to increase linearly.

Finally a comparison of the transmission spectrum at 0 V bias with the partial density of states, related to the C_{60} in such junction, can be performed as shown in picture 9.8. In particular it can be noticed that the DOS presents 3 peaks below the Fermi level and one above it. However they have a small linewidth, hence these states can be considered almost localized, so the transmission for them is not expected to be strong. In fact at the on the energy corresponding to the DOS peaks the transmission spectrum small peaks added to the general behavior, as highlighted by the dotted yellow lines in picture 9.8.

Furthermore in this case it can be noticed how the influence of the electrodes affect the

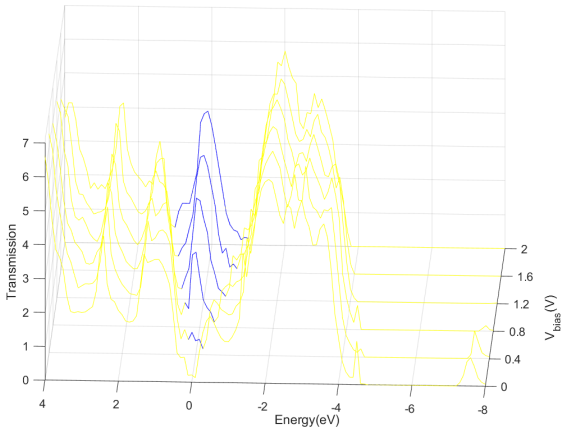

Figure 9.7: Transmission spectra at different bias voltage, with a focus on the region into the bias window (represented in blue)

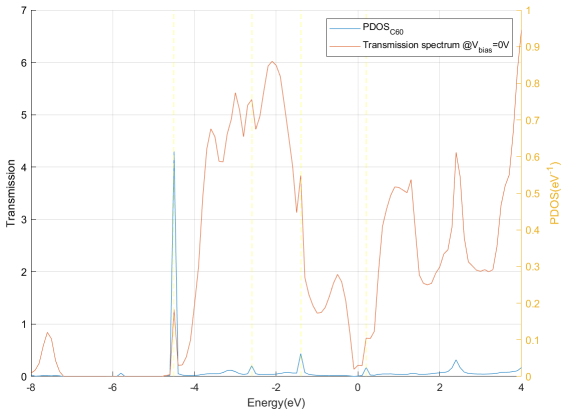

Figure 9.8: Comparison between the transmission spectrum and the partial DOS related to the C_{60} in the middle of the two electrodes

peak position in the fullerene, the obtained data with this simulation and the calculation made on the bulk fullerene are shown in table 9.7. In this case a partial agreement with the measurements is achieved, assuming that the HOMO resulting from the computation was not visible by UPS measurement. In particular when looking at the UPS spectrum (in figure 10.13) a very low peak is visible at 1.5 eV, but the dimensions are comparable to the noise, so such hypothesis is not reliable, hence further more accurate investigations are needed.

	Molecular junction C_{60} DOS	Bulk C_{60} DOS	UPS measurement
LUMO	0.2 eV	0.86 eV	-
HOMO	−1.4 eV	−0.78 eV	−2.85 eV
HOMO - 1	−2.6 eV	−2 eV	−4.18 eV
HOMO - 2	−4.5 eV	−3.6 eV	−6.45 eV

Table 9.7: Comparison between calculated and measured energy levels of C_{60}, referred to the Fermi energy level, supposed to be at 0 eV

Chapter 10

Characterization of a device

10.1 Device fabrication

The device that wanted to be under analysis is a MOSFET realized by means of:

- Fullerenes C_{60}, as semiconductive material in the active region;
- Bismuth as metal for the electrodes (so Source, Drain and Gate);
- Bismuth oxide as gate oxide.

The geometry chosen for the device is the one shown in 10.1, where the Source and Drain electrodes are at the bottom of the structure, and the Gate is on the top of the structure, separated from the 2 electrodes by the fullerenes and the gate oxide layers (so having the so called *bottom-contact top gate* structure).

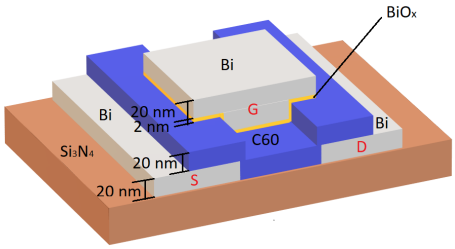

Figure 10.1: 3D model of the transistor

Regarding the dimensions of the structure the thicknesses are all in the nanometer scale (as shown in the 3D model in figure 10.1), in order to try to study a thin film device and having a behavior closer to the quantum simulations on a molecular device. Instead the other two dimensions are in the macroscale, determined by the available masking techniques (shadow masking with sample holder arms and aluminum foil). Indeed the dimensions are in the order of some millimeters.

The structure has been realized by means of PVD, using a substrate in Silicon (p-type with <100> orientation) passivated with 50 nm ofSi_3N_4 and covered by a resist film removed before the deposition steps.

10.1.1 Substrate preparation

In order to have a flat substrate and known electronic properties, the resist film has been removed following a cleaning procedure:

- 15 s sonication in acetone
- 10 min soaking in acetone
- cleaning of the surface through an acetone wet tissue, in order to remove the last residuals of resist on it

Afterward another cleaning procedure has been adopted in order to remove other further impurities that can contaminate the UHV system where the deposition and XPS analysis occurs.

- 10 min sonication in acetone
- 10 min sonication in isopropanol
- 10 min sonication in deionized (DI) water
- removal of water drops through a gentle N_2 flow, in order to not have any residuals left from water evaporation
- drying 40 min in the oven at 100 °C

10.1.2 Layers deposition

The cleaning procedure allows the sample to go into the UHV system, after the masking procedure, where there is need of cleaned tools and gloves to not introduce new impurities. The subsequent fabrication of the device follows the below mentioned steps:

STEP 1 : Source and drain masking, where the active area has been shadowed by an aluminum foil wounded around the sample;

STEP 2 : deposition of 20 nm of Bi at 0.15 Å s^{-1};

STEP 3 : masking of the active area, by means of aluminum foil in order to cover only a part of the deposited electrodes (that have to be exposed to be reached for the electrical and physical measurements);

STEP 4 : deposition of 20 nm of C_{60} at 0.03 Å s^{-1};

STEP 5 : gate masking;

STEP 6 : deposition of 2 nm of Bi at 0.05 Å s^{-1};

STEP 7 : venting of the chamber for 40 min in order to oxidize the Bi film to the air and obtain the gate oxide.

STEP 8 : deposition of 20 nm of Bi at 0.15 Å s^{-1};

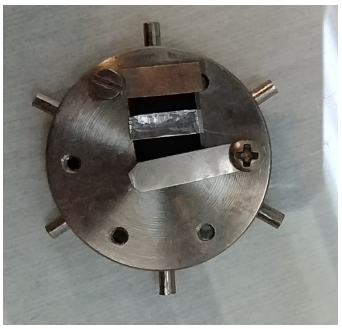

(a) STEP 1

(b) STEP 2

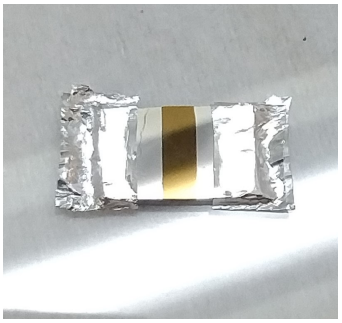

(c) STEP 3

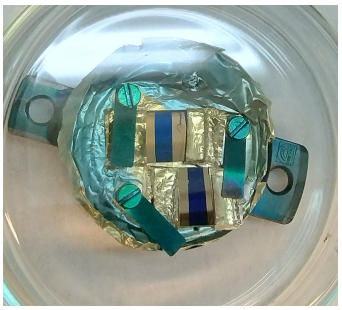

(d) STEP 4

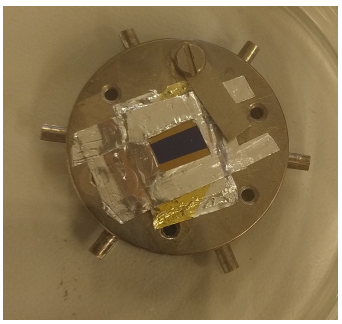

(e) STEP 5

(f) STEP 6, STEP 7 and STEP 8

It is important to notice that the masking procedures occurred at open air, so also the Source and Drain electrodes have been oxidized, as well as the fullerene layer which as shown in literature [19] can incorporate oxygen. Actually in fullerenes there is no true oxidation, even if hereinafter it will be referred as oxidation to highlight the performance degradation due to oxygen exposure. In particular regarding the fullerene layer both light and oxygen exposure influences negatively the electrical performances of the material, by means of bulk oxidation[19] and photopolymerization[51], where a covalent bond is formed between two C60 molecules.
The so prepared samples are two, with slight geometrical differences in the active area (measured by a caliper).

10.2 Characterization

The properties of the so fabricated device have been investigated trough several methods in order to extract both the topographical (AFM) and interface properties (SKPFM and

	channel length (mm)	width(mm)
sample 1	2.8	7.3
sample 2	2.3-2.8	9.5

Table 10.1: Power consumption of all the deposition steps

photoelectron spectroscopy) .

10.2.1 Atomic force microscopy (AFM)

The AFM probing investigated all the possible boundaries between region with different height and also all the flat surfaces in each different region.
Indeed the obtained results are: the actual geometry of the device, the length of the boundaries and the roughness of each flat surface.
From the first analysis it can be seen that the measured heights for each region transition are in agreement with the expected ones with a maximum error of 5.3 nm (over the 20 nm expected in the fullerenes layer below the gate), as shown in 10.3, where each different region has been named in a different way (in red in figure 10.3).

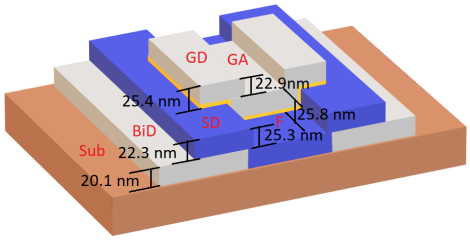

Figure 10.3: 3D model extracted from the AFM measurements

Furthermore the space over which the boundaries extend can be important to evaluate the masking procedure. Considering all of them the medium length is around 15 µm for the masking with the aluminum foil, while around 9 µm for the masking with the sample holder arm. So both masking methods are not suitable for defining dimensions in the order of 10 µm and below, without considering the uncertainty introduced by the human capabilities in placing the masking (even larger than this magnitudes). The measured length are summarized in table 10.2.

Finally the roughness can be useful to determine the scale and the application at which the deposited material can be employed with a physical deposition. Indeed if it can be suitable for those application where there's need of a very flat surface (electronic device) or a very rough one (e.g. electrodes in electrochemical cells, where an higher surface area correspond to an higher capacity). The roughness is calculated by its rms value, which can take into account the distribution of the height of the grain and also their density

boundary	length (µm)
Sub and BiD	22
BiD and SD	14.5
SD and GD	16.5
GD and GA	7.5
GA and F	21
F and SD	11

Table 10.2: Extension of the boundary over the sample

into the surface, while the other parameter useful for the before mentioned analysis is the surface area.

	BiD	F	GA	GD	SD	Sub
	5x5 µm2	5x5 µm2	5x5 µm2	5x5 µm2	5x5 µm2	5x5 µm2
RMS (Sq), nm	3.631	1.352	15.53	9.14	4.04	2.13
Surface area, µm2	25.57	25.33	26.77	27.61	25.78	25.73

As result the substrate shows to be very flat, even if the C_{60}(i.e. region F) deposited over it has the lowest roughness, while still showing a good flatness when deposited over the Bismuth (i.e. region SD).
Instead the Bismuth show generally higher roughness, when deposited over the substrate (i.e. region BiD) is almost flat as well as the substrate. While the roughness increases when deposited over the fullerenes (i.e. regions GA and GD). This behaviour is clearer when looking at figure 10.4, in particular at the maximum level reached by the grains in the surface.

10.2.2 Scanning Kelivin Probe Force Microscopy(SKPFM)

The SKPFM measurement can give an idea about how the interface is characterized by looking at the surface potential at the boundaries between two different regions. This could not give the exact value of the potentials present at the actual interface since they differ from the surface ones because of the reciprocal influence of the two materials, as explained in the theoretical section.
Furthermore the SKPFM over the surface of one material is useful to determine how the different grains formed during the deposition show different vacuum levels and so work functions[26].
The measurements considered two kind of grounding by means of a conductive carbon tape, so connecting the region of interest in the structure to the bottom side of the sample where the reference level connection occurs (so also connecting electrically the bottom side of the substrate with the region of interest at the top of the sample). In particular the first taping (only used for the measurements at the boundaries between two different regions) connects on top of the substrate , while the second taping (employed also for the

measurements on one region) connects the BiD region (so the Source, or Drain, electrode to the reference level).

Regarding the analysis on the lone regions the differences in potential among grains and valleys can be seen from figure 10.4, where the grains present higher potential surface with the respect to the other regions. Therefore both the roughness (in RMS) and maximum difference in potential value have been summarized in table 10.3, highlighting that the maximum height reached by a grain is around 300 mV. However regarding the grounding connection of the sample, it is the second adopted one, or better the one represented by a black taping in figure10.5.

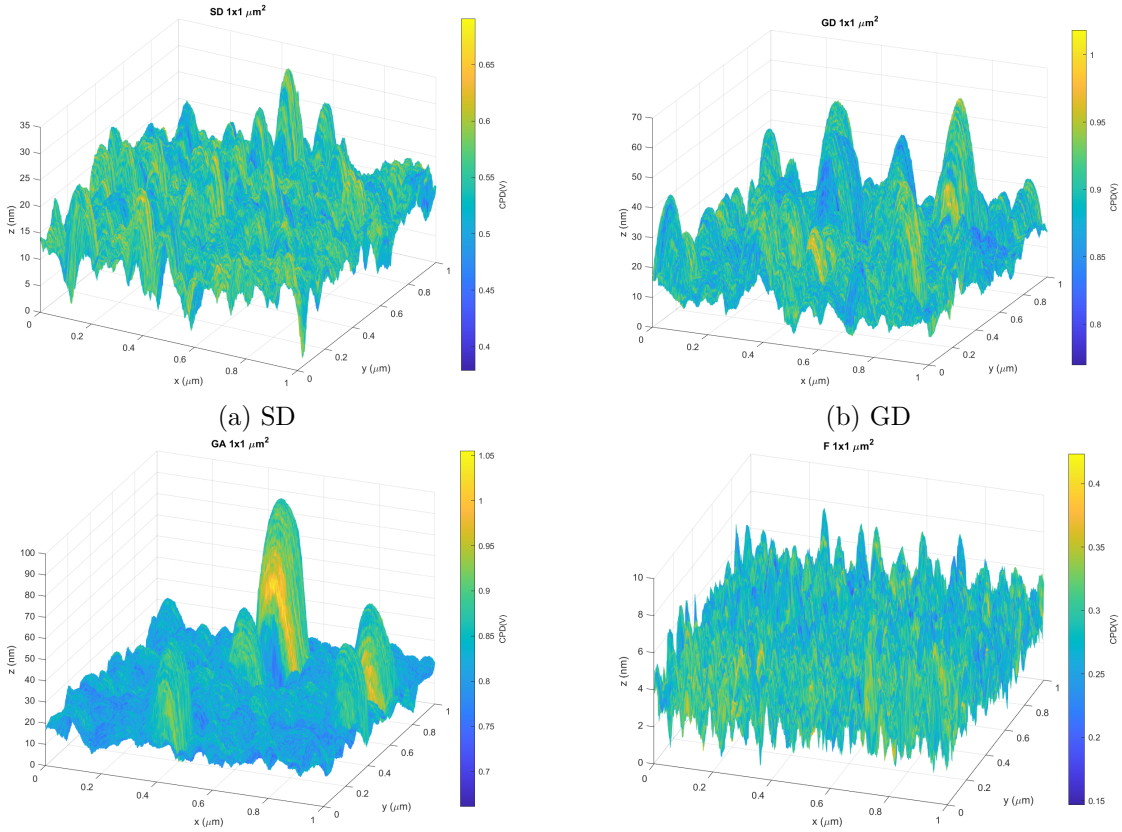

(a) SD (b) GD

(c) GA (d) F

Figure 10.4: Topography and surface potential of regions

Regarding the analysis on the behaviour of surface potential at the boundaries between two different regions, it can be a measure of how the interface is. In particular it shows the band bending due to the interface between a p-type material (i.e. C_{60}) and an n-type one (i.e. bismuth oxide), even if the exact length of the bent regions cannot be found because of a not sharp transition from one region to the other.

	F	GA	GD	SD
	1x1 μm^2	1x1 μm^2	1x1 μm^2	1x1 μm^2
RMS (Sq),mV	31.5	35.04	28.18	33.88
$\Delta V = Vmax - Vmin$, mV	276.8	394	248	311.6

Table 10.3: Roughness and voltage differences in the surface potentials

The two aforementioned taping are employed both in order to understand which connection can guarantee the alignment of Fermi levels in the whole structure, and so a good measure. Indeed the first one (represented in red in figure 10.5) is placed on the substrate, while the second one (represented in red in figure 10.5) is connected to the Source (or equivalently Drain) region, here named BiD.

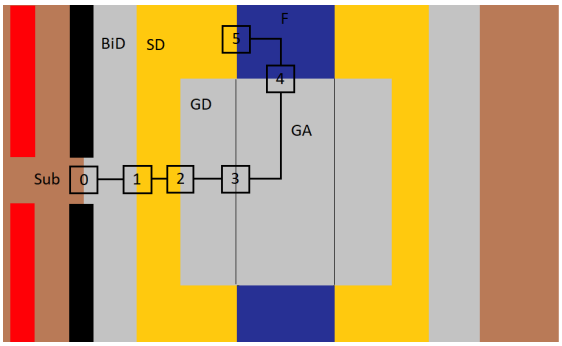

Figure 10.5: Different groundings (or taping) and route of the potential profile

Therefore the measurements occurred over all the boundaries for both taping, according to the order shown in 10.5, where the region 0 is detected only in case of taping 1, since it is the area where the second taping is placed. Therefore, while showing the measurements with the later taping, this region will be represented by a null potential, even if without any physical meaning. In particular the measurements with the second taping considered 3 different biases($-0.5\,V$, $0\,V$ and $0.5\,V$), in order to investigate how different biases can stimulate the structure, but trying to not damage it with to high voltage, so electric field, because of its very thin thickness. While the first one has no bias applied. Indeed in order to evaluate these measurements at first a unique profile has been extracted, merging the measurements of all the boundaries in the order defined in figure 10.5.

However these profiles present a voltage difference between the end of a scan and the start of another one, that can be attributed to the built in voltage of the interface that have not been taken into account by the measurement in that particular boundary, but which are biased by the instrument together with the surface junction, since placed beneath it. However they have not been further investigated, thus quantified, focusing only at the behavior at the transitions from one layer to another. Indeed the profile have been leveled to look at a first glance how all the junctions behave. However in the comparison

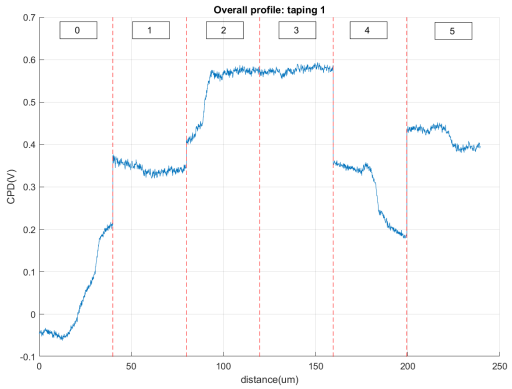

(a) Overall potential profile with the taping 1

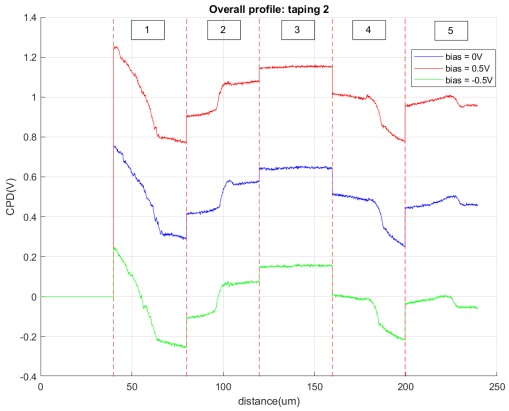

(b) Overall potential profile with the taping 2

Figure 10.6: Overall potential profile

among the different biases the curves show a similar behavior, but shifted by a voltage equal to the applied bias.
Moreover also a comparison between the 2 taping and the different biases can be performed, as it is shown subsequently.

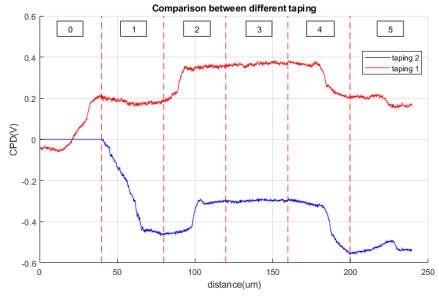

(a) Comparison between different taping

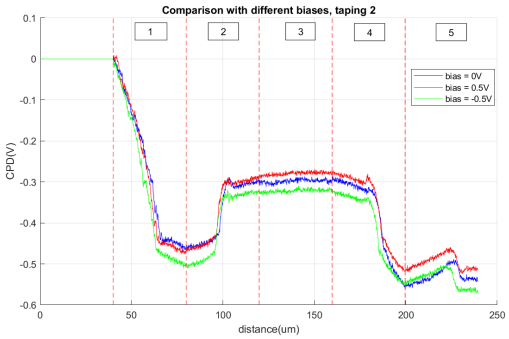

(b) Comparison between different biases

Figure 10.7: Comparisons

From the comparison between the two different taping the region characterized by the gate (spread over region 2, 3 and 4),is almost flat, in agreement to a common work function due to the presence of only bismuth.
Instead in regions 2 and 4, where there is the $C_{60}-Bi_{Gate}$ interface, it is visible the presence of a pn junction with the C_{60} side working as p-type and the Bi one as n-type, by means of a concave and a convex curve in the respective side. Moreover at the Bi side of the junction there is a bump in the curve, which can be attributed to a not sharp transition, and so a not uniform charge distribution of this interface, and will be investigated later in detail.

Instead also some differences can be found:

- at the $Bi_{Drain} - C_{60}$ interface (in region 1) with the first taping the potential is constant, being in agreement with the UPS measurements (see table 10.4), where both layer have almost the same work function. While with the second taping the potential increase going into the Bi layer toward the tape, so this can be attributed to a charging of this area, since there is also no flat region of this behaviour.
- at the $C_{60,substrate} - C_{60,Drain}$, there is an interface behavior in both taping, but in the first one the two flat levels are slightly different (and this can be due to the effect of the different layers beneath them), while in case of taping 2 the two flat regions show similar potential, even if there is at the junction a change in behavior. This difference has not been investigated, since it needs further measurements (determine the work function of the $C_{60,substrate}$).

Finally in the taping 1 also the interface $Substrate - Bi_{Drain}$ can be seen, by an increasing of the potential toward the Bi side.
Instead, looking deeply into the behavior at the interface, the charge distribution can be estimated by means of a double integration of the Poisson equation, but normalizing the charge to the relative dielectric constant, because is difficult to separate the contribution of the charge due to the C_{60} layer from the Bi one.

$$\frac{d^2\phi(x)}{dx^2} = -\frac{\rho(x)}{\epsilon} = -(\frac{\rho_{C60}(x)}{\epsilon_{C60}} + \frac{\rho_{Bi}(x)}{\epsilon_{Bi}})$$

Starting from these considerations the behavior of the charge density along the boundary is computed, while still including the dielectric constant component (as shown in figure 10.8a). In particular a negative charge and a positive charge regions are nearby, and the transition between them occurs when the topography is at around a third of the boundary height. Moreover it can be noticed how the potential decays in a longer distance rather than the extension of the charge regions aforementioned.
In this scenario it is also important to highlight that the vertical interface Bi(or BiOx)-C_{60} creates a depleted region at the interface as shown at the right side of the figure 10.8b. Therefore, when such interface is interrupted, because there is no more bismuth deposited, the charge in the C_{60} layer will diminish going further from the boundary, according to the relative depletion region extension.
However, by taking into account also the starting reasoning, it can be expected that the presence of negative charges just outside the boundary (still supposing it as sharp, different from our case), will create a negative charge region also on the horizontal plane. As a consequence, on the opposite side of the horizontal boundary a positive charge accumulates and will be extinguished in a certain space. This further charge accumulated at the horizontal boundary, that adds to the one due to the vertical interface, characterizes the bump present in the potential.
The previous reasoning was applied to a sharp topographical transition, but works well also in case of a not sharp transition, where the boundary of the charges occurs after the boundary start to develop, indeed when the contribution of bismuth over C_{60} starts

to be no more negligible with respect to where the topography is at its maximum. This description has been represented in figure 10.8b.

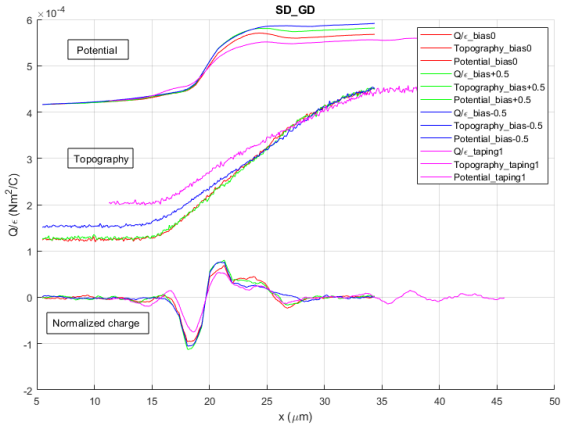

(a) Interface charge distribution on the horizontal plane (the top plot represents the different potential measurements, the middle one the topography, while the bottom one the computed charge density)

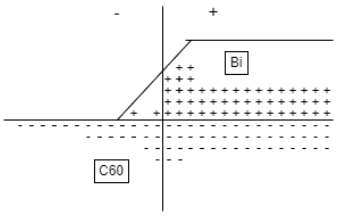

(b) Idea of the interface charge distribution on both horizontal and vertical plane

10.2.3 Photoelectron spectroscopy

Photoelectron spectroscopy in this study has been useful to identify the energy levels and address the causes. In particular the work function and the distance of the highest valence levels from the Fermi level have been measured. While the nature of the top most layer of the electrode has been verified.
Measurements were performed on three different regions of the completed device and on fullerene layer before exposure to air. The first three detected regions are shown in figure 10.9:

1 the drain (or source) bismuth electrode;

2 the C_{60} layer over the bismuth drain;

3 the gate electrode.

The employed methods are both ultraviolet and x-ray photoelectron spectroscopy, UPS and XPS respectively.
Considering the UPS measurements, shown in picture 10.10, different work functions for each detected region were found. In particular the difference of 0.3 eV between the gate and the drain electrode work function can be attributed to the presence of a dipole at the interface between the C_{60} layer beneath an the bismuth one, corresponding to the electrodes, whose electric field can be sensed on the surface of the gate electrode.
Instead regarding the distance of the valence band edge and the Fermi level in the bismuth

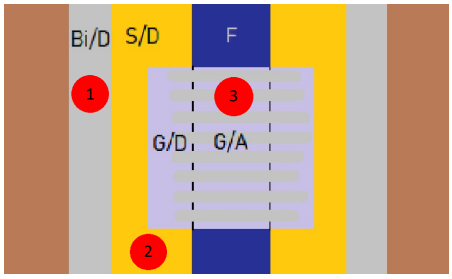

Figure 10.9: Representation of measurement spot position: 1.Bismuth over the substrate 2.C_{60} over the bismuth 3. Bismuth over the C_{60} on the substrate

electrodes, it is not null (i.e. equal to 2.5 eV, showing the effect of the native oxide in the topmost layer of the electrodes. In fact the valence band region measured by XPS show the metallic behavior, since the detection depth obtained with it is much larger than the native oxide thickness, supposed to be around 2 nm, as well as UPS detection depth, because of the lower energy of the ray. Indeed the distance of the valence band edge from the Fermi level is almost null, as it can be seen in picture 10.11, where the region above the Fermi level as negligible photoelectron contribution(i.e. counts per second) with respect to the region below it.

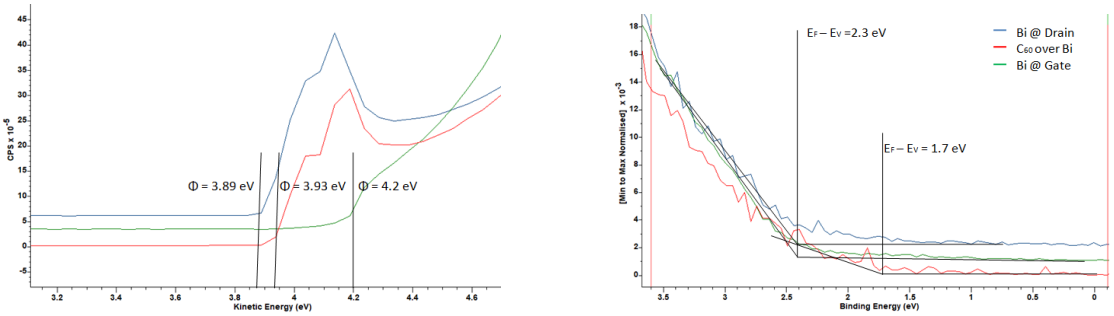

Figure 10.10: Results of the three measurements, were the blue line, the red and green ones correspond to the spots 1, 2 and 3 respectively. On the left the work function measurements are shown, while on the right the difference between Fermi and valence energy level is present.

The hypothesis of oxidation of bismuth due to air exposure is confirmed by the XPS results, where both signals of bismuth oxide and metallic bismuth are present, as it can be shown in picture 10.12. In particular the shown spectra refers to the gate electrode region, since in these contributions from nearby regions, with other materials, are not present. Indeed the detection area has a diameter higher than 1 mm, which coincides with the dimension of exposed drain and source electrodes.

Analyzing in details the shown XPS spectrum the peak splitting due to spin orbit coupling effect is visible, indeed the signal of the metallic and oxidized bismuth, together with a satellite peak, is present twice in the spectrum with a shift of 5.3 eV, as expected

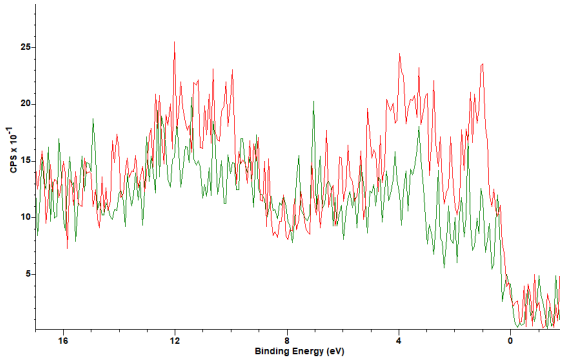

Figure 10.11: Valence band of drain and gate electrode regions, respectively represented by the green and red curves.

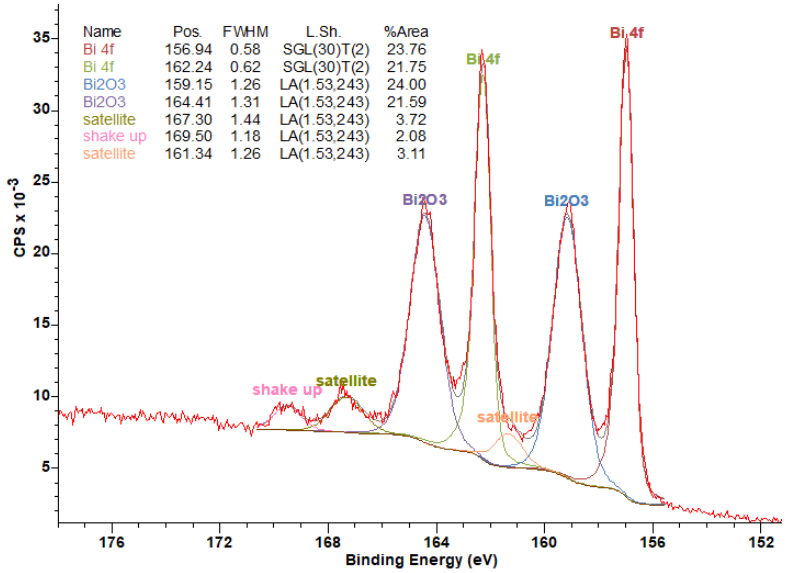

Figure 10.12: XPS fitting of the Bi 4f spectrum measured from the gate electrode region, with information on the fitting peaks.

[52]. Moreover the peak at lower binding energies, corresponding to the first peak of the metallic bismuth, is at 156.94 eV, according to the value found in literature [52], hence there is no charging in this layer.
Instead by looking at the oxide peak they are shifted from the respective metallic peak by 2.2 eV and 2.17 eV, which is lower than the value of 2.4 eV reported in literature [52] for stoichiometric bismuth oxide Bi_2O_3. Such behavior is indicative of a not completely stoichiometric oxide, having instead a lack of oxygen, in fact the oxygen that has higher electronegativity tends to cause higher binding energy to electrons coming from oxidized species, rather than to those ones coming from the pure one.
Furthermore, also the lineshape is important in this case, indeed the metallic peaks have to

present a tail toward higher binding energy, against the oxidized or non metallic species. While, regarding the satellite peaks, they are caused by the electron cloud oscillations after an electron has been emitted, so has been create a vacancy to occupy again.
Instead looking at the fullerene layer it would have been expected to have the energy levels visible, while this does not occur for the layer exposed to air, even if there are differences with respect to the bismuth behavior. In fact air exposure causes carbon species to adsorb over the surface, interfering with the HOMO levels of the beneath fullerene layer, hence hiding them. Moreover the measurement has been conducted over a region of the same dimensions of the detection area (around 1 mm large), thus the nearby materials are sensed by the instrument, adding noise to the measurement, which further hide the HOMO levels.
However they can be visible by *in-situ* measurement on fullerene, that in fact was not exposed to the air, so it is lack of other carbon species. These considerations are in agreement with the results, since the measured work function does not vary among the two situations, as shown in picture 10.13.

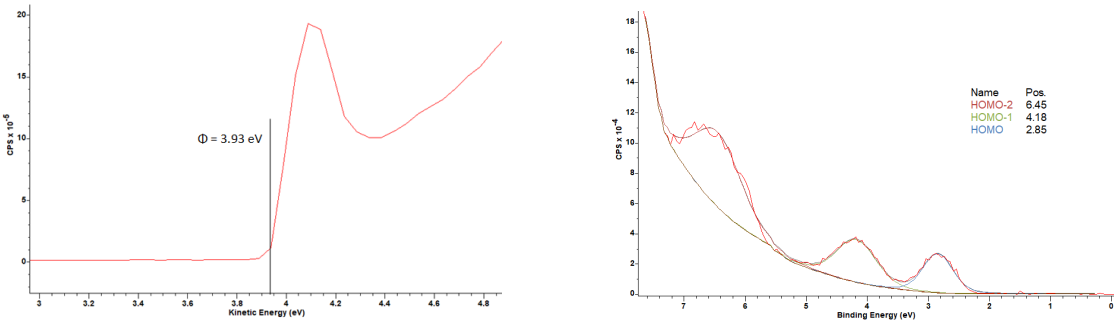

Figure 10.13: Work function (on the left) and valence band region (on the right) analyses of the C_{60} layer deposited over the substrate, before the exposure to the air, hence before the device has been completed.

The obtained results are summarized and gather together in the following table 10.4.

	After air exposure		Before air exposure	
	Φ (eV)	$E_F - HOMO (or E_V)$ (eV)	Φ (eV)	$E_F - HOMO (or E_V)$ (eV)
Bi_{Drain}	3.89	2.5	-	-
C_{60}	3.93	1.7	3.93	2.85
Bi_{Gate}	4.2	2.5	-	-

Table 10.4: Work function and distance of the HOMO to the Fermi level measured by UPS

Part VI

Conclusions

Chapter 11

Conclusions and future perspectives

This work highlights the importance of evaluating the environmental impact of a device. Where the analysis has to consider each material involved into the device and all the phases required to fabricate, use and dispose the device. In this case study on C_{60} the synthesis and deposition of the material have been characterized by energy requirements and solvent loss, while the material itself has been analysed by its features to be easily disposed (so in this case only by their toxicity), according to the proposed scheme (see chapter 7). However such analysis has not been conducted for the other material taken into account (i.e. Bismuth).
Indeed from the synthesis of the material 12.7 GJ per Kg_{C60} and 48.55 L per Kg_{C60} of o-xylene loss are required and the device fabrication needs 300 MJ of energy (171.3 MJ and 128.7 MJ for the deposition and the turning on and off, respectively). The energy requirements define the scope 2 emissions, resulting to be 2681 kg of CO_{2eq} per Kg_{C60} and 63.3 kg of CO_{2eq} due to the deposition, referring to Poland emissions per unit of energy. Within the proposed scheme the power consumption of a device based on C_{60} has not been characterized, as well as for the device lifetime and the raw material extraction environmental impact.
Instead regarding the harmfulness of C_{60}, it presents mild to no toxicity, depending on the environmental, physical and chemical conditions. However further studies have to be conducted in order to attribute the effect on toxicity of each impacting feature or agent, by measuring the minimum amount of C_{60} which can cause a not negligible response of the biological system under test. Also the tested organisms or cells have to be classified, aiming to find a method to assess the harmfulness for the environment caused by the free disposal of such material.
Furthermore the conducted analysis on the sustainability of the material itself lacks of insights on the possible disposal techniques and consequently the toxicity of eventual by-products.
Within this perspective a method to quantify the environmental compatibility is needed to perform comparison among different materials. In addition to this, for each material

the possible syntheses, depositions and combinations with other materials to obtain a device can be gathered together into a database. It would work as useful tool to optimize the fabrication processes and the device from an environmental point of view, rather than performances (in case also performances of the studied devices are taken into account). In order to achieve this result there is need of cooperation among different studies and the definition of a unique paradigm to characterize the environmental and technical performances, in a manner that different materials can be compared each other.
The device fabrication and the subsequent measurements have been based on this perspective. In particular the study focuses on the analysis of the interfaces created in a transistor-like structure, with electrode made by bismuth and the active area by C_{60}, while the naturally oxidized bismuth over fullerenes characterizes the gate oxide. However the oxidation of the electrodes due to the air exposure, during the masking, avoids a direct contact between Bi and C_{60}, hence it is not expected to have good electrical performances. Therefore the resulting structure is useful to study the interface between Bi and C_{60}.
For this purpose the simulations have been used to support the measurement results. In particular from UPS it was possible to determine the work function and the energy levels below the Fermi level, which compared to the simulation results revealed to be consistent in the bismuth case (3.89 eV instead of the computed 3.69 eV). While regarding C_{60} the obtained results are different, without taking into account the work function, where there is lack of the simulated result.
Moreover the UPS measurements has been performed on all the areas that have been investigated through SKPFM, providing coherent results: the potential steps in the boundary regions revealed by SKPFM are equivalent to the differences in the work functions, detected by UPS, of the two different layer present in that boundary.
Regarding the surfaces, they have been analyzed both by topography and by potential topography. The former revealed vertical dimensions in agreement with the desired one, describing this fabrication process as repeatable, and roughness of each layers compatible to the chosen vertical dimensions, but not to ones below 4-5nm (higher roughness of the layers deposited before the top gate bismuth). Instead the latter highlighted a surface potential change in the range between 250 mV and 400 mV, corresponding to the presence of a grain, hence it has to be taken into account during microfabrication processes.
Finally a proof of a working device based on bismuth and C_{60} is provided by the simulation a molecular junction, where there is an almost low voltage threshold (around 0.4 eV, above which the current increases with an higher rate, hence a switching application can be addressed to it. However the computation were performed with a low resolution over the bias voltage, so a more accurate value can be found with further investigation. Furthermore the switching behavior has to be evaluated also by the $\frac{I_{ON}}{I_{OFF}}$ ratio and the speed performances.
However further analyses and investigation are needed in order to have a device working with decent performances, enough to allocate it into a market sector. In fact at first there is need to better understand the interface, analysing also through simulation how the potential energy changes when the two material are put in contact and also the influence of the thin layer of oxide. This will explain a static behavior, but studies on the dynamic

behavior are important to determine the electrical performances, hence the suitable application of a device based on this interface. Therefore, a device like a transistor can be studies to better understand the electrical performances and the field of application. Finally the structure can be optimized by doping the active material to enhance conductivity (usually low in organic materials with respect to inorganic ones). The concept here presented can be subsequently applied to other materials (metals,semiconductors and insulators) of interest in the field of green electronics, with the aim to find optimized structures competitive in the global semiconductor market.
All the considerations done until now aimed to find a way toward new technologies that can have a much lower and even negligible impact on the environment than actual one, but the reduction of the environmental impact pass throughout also the reduction of consumption, which has to go hand in hand with the technological innovation.

Bibliography

[1] IPCC:Stocker et al. *Climate Change 2013: The Physical Science Basis. Contribution of Working Group I to the Fifth Assessment Report of the Intergovernmental Panel on Climate Change*. https://www.ipcc.ch/site/assets/uploads/2018/02/WG1AR5_all_final.pdf. 2013.

[2] Jalali-Asadabadi et al. «Electronic Structure of Crystalline Buckyballs: fcc-C60». In: *Journal of Electronic Materials* 45 (2016). Published: 16 October 2015, pp. 339–348.

[3] Xflroang Zhou et al. «Solubility of Fullerene C60 and C70 in Toluene, o-Xylene and Carbon Disulfide at Various Temperatures». In: *Fullerene Science and Technology* 5.1 (1997), pp. 285–290. DOI: 10.1080/15363839708011990. eprint: https://doi.org/10.1080/15363839708011990. URL: https://doi.org/10.1080/15363839708011990.

[4] John M. Alford et al. «Fullerene production in sooting flames from 1,2,3,4-tetrahydronaphthalene». In: *Carbon* 46.12 (2008), pp. 1623–1625. ISSN: 0008-6223. DOI: https://doi.org/10.1016/j.carbon.2008.07.004. URL: https://www.sciencedirect.com/science/article/pii/S0008622308003394.

[5] Annick Anctil et al. «Material and Energy Intensity of Fullerene Production». In: *Environmental Science & Technology* 45.6 (2011). PMID: 21332197, pp. 2353–2359. DOI: 10.1021/es103860a. eprint: https://doi.org/10.1021/es103860a. URL: https://doi.org/10.1021/es103860a.

[6] Zaeem Bin Babar and Zarook Shareefdeen. «Management and control of air emissions from electronic industries». In: *Springer-Verlag Berlin Heidelberg* (Mar. 2013). Received: 16 November 2012 / Accepted: 21 February 2013 / Published online: 6 March 2013.

[7] Cornelis P. Baldé et al. *Global E-waste Monitor 2024*. Technical Report. Geneva/Bonn: International Telecommunication Union (ITU), United Nations Institute for Training, and Research (UNITAR), 2024.

[8] Cornelis P. Baldé et al. *Global E-waste Monitor 2024*. Technical Report. Geneva/Bonn: International Telecommunication Union (ITU), United Nations Institute for Training, and Research (UNITAR), 2024. URL: https://ewastemonitor.info/wp-content/uploads/2024/03/GEM_2024_18-03_web_page_per_page_web.pdf.

[9] Carbon Footprint Ltd. *Emissions Factors and Sources for 2022*. Technical Report. 2023. URL: https://www.carbonfootprint.com/docs/2023_02_emissions_factors_sources_for_2022_electricity_v10.pdf.

[10] Gi Doo Cha et al. «Bioresorbable Electronic Implants: History, Materials, Fabrication, Devices, and Clinical Applications». In: *Advanced Healthcare Materials* 8.7 (2019). First published: 08 April 2019, Citations: 89, p. 1801660. DOI: 10.1002/adhm.201801660.

[11] Y. Choi, J. Koo, and J.A. Rogers. «Inorganic materials for transient electronics in biomedical applications». In: *MRS Bulletin* 45 (2020). Published 04 October 2020, Issue Date: February 2020, pp. 103–112. DOI: 10.1557/mrs.2020.25.

[12] European Commission. *Communication from the Commission to the European Parliament, the Council, the European Economic and Social Committee and the Committee of the Regions: A European Strategy for Data*. European Commission. COM(2020) 474 final. 2020. URL: https://eur-lex.europa.eu/legal-content/EN/TXT/?uri=CELEX:52020DC0474.

[13] McKinsey & Company. *Here is how the mining industry can respond to climate change*. 2023. URL: https://www.mckinsey.com/capabilities/sustainability/our-insights/sustainability-blog/here-is-how-the-mining-industry-can-respond-to-climate-change.

[14] Erika Alessia Di Liberto et al. «Biodegradation of Polystyrene by Plastic-Eating Tenebrionidae Larvae». In: *Polymers* 16.10 (2024). ISSN: 2073-4360. DOI: 10.3390/polym16101404. URL: https://www.mdpi.com/2073-4360/16/10/1404.

[15] Scott C. Doney et al. «The Impacts of Ocean Acidification on Marine Ecosystems and Reliant Human Communities». In: *Annual Review of Environment and Resources* 45 (2020). First published as a Review in Advance on June 24, 2020, pp. 83–112. DOI: 10.1146/annurev-environ-012320-083019. URL: https://doi.org/10.1146/annurev-environ-012320-083019.

[16] EPA. *Ozone-Depleting Substances*. https://www.epa.gov/ozone-layer-protection/ozone-depleting-substances. 2024.

[17] R. M. Fleming et al. «Crystalline Fullerenes: Round Pegs in Square Holes». In: *Fullerenes*. Copyright © 1992 American Chemical Society. American Chemical Society, Jan. 6, 1992, pp. 25–39. DOI: 10.1021/bk-1992-0481.ch002.

[18] Yu. S. Grushko, V. P. Sedov, and Viktor Abramovich Shilin. «Technology for manufacture of pure fullerenes C60, C70 and a concentrate of higher fullerenes». In: *Russian Journal of Applied Chemistry* 80 (2007), pp. 448–455. URL: https://api.semanticscholar.org/CorpusID:101802951.

[19] A. Hamed et al. «Effects of oxygen and illumination on the in situ conductivity of C_{60} thin films». In: *Phys. Rev. B* 47 (16 Apr. 1993), pp. 10873–10880. DOI: 10.1103/PhysRevB.47.10873. URL: https://link.aps.org/doi/10.1103/PhysRevB.47.10873.

[20] Seyed M. Heidari et al. «Environmental, cost, and chemical hazards of using alternative green solvents for fullerene (C60) purification». In: *Green Chem.* 25 (11 2023), pp. 4350–4361. DOI: 10.1039/D3GC00859B. URL: http://dx.doi.org/10.1039/D3GC00859B.

[21] Paul A. Heiney. «Structure, dynamics and ordering transition of solid C60». In: *Journal of Physics and Chemistry of Solids* 53.11 (1992), pp. 1333–1352. ISSN: 0022-3697. DOI: https://doi.org/10.1016/0022-3697(92)90231-2. URL: https://www.sciencedirect.com/science/article/pii/0022369792902312.

[22] Theo Henckens. «Scarce mineral resources: Extraction, consumption and limits of sustainability». In: *Journal Name* (2021).

[23] Intergovernmental Panel on Climate Change. *Appendix 8.A*. Fifth Assessment Report, p. 731. Archived (PDF) from the original on 13 October 2017. Retrieved 6 November 2017. 2017. URL: https://www.ipcc.ch/report/ar5/syr/.

[24] Intergovernmental Panel on Climate Change (IPCC). *IPCC AR6 Synthesis Report: Climate Change 2023*. https://www.ipcc.ch/report/ar6/syr/downloads/report/IPCC_AR6_SYR_FullVolume.pdf. Section 4.2. 2023.

[25] IPCC. $IPCC_AR6_SYR_FullVolume$. https://www.ipcc.ch/report/ar6/syr/downloads/report/IPCC_AR6_SYR_FullVolume.pdf. 2023.

[26] Hisao Ishii et al. «Energy Level Alignment and Interfacial Electronic Structures at Organic/Metal and Organic/Organic Interfaces». In: *Advanced Materials* 11.8 (1999), pp. 605–610. DOI: 10.1002/(SICI)1521-4095(199906)11:8<605::AID-ADMA605>3.0.CO;2-Q.

[27] Anton W Jensen, Stephen R Wilson, and David I Schuster. «Biological applications of fullerenes». In: *Bioorganic & medicinal chemistry* 4.6 (1996), pp. 767–779.

[28] Helinor J Johnston et al. «The biological mechanisms and physicochemical characteristics responsible for driving fullerene toxicity». In: *Toxicological Sciences* 114.2 (2010), pp. 162–182.

[29] Y. Jung et al. «High-performance green flexible electronics based on biodegradable cellulose nanofibril paper». In: *Nature Communications* 6 (2015), p. 7170. DOI: 10.1038/ncomms8170.

[30] Yei Hwan Jung et al. «High-performance green semiconductor devices: materials, designs, and fabrication». In: *Semiconductor Science and Technology* 32.6 (2017). Published 18 May 2017, © 2017 IOP Publishing Ltd, p. 063002. DOI: 10.1088/1361-6641/aa6f88.

[31] Kui S. Kwok et al. «Separation of fullerenes C60 and C70 using a crystallization-based process». In: *Aiche Journal* 56 (2009), pp. 1801–1812. URL: https://api.semanticscholar.org/CorpusID:95309701.

[32] *Kyoto Protocol Reference Manual on Accounting of Emissions and Assigned Amounts*. https://unfccc.int/resource/docs/publications/08_unfccc_kp_ref_manual.pdf. United Nations Framework Convention on Climate Change (UNFCCC), 2008.

[33] NOAA-Chemical sciences laboratory. *Scientific Assessment of Ozone Depletion: 2010*. https://csl.noaa.gov/assessments/ozone/2010/executivesummary/index.html. 2010.

[34] Hyunkyung Lee, Yongxun Jin, and Seungkwan Hong. «Recent transitions in ultrapure water (UPW) technology: Rising role of reverse osmosis (RO)». In: *Desalination* 399 (2016), pp. 185–197. ISSN: 0011-9164. DOI: https://doi.org/10.1016/j.desal.2016.09.003. URL: https://www.sciencedirect.com/science/article/pii/S0011916416312474.

[35] J.-Y. Lee et al. «Future Global Climate: Scenario-Based Projections and Near-Term Information». In: *Climate Change 2021: The Physical Science Basis. Contribution of Working Group I to the Sixth Assessment Report of the Intergovernmental Panel on Climate Change*. Ed. by V. Masson-Delmotte et al. Cambridge, United Kingdom and New York, NY, USA: Cambridge University Press, 2021, pp. 553–672. DOI: 10.1017/97810091.

[36] Wenhui Li et al. «Biodegradable Materials and Green Processing for Green Electronics». In: *Advanced Materials* 32.29 (2020). DOI: 10.1002/adma.202001591.

[37] Yuyang Li et al. «Experimental and kinetic modeling study of tetralin pyrolysis at low pressure». In: *Proceedings of the Combustion Institute* 34.1 (2013), pp. 1739–1748. ISSN: 1540-7489. DOI: https://doi.org/10.1016/j.proci.2012.05.002. URL: https://www.sciencedirect.com/science/article/pii/S154074891200003X.

[38] E. Subramanian M. Ahila M. Malligavathy and D. Pathinettam Padiyan. «Effect of anodization time on the growth of twinned pyramid crystals of bismite from polyhedral bismuth particle by facile electrolysis-based oxidation». In: *Particulate Science and Technology* 36.6 (2018), pp. 655–659. DOI: 10.1080/02726351.2017.1287793. eprint: https://doi.org/10.1080/02726351.2017.1287793. URL: https://doi.org/10.1080/02726351.2017.1287793.

[39] George H. Major et al. «Practical guide for curve fitting in x-ray photoelectron spectroscopy». In: *Journal of Vacuum Science Technology A* 38.6 (Oct. 2020), p. 061203. ISSN: 0734-2101. DOI: 10.1116/6.0000377. URL: https://doi.org/10.1116/6.0000377.

[40] Nemi Malhotra et al. «An update report on the biosafety and potential toxicity of fullerene-based nanomaterials toward aquatic animals». In: *Oxidative Medicine and Cellular Longevity* 2021 (2021).

[41] V. Masson-Delmotte et al., eds. *Climate Change 2021: The Physical Science Basis*. Cambridge, United Kingdom and New York, NY, USA: Cambridge University Press, 2021, p. 2391. DOI: 10.1017/9781009157896.

[42] Hanan H. Mohamed. «Chapter 1 - Introduction to green processing for sustainable materials». In: *Sustainable Materials and Green Processing for Energy Conversion*. Ed. by Kuan Yew Cheong and Allen Apblett. Elsevier, 2022, pp. 1–42. ISBN: 978-0-12-822838-8. DOI: https://doi.org/10.1016/B978-0-12-822838-8.00004-1. URL: https://www.sciencedirect.com/science/article/pii/B9780128228388000041.

[43] Camilo Mora et al. «Biotic and Human Vulnerability to Projected Changes in Ocean Biogeochemistry over the 21st Century». In: *PLoS Biology* 11.10 (Oct. 2013). Ed. by Georgina M. Mace, e1001682. DOI: 10.1371/journal.pbio.1001682.

[44] Prashant Nagapurkar, Paulomi Nandy, and Sachin Nimbalkar. «Cleaner Chips: Decarbonization in Semiconductor Manufacturing». In: *Sustainability* 16.1 (2024). ISSN: 2071-1050. DOI: 10.3390/su16010218. URL: https://www.mdpi.com/2071-1050/16/1/218.

[45] Author Name. «Title of the Thesis». MA thesis. Turin, Italy: Politecnico di Torino, 2023. URL: https://webthesis.biblio.polito.it/28560/.

[46] ABC News. *Blood Cobalt*. 2022. URL: https://www.abc.net.au/news/2022-02-24/blood-cobalt/13769990.

[47] NOAA. *Global Time Series*. https://www.ncei.noaa.gov/access/monitoring/climate-at-a-glance/global/time-series/globe/land_ocean/ytd/11/1850-2023?filter=true&filterType=binomial. 2023.

[48] NASA Earth Observatory. *Ozone: What Is It, and Why Do We Care About It?* https://earthobservatory.nasa.gov/features/Ozone/ozone_2.php. 2021.

[49] NASA-Earth observatory. *Ozone Balance in the Stratosphere*. https://earthobservatory.nasa.gov/features/Ozone/ozone_2.php. 1999.

[50] J. Obu. «How Much of the Earth's Surface is Underlain by Permafrost?» In: *Journal of Geophysical Research: Earth Surface* 126.6 (2021). First published: 23 April 2021, e2021JF006123. DOI: 10.1029/2021JF006123. URL: https://doi.org/10.1029/2021JF006123.

[51] Jun Onoe, Aiko Nakao, and Kazuo Takeuchi. «XPS study of a photopolymerized C_{60} film». In: *Phys. Rev. B* 55 (15 Apr. 1997), pp. 10051–10056. DOI: 10.1103/PhysRevB.55.10051. URL: https://link.aps.org/doi/10.1103/PhysRevB.55.10051.

[52] Author's Name or Organization. *Bismuth Information*. Website. 2024. URL: https://www.xpsfitting.com/search/label/Bismuth.

[53] Tim Osborn. *CRU Temperature Diagnostics: Time Series Analysis*. https://crudata.uea.ac.uk/~timo/diag/tempdiag.htm. Accessed: 2024-09-05. 2024.

[54] Andreas Oschlies et al. «Drivers and mechanisms of ocean deoxygenation». In: *Nature Geoscience* 11.7 (2018), pp. 467–473. ISSN: 1752-0908. DOI: 10.1038/s41561-018-0152-2. URL: https://doi.org/10.1038/s41561-018-0152-2.

[55] *Paris Agreement*. https://unfccc.int/resource/docs/2015/cop21/eng/l09r01.pdf. United Nations Framework Convention on Climate Change (UNFCCC), 2015.

[56] H.-O. Pörtner et al., eds. *Climate Change 2022: Impacts, Adaptation, and Vulnerability*. Cambridge, UK and New York, NY, USA: Cambridge University Press, 2022, p. 3056. DOI: 10.1017/9781009325844.

[57] QuantumATK. *Work Function of Ag(100)*. 2023. URL: https://docs.quantumatk.com/tutorials/work_function_ag_100/work_function_ag_100.html.

[58] Hannah Ritchie and Max Roser. *Emissions by Sector*. https://ourworldindata.org/emissions-by-sector. 2020.

[59] Hannah Ritchie and Max Roser. *Greenhouse Gas Emissions*. https://ourworldindata.org/greenhouse-gas-emissions. 2020.

[60] Alexander G. Shard. «Practical guides for x-ray photoelectron spectroscopy: Quantitative XPS». In: *Journal of Vacuum Science Technology A* 38.4 (July 2020), p. 041201. ISSN: 0734-2101. DOI: 10.1116/1.5141395. URL: https://doi.org/10.1116/1.5141395.

[61] Jun-Seok Shim, John A. Rogers, and Seung-Kyun Kang. «Physically transient electronic materials and devices». In: *Materials Science and Engineering: R: Reports* 145 (2021), p. 100624. ISSN: 0927-796X. DOI: https://doi.org/10.1016/j.mser.2021.100624. URL: https://www.sciencedirect.com/science/article/pii/S0927796X2100019X.

[62] National Institute of Standards and Technology (NIST). *X-ray Photoelectron Spectroscopy (XPS) Database*. Accessed: 2024-10-06. 2024. URL: https://srdata.nist.gov/xps/.

[63] Fred A. Stevie and Carrie L. Donley. «Introduction to x-ray photoelectron spectroscopy». In: *Journal of Vacuum Science Technology A* 38.6 (Sept. 2020), p. 063204. ISSN: 0734-2101. DOI: 10.1116/6.0000412. URL: https://doi.org/10.1116/6.0000412.

[64] Inc. Synopsys. *Quantum ATK User Manual*. 2021.

[65] Park Systems. *Tapping Mode*. URL: https://www.parksystems.com/en/products/research-afm/AFM-modes/imaging-modes/tapping-mode.

[66] Park Systems. *True Non-Contact Mode*. URL: https://www.parksystems.com/en/products/research-afm/AFM-modes/imaging-modes/TrueNon-ContactMode.

[67] Massachusetts Institute of Technology. *Permafrost*. https://climate.mit.edu/explainers/permafrost. 2022.

[68] TSMC. *TSMC 2021 Sustainability Report*. https://esg.tsmc.com/download/file/2021$_s$*ustainabilityR*
all.pdf. 2021.

[69] *United Nations Framework Convention on Climate Change*. https://unfccc.int/files/essential_background/background_publications_htmlpdf/application/pdf/conveng.pdf. United Nations, 1992.

[70] NASA Ozone Wacth. *What is ozone?* https://ozonewatch.gsfc.nasa.gov/facts/SH.html. 2021.

[71] S. Widdicombe et al. «Unifying biological field observations to detect and compare ocean acidification impacts across marine species and ecosystems: what to monitor and why». In: *Ocean Science* 19.1 (2023), pp. 101–119. DOI: 10.5194/os-19-101-2023. URL: https://os.copernicus.org/articles/19/101/2023/.

[72] World Meteorological Organization (WMO). *About GCOS and the UNFCCC*. 2023. URL: https://gcos.wmo.int/en/about/UNFCCC.

[73] *XPS Fitting*. 2024. URL: https://www.xpsfitting.com/.

[74] Juhi Yadav, Avinash Kumar, and Rahul Mohan. «Dramatic Decline of Arctic Sea Ice Linked to Global Warming». In: *Natural Hazards* 103.3 (2020). Published online: 21 May 2020, pp. 2617–2621. DOI: 10.1007/s11069-020-04064-y. URL: https://doi.org/10.1007/s11069-020-04064-y.

[75] Yanbao Zhao, Zhijun Zhang, and Hongxin Dang. «A simple way to prepare bismuth nanoparticles». In: *Materials Letters* 58.5 (2004), pp. 790–793. ISSN: 0167-577X. DOI: https://doi.org/10.1016/j.matlet.2003.07.013. URL: https://www.sciencedirect.com/science/article/pii/S0167577X03006189.